Dissertation

In vivo study of the two-component signaling network in *Escherichia coli*

Erik Sommer

December 2011

Dissertation
submitted to the
Combined Faculties for the Natural Sciences and for Mathematics
of the Ruperto-Carola University of Heidelberg, Germany
for the degree of
Doctor of Natural Sciences

presented by

Diplom-Biologe Erik Sommer
born in Wiesbaden-Sonnenberg
Oral examination: February 2012

In vivo study of the two-component signaling network in *Escherichia coli*

Referees: Prof. Dr. Victor Sourjik
PD Dr. Axel Mogk

Für meine Familie

Acknowledgements

First and foremost, I would like to express my sincere gratitude to Prof. Dr. Victor Sourjik for his supervision, encouragement and support throughout the last years.

Also, I am very grateful to PD Dr. Axel Mogk for his kind guidance, helpful discussions and valuable advice.

I want to thank Prof. Dr. Bernhard Hauer from the University of Stuttgart for being member of my TAC during the last years, for the fruitful discussions and his helpful suggestions.

This work is part of a collaboration with Prof. Dr. Ady Vaknin and Dr. Moriah Koler at the Racah Institute of Physics, Hebrew University Jerusalem, Israel. I wish to thank them for the fruitful collaboration during the last years.

I am grateful as well to all the present and former colleagues in the Sourjik lab for giving me indispensible help and support and creating a wonderful working environment.
Especially, I would like to thank Anette Müller for her help during this project, her patience with me and the nice co-working atmosphere. David Kentner I like to thank for providing plasmids and helpful discussions regarding cloning strategies. Abiola Pollard I would like to thank for her proof-reading of my manuscript and very helpful suggestions.

Ein riesiges Dankeschön geht an meine Eltern und meinen Bruder für Ihre Geduld, Aufmunterung und Unterstützung während der letzten Jahre. Ohne Euch hätte ich das nicht geschafft!

Zum Schluss möchte ich mich bei meiner Liebsten, Madeleine, ganz herzlich bedanken. Es ist ein großes Glück, daß ich Dich getroffen habe. Vielen Dank, daß Du immer für mich da bist!

Contents

Zusammenfassung

Mikroorganismen verwenden meist “Zweikomponentensysteme” zur Wahrnehmung ihrer Umweltbedingungen und man findet sie in unterschiedlicher Zahl in den Genomen fast aller Bakterien und Archaeen. Ein typisches Zweikomponentensystem besteht aus einer Histidinkinase als Sensor und einem Antwortregulator, welcher von der Kinase phosphoryliert wird. Der Antwortregulator fungiert meist als Transkriptionsfaktor und reguliert die Genexpression. Aufgrund ihrer Verbreitung in Mikroorganismen ermöglicht ein grundlegendes Verständnis der Funktionsweise von Zweikomponentensystemen Einblicke in die Mechanismen prokaryotischer Signalverarbeitung. Trotz einiger *in vitro* Studien fehlt bisher die Beschreibung eines vollständigen Netzwerkes von Zweikomponentensystemen *in vivo*. In einer systemweiten Studie im Bakterium *Escherichia coli* haben wir die Lokalisierung von Signaltransduktionsproteinen und die Wechselwirkungen zwischen Systemen auf verschiedenen Ebenen untersucht. Dafür konstruierten wir eine umfassende Bibliothek von fluoreszenten Kinase- und Regulatorfusionen und analysierten ihre Lokalisierung innerhalb der Zelle mittels Fluorezenzmikroskopie. Wir sahen für die meisten Sensoren eine intrinsische Tendenz zur Komplexbildung, welche wahrscheinlich ein Gerüst zur Informationsverarbeitung bietet und Systeme gegen störende Einflüsse von außen schützt. Mittels systematischer *in vivo* FRET-Mikroskopie untersuchten wir systematisch die Interaktionen zwischen den einzelnen Proteinen. Für die meisten Sensoren konnten wir die Bildung von Dimeren oder Oligomeren *in vivo* bestätigen. Den Sensor BaeS charakterisierten wir durch die induzierte Konformationsänderung auf Grund von Stimulationen. Zusätzlich fanden wir einige Signaltransduktionswege, welche auf Sensorebene oder zwischen Kinasen und nicht zugehörigen Regulatoren interagieren. Diese bilden eine weitere Ebene der Signalverarbeitung. Mittels Durchflusszytometrie und einer fluoreszenten Promotorkollektion konnten wir für einige dieser Interaktionen die physiologische Relevanz auf Genexpressionsebene bestätigen. Jedoch fanden wir keinen Effekt der meisten beschriebenen Stimuli auf die Genexpression von Zweikomponentensystemen. Abschließend liefern unsere Ergebnisse ein detailierteres Verständnis der räumlichen Organisation von *E. coli* Zweikomponentensystemen und deren Wechselwirkungen untereinander. Diese erweitern das Verständnis bakterieller Signaltransduktion.

Summary

Microorganisms commonly use 'two-component' signaling systems for sensing environmental conditions, with members being present in nearly all bacterial and archaeal genomes in different numbers. Prototypical two-component systems are comprised of a sensory histidine kinase and a response regulator protein that is phosphorylated by the kinase. The regulator typically acts as a transcription factor regulating gene expression. Due to their prevalence in microorganisms, a basic understanding of the principles of two-component systems provides insights into mechanisms of prokaryotic signaling circuits. Apart from a few studies performed *in vitro*, the signaling properties of a whole bacterial two-component network *in vivo* remains largely unclear. Using a system level approach, we characterized the localization of signaling proteins and the interactions between pathways on different levels in the model bacterium *Escherichia coli*. We constructed a comprehensive library of fluorescent protein fusions to kinases and regulators from two-component systems, and applied fluorescence microscopy to analyze their spatial organization within the cell. We found that most of the sensors exhibit a intrinsic tendency for cluster formation, which might provide a scaffold for information processing and insulation against detrimental noise from other sources. We used *in vivo* FRET microscopy tools to study protein interactions in a systematic way. For kinases, we could confirm the formation of sensor dimers or higher order oligomers *in vivo* in most of the cases. For the sensor BaeS, we characterized the change of sensor confirmation upon stimulation. Additionally, we identified a few pathways exhibiting interconnections on the sensor level and between sensors and non-cognate regulators, providing an additional layer of information processing. We could confirm the physiological relevance of some of these pathway interconnections on the gene expression level, using flow cytometry measurements of a fluorescent promotor library. Moreover, using this library we found most of the reported stimuli not affecting two-component gene expression. Taken together, our data provide a deeper understanding of cellular organization within and interconnections between different two-component systems in *E. coli*. The results of this study can broaden the understanding of cell signaling principles in bacteria.

1 Introduction

1.1 Bacterial signaling

Microorganisms are the oldest and most successful form of life and ubiquitous in the earth´s biosphere. Notwithstanding the majority of prokaryotes remains to be characterized [1], they outnumber all other species and despite their small size, they account for a biomass exceeding those formed by all other higher organisms [2, 3]. Prokaryotes occupy all possible habitats either as free living single cells, in cell communities or as symbionts or parasites in close association with other organisms. Because of differences in lifestyles, they must sense and respond to a large variety of external and internal signals. These include for example changes in metabolism, nutrient availability, stress-responses, signals for biofilm formation or virulence factors. To perform this tasks prokaryotes developed several different ways of receiving signals and transmitting the input to an appropriate response inside the cell [4]. The successful processing of information and responding appropriately allows adaptation, maintainance of viability, and the movement towards more favourable conditions. In most cases, cellular responses operate on a genetic level, converting a received signal into a changed gene expression pattern.

The signal transduction systems developed by prokaryotes can be classified in three major classes, depending on the location of the stimulus source:

- transmembrane signaling
- cell-cell communication and
- intracellular signal transduction.

These classes contain different architectures of sensory transduction networks, which are encoded into the bacterial genomes. The most prevalent and evolutionarily oldest pathways are so-called one-component systems [5], which are ubiquitous among bacteria and archaea. The second most frequent bacterial signaling pathways are two-component systems (TCS) which are the subject of this study. Additionally, there is a range of different signal transduction systems such as phosphotransferase systems (PTS) [6] and signaling systems

mediated by small molecules like cyclic-di-GMP, cAMP or ppGpp [7, 8] or small regulatory RNAs [9]. This work focuses on the signaling network of two-component systems in the gram-negative enterobacterium *Escherichia coli* K-12 [10, 11], a commonly used model organism in (molecular) microbiology.

1.2 Two-component systems

Two-component systems (TCS) are one of the most widespread signaling systems in prokaryotes and lower eukaryotes, with pathways being present in nearly all bacteria and many archaea in different numbers (*Bacillus subtilis*: 32, *Helicobacter pylori*: 3, *Methanobacterium thermoautotrophicum*: 29, *Ktedonobacter racemifer DSM 44963*: 366) [12]. They also occur in eukaryotes like the budding yeast *Saccharomyces cerevisiae*, the slime mold *Dictyostelium discoideum* or the plant *Arabidopsis thaliana* with 1, 11 and 4 systems, respectively [13, 14]. The number of systems seems thereby to depend on the organism´s environment and the number of signals it is exposed to, with free living bacteria harbouring more systems than parasites [15, 16]. Additionally, TCS numbers exhibit a positive correlation with the genome size [5]. Interestingly, TCS seem to be completely absent from the animal kingdom [17], as so far no genes coding for sensors or regulators have been found in the genomes of *Caenorhabditis elegans* [18], *Drosophila melanogaster* [19] or *Homo sapiens* [20]. This fact makes them an attractive target for new kinds of specific antimicrobial agents [21, 22]. What makes them suitable to study basic principles of signal transduction is the relatively simple layout and the modularity in their design (Figure 1.1).

They are comprised out of only two proteins, a sensor histidine kinase (HK) and a cytoplasmic response regulator (RR) [13]. Upon activation through a certain stimulus, the sensor kinase gets autophoshorylated at a histidine residue. The phosphoryl group is subsequently transferred to a specific aspartate residue on the response regulator that acts in most of the cases as a transcription factor regulating downstream gene expression. There are kinases, referred to as orthodox kinases, that perform a direct phosphotransfer from the sensor to the response regulator. Additionally, there are more elaborate ways of phosphotransfer such as hybrid kinases or phosphorelays [13, 23] (Figure 1.2). Those sensors include additional intramolecular domains harbouring Asp and His residues, allowing a multistep phosphotransfer within the kinase before phosphorylation of the response regulator. Those systems account for about 25 % of all known two-component sensors [24]. It is not clear why some pathways are designed as phosphorelays instead of a orthodox two-component system. It is believed that those multistep relays allow further control of

the signal transduction cascade as for example exhibited by the regulation of *B. subtilis* sporulation [25]. Another hypothesis is that multiple steps could provide a filter against noise in the input signals [26], but this has yet to be confirmed experimentally. In *E. coli*, 5 out of 30 sensors (ArcB, BarA, EvgS, RcsC, TorS) are hybrid kinases [15]. An overview

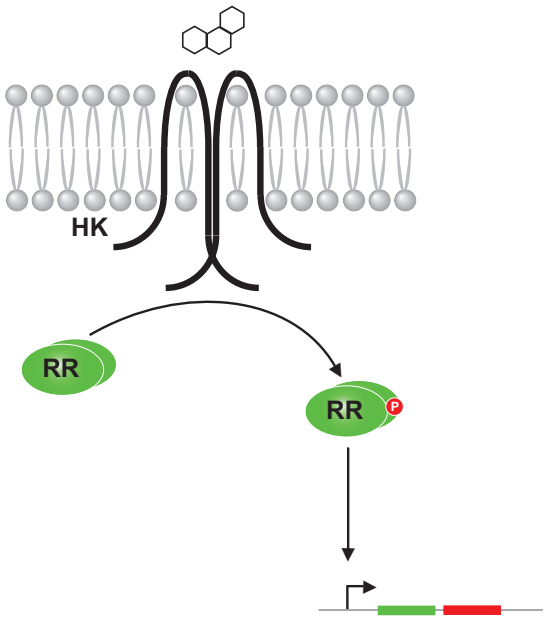

Figure 1.1: **Schematic representation of two-component systems architecture.** A prototypical two-component system contains a histidine kinase dimer (**HK**) located in the cytoplasmic membrane, acting as a sensor. **RR** represents the cytoplasmic dimeric response regulator, which is phosphorylated (**P**) through the kinase resulting in binding to a promotor region on the genome. The polycyclic hydrocarbon structure symbolizes the (periplasmic) stimulus of the system.

of all TCS from *E. coli* is depicted in Table 1.1. TCS show a high degree of homology between different systems and even organisms [27]. Given that, a basic understanding of the principles of two-component system would provide the insight into the mechanisms of virulence or pathogenicity [28] or allow construction of novel signaling circuits and genetic networks using synthetic biology or metabolic engineering [29, 30].

Table 1.1: **Overview of two-component systems in *Escherichia coli*.** A list of all identified two-component systems in *E. coli* with their corresponding downstream target promotor and stimuli. Modified after [4].

Family[1]	Histidine kinase	Response regulator	Promotor	Stimulus	Involved process
CitB	CitA	CitB	*citC*, *citT*	citrate	citrate uptake
	DcuS	DcuR	*dcuB*	fumarate	C_4-metabolism
LytT	LytS (=YehU)[2]	LytR (=YehT)[2]	*lrgA*		mureine hydrolase activity
	YpdA	YpdB	n.d.	n.d.	n.d.
NarL	BarA	UvrY	*csrB*	pH	carbon storage, pilus adherence
	EvgS	EvgA	*emrK*	ubiquinone	antibiotic resistance
	NarQ	NarP	*fdnG*, *frdA*,	$NaNO_2$, $NaNO_3$	anaerobic respiration
	NarX	NarL	*nrfA*, *ytfE*		
	RcsC	RcsB (=YojN)[2]	*wza*	undecaprenyl(pyro)phosphate	capsule synthesis, motility
	UhpB	UhpA	*uhpT*	glucose-6-phosphate	glucose-6-phosphate transport
	-	FimZ (=YbcA)[2]	*ampC*	n.d.	β-lactam resistance
NtrC	AtoS	AtoC	*atoD*	acetoacetate	acetoacetate metabolism
	HydH (=ZraS)[2]	HydG (=ZraR)[2]	*zraP*	$ZnCl_2$, $PbCl_2$	Zn^{2+} tolerance
	NtrB (=GlnL)[2]	NtrC (=GlnG)[2]	*glnA*	α-ketoglutarate	nitrogen metabolism
	YfhK	YfhA	n.d.	n.d.	n.d.
OmpR	ArcB	ArcA	*sdhC*	D-lactate, acetate	(an)aerobiosis
	BaeS	BaeR	*mdtA*	Indole, $CuSO_4$, $ZnSO_4$	multidrug and metal resistance
	BasS	BasR	*tdcB*, *ygjJ*	$FeSO_4$	iron response
	CpxA	CpxR	*htrA*	pH	cell envelope protein folding
	CreC	CreB	*creA*	n.d.	regulation intermediary metabolism
	CusS	CusR	*cusC*	$CuSO_4$	copper resistance
	EnvZ	OmpR	*ompC*, *pstS*	sucrose, NaCl, KCl	outer membrane porin production
	KdpD	KdpE	*kdpA*	K^+, ionic strength	high affinity K^+transport
	PhoQ	PhoP	*phoA*	antimicrobial peptides, Mg^{2+}	bacterial virulence
	PhoR	PhoB		phosphate, Mg^{2+}	phosphate limitation
	RstB	RstA	*asr*	$ZnCl_2$, $MgCl_2$	Mg^{2+}-stimulon
	QseC	QseB	*flhD*	(nor)epinephrine, AI-3	cell density, quorum sensing
	TorS	TorR	*torC*	trimethylamine-N-oxide	trimethylamine metabolism
	YedV	YedW	n.d.	n.d.	metal homeostasis
others	-	RssB	*rpoS*	n.d.	sigma S proteolysis
CheA[3]	CheA	CheB	*fliF*, *motA*	Asp, Ser	chemotaxis
		CheY			

1: Classification based on Effector domains of response regulators

2: Alternative nomenclature from literature and databases

3: Proteins from chemotaxis, which were not included in our experiments; **n.d.**: no stimulus or involved process defined

1.2.1 Histidine kinases

Stimulus perception in two-component systems is performed by sensor or histidine kinases [13, 23]. The basic principle of kinase domain organization is shown in Figure 1.2, the structural details are depicted in Figure 1.3.

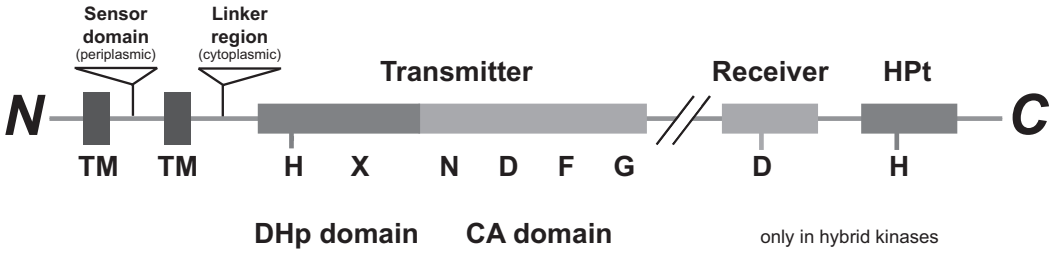

Figure 1.2: **Domain organization of histidine kinases.** Majority of sensors contain a N-terminal (periplasmic) sensing domain for stimulus perception, which is surrounded by two transmembrane (**TM**) domains. The following linker region connects the TM with the cytoplasmic transmitter module, containing the DHp and CA domains. DHp harbours the conserved histidine residue (**H**). Single letters describe homology motifs inside the module (details: see text). Hybrid kinases additionally contain C-terminal Receiver and HPt domains with additional histidine and aspartate (**D**) residues building a phosphorelay. (modified after [23])

It contains two N-terminal transmembrane domains (TM), which surround a sensor domain for periplasmic sensing kinases (details, see below). On the cytoplasmic side the TM region is followed by a HAMP domain (named after their conservation among histidine kinases, adenylyl cyclases, methyl-accepting proteins, phosphatases), transmitting information via a piston-like movement from the outside to the cytoplasmic parts of the sensor. The following transmitter part is composed of two domains, the DHp (dimerization and histidine phosphotransfer) and the CA (catalytic activity and ATPase) domain. The DHp domain contains a conserved histidine residue that is involved in the signal transmission through phosphorylation. The CA domain is responsible for catalyzing autophosphorylation of the sensor using ATP, which binds to the ATP-lid between the G1 and G2 boxes of the CA domain.

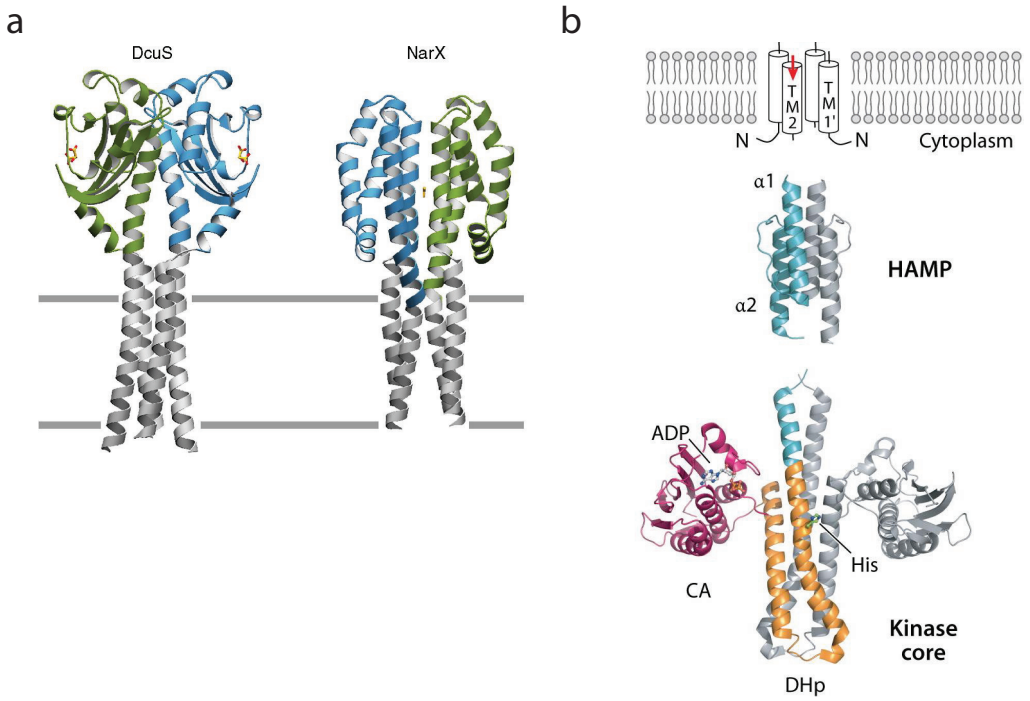

Figure 1.3: **3D structures of common histidine kinase domains.** **(a)** Alternative designs for periplasmic sensing domains showing structures from *E. coli* DcuS and NarX sensors. Individual monomers are depicted in green and blue, respectively, modeled TM domains are shown in grey. The corresponding signal molecules malate and nitrate bound to DcuS and NarX, respectively, are depicted in yellow. **(b)** Structural representation of cytoplasmic HK domains with the HAMP domain from *Archaeoglobus fulgidus* Af1503 (**HAMP**) and the transmitter domain from *Thermotoga maritima* HK853 (**Kinase core**). All domains exhibit a dimeric structure and are shown in different colours. Red arrow in TM2 represents proposed piston-like movement upon stimulation for signal transmission. Conserved His-residue in the kinase core is shown as green pentagon. Violet 3D structure represents a RR which accesses the kinase phosphorylation site. (modified after [24, 31])

Classification of sensor kinases into families or groups is difficult given the large variation in sequence and 3D-structure. Grebe and co-workers grouped the histidine kinases in 11 different families, based on sequence homologies in their different domains [27]. The kinases contain six different amino acid motifs (called the H, X, N, D, F and G box), which have a high degree of conservation between different sensors. Additionally, sensors of certain kinase subfamilies have the tendency to group with regulators from a specific RR subfamily (see below, section 1.2.2) [27], indicating co-evolution of the two proteins. This classification of bacterial sensors is strictly based on sequence data, neglecting any functional properties of the kinases. Therefore, Mascher and colleagues suggested to group

histidine kinases based on domain architecture and topology, which leads to a classification related to the sensor function [23]. The most common design of kinases includes a sensing domain exposed to the periplasmic space, interacting directly or indirectly with extracellular signals. Those sensors are typically involved in the sensing of nutrients or soluble substances from the cellular environment. The second largest class are kinases that sense signals from the cytoplasm. They are either anchored to the cytoplasmic membrane or are soluble proteins, detecting exclusively cytoplasmic solutes or signals from metabolic or developmental processes in the cell. A third class of kinases detect membrane-associated or membrane interface signals like turgor pressure, mechanical stress and electrochemical gradients. For theses sensors, stimulus perception is performed by the membrane spanning helices or a combination of one transmembrane helix and one cytoplasmic domain at the N-terminus. One exception from the usual kinase construction is the *E. coli* citrate sensor CitA, which contains one periplasmic and one cytosolic sensor domain [32], resulting from domain duplication during evolution of the protein.

There are 14 different types of sensor domains [5]. About a third of all sensors use a PAS 3D-structure (Per-ARNT-Sim) as sensory domain [24], formed by a five-stranded β-sheet and five α-helices [33, 34]. PAS domains are a universal signaling structure which are widespread in biology [35], sensing a variety of environmental cues. Interestingly, they show only conservation on structural level but not within their amino acid sequence [36]. The sensing domain is connected to a cytoplasmic autokinase domain by a membrane spanning linker region. Transmembrane domains are found in the vast majority (∼83 %) of sensor kinases [37] in numbers up to 20 TM regions per protein [23]. The autokinase domain consists of a long α-hairpin (DHp domain), responsible for dimerization and histidine phosphotransfer (Figure 1.3). Two DHp domains form a four-helix bundle via the dimerization interface. Additionally, the DHp domain contains a conserved histidine residue, which acts as phosphorylatable target in the first step of the phosphotransfer reaction. The C-terminal end of the sensor kinase is formed by the globular catalytic and ATP binding domain (CA), which is connected to the DHp domain via a short linker. ATP binding at the CA domain requires the presence of Mg^{2+} as a bivalent cofactor [38]. Most histidine kinases are thought to function as dimers, and there is much structural and biochemical evidence to support this assertion [39, 40]. Nevertheless, the majority of experiments are derived *in vitro* so far [41, 42, 43], meaning that a systematic investigation has yet to be performed in living cells. This is especially important, because the existence of monomeric sensor kinases was reported by Fabret and colleagues for *Bacillus subtilis* [44], emphasizing the variations in design principles within prokaryotic two-component sensors.

Biochemically, histidine kinases catalyze three different kinds of phosphotransfer re-

actions: (i) their own autophosphorylation (phosphotransfer from ATP to the histidine residue), (ii) transphosphorylation from His∼P towards an Asp residue of the response regulator and (iii) dephosphorylation of the response regulator Asp residue [13].

(i) Autophosphorylation: $\text{HK-His} + \text{ATP} \leftrightharpoons \text{HK-His}\sim\text{P} + \text{ADP}$

(ii) Phosphotransfer: $\text{HK-His}\sim\text{P} + \text{RR-Asp} \leftrightharpoons \text{HK-His} + \text{RR-Asp}\sim\text{P}$

(iii) Dephosphorylation: $\text{RR-Asp}\sim\text{P} + \text{H}_2\text{O} \leftrightharpoons \text{RR-Asp} + \text{P}_\text{i}$

Autophosphoralytion within a kinase dimer was long believed to take place exclusively in *trans*, meaning that the phosphoryl group of ATP bound to one monomer is used to phosphorylate the His residue of the other monomer. This has been shown experimentally for the sensors AtoS [45], EnvZ [46], KdpD [41], NRII [47] and the non-canonical kinase CheA [48, 49]. Nevertheless, recent experiments on a sensor kinase from *Thermotoga maritima* showed autophosphorylation within the same monomer [50], hinting to at least one exception of the paradigm assumed so far.

To ensure a proper performance of signal processing and a return to the basic ´off´state of the pathway, cells have to limit the response temporarily. One possibility to achieve this is to limit the half-live of a phosphorylated protein residue. Experiments showed that the half-lives of phosphorylated kinases is not that different independent of the kind of signaling pathway they are involved in. They range from about 30 to 90 minutes for the full-length proteins investigated [51, 52], and it seems that the temporal adjustment in signaling is rather performed through half-live of the response regulator phosphorylation (see below, section 1.2.2).

1.2.2 Response regulators

The second protein involved in TCS signal transduction is called the response regulator (RR). Response regulators, as histidine kinases, exhibit a modular architecture harbouring two different domains, a highly conserved N-terminal receiver and a variable C-terminal effector (output) domain. This modularity in design allows for a perfect adaptation to the needs of different regulatory mechanisms. A structural overview of the response regulator domain organization and effector domain distribution is shown in Figure 1.4.

Response regulators connect the sensor kinase with a downstream target inside the cell. This is in most cases a promotor sequence, as the majority (63 %) of RRs function as

transcription factors with a DNA binding domain [15]. *E. coli* has a high number of response regulators that bind DNA, 27 out of 32 control gene expression, three contain a receiver domain, only and two include a unique output domain [5, 12]. Based on their DNA binding domains, RRs are grouped in three major families [53], OmpR, NarL and NtrC, with OmpR being the most abundant family in *E. coli* with 14 members (Table 1.1). Nevertheless, there are some exceptions to the prototypical design principle. Some RRs have a enzymatic subunit as C-terminal effectors like the methylesterase CheB from the *E. coli* chemotaxis pathway [54] or the cAMP phosphodiesterase from *Dictyostelium* [55, 56]. About 15 % of bacterial and 50 % of archaeal response regulators lacks the effector domain completely[57], for example CheY from chemotaxis [15] or the sporulation factor Spo0F from *B. subtilis* [58, 59].

The N-terminal receiver domain (REC) functions as a phosphorylation-mediated switch. Their structure contains a five-stranded parallel β-sheet, which is sorrounded by five α-helices [60, 61] as shown in Figure 1.4a. The REC domain is involved in phosphorylation through the cognate sensor via using a conserved Asp residue, generating a high energy acyl phosphate. Subsequently this binding energy is used to drive a conformational change affecting a large surface of the REC domain, shifting the equilibrium from one state to another, usually inactive to active. This switching subsequently controls the activity of the downstream effector domain of the regulator, with a mechanism similar to the energy coupled conformational change in P-type ion-translocating ATPases [60]. The REC domain is able to perform two kinds of enzymatic reactions, phophotransfer from the kinase and autodephosphorylation. The ability for phosphotransfer has been shown experimentally by adding small phosphodonor molecules like acetyl phosphate or carbamoyl phosphate to regulators, phosphorylating the Asp residue independent of the presence of a kinase [62]. Nevertheless, the phosphorylation rate of a regulator through a kinase is faster than the rate of autophosphoralytion [63, 64], ensuring a high degree of signaling specificity *in vivo*. The intrinsic ability of autodephosphorylation serves to limit the lifetime of the elicited response after a signaling event, and is therefore a critical step in the signal transmission. There has been a wide range of dephosphorylation rates reported, ranging from 0.28 s^{-1} for CheY6 from *Rhodobacter sphaeroides* [65] up to 0.25 $week^{-1}$ for RedF from *Myxococcus xanthus* [66]. These huge differences represent the different timescales of the single pathways they are involved in, ranging from fast processes like chemotactic sensing to regulation of developmental processes in slow growing bacteria. As the half-live of phosphorylated kinases is relatively stable and conserved between sensors (see section 1.2.1), temporal adjustments of two-component signaling pathways take place at the response regulator level.

In many two-component regulators (e.g. NtrC∼P and CheY∼P), dephosphorylation is performed through the phosphatase activity of other proteins. Mechanistically, rather the intrinsic ability of the regulator to dephosphorylate is stimulated instead of direct dephosphorylation performed by the auxiliary phosphatase [67, 68, 69].

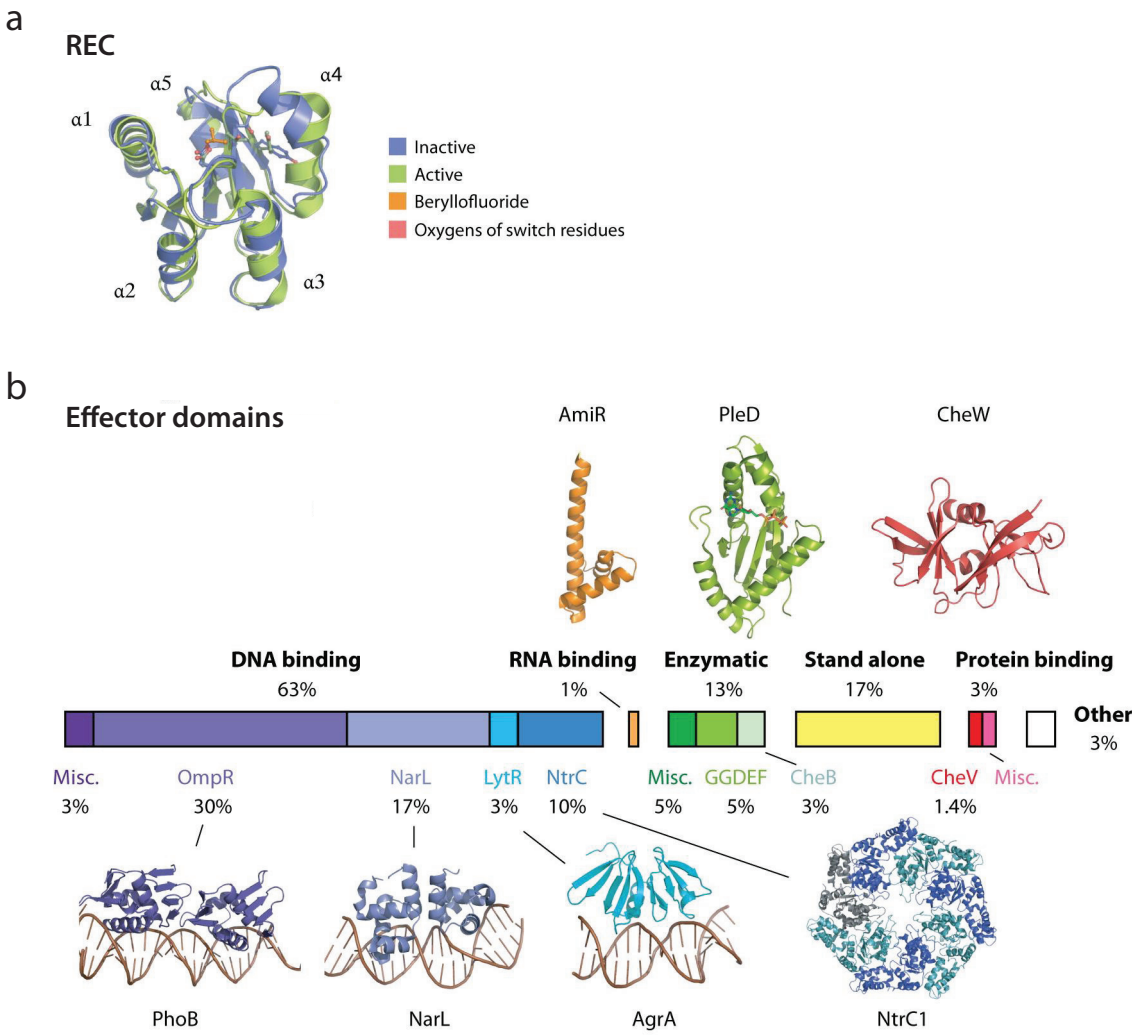

Figure 1.4: **3D structures of different response regulator domains.(a)** The active and inactive receiver domain structure (**REC**) from *E. coli* PhoB shown in green and blue, respectively. Sorrounding α-helices are numbered and switching residues are coloured in red. BeF_3 (orange) substitutes ATP as structural analogue for crystallization. **(b)** Distribution of functional classes among the effector domains of different RR families. Family names are shown in colour beneath the bar, and for every family a representative 3D structure is shown using the same colour coding. (modified after [24])

Effector domains within response regulators are quite diverse [13], even within a single family (see Figure 1.4b for details). The members of the OmpR family for example define a subclass of winged-helix transcription factors. Thereby, the protein fold is structurally conserved within the family, forming a helix interacting with the major groove of the DNA and the adjacent wings interacting with the minor groove [70, 15]. Regulators of the NarL family are characterized by a four-helix DNA binding domain [71], containing a typical helix-turn-helix motif. The third major response regulator family, NtrC, represents structurally the most diverse group, with two domains forming the effector part: an ATPase domain and a helix-turn-helix DNA binding motif [72, 73, 74].

1.3 Signal processing in two-component systems

Despite the classical linear pathway design (Figure 1.5a), there is some complexity in the regulatory circuits of two-component systems via branched pathways [75]. For example bacterial chemotaxis is a ´one-to-many´ pathway (Figure 1.5b), where a single kinase CheA phosphorylates different response regulators CheY and CheB competitively [76, 77, 78]. An exemplification of a ´many-to-one´ architecture is the quorum sensing signaling pathway from the marine bacterium *Vibrio harveyi* (Figure 1.5c). In this network, three different hybrid kinases (LuxN, LuxQ and CqsS), respond to different autoinducers and converge information via phosphorylation of the RR protein LuxU to integrate three different autoinducer signals into one pathway [9]. Another example is the sporulation phosphorelay of *B. subtilis* [79], where the four kinases KinA-D phosphorylate the regulator Spo0F, the first part of a signaling cascade switching between sporulation or the entry into stationary phase. It should be mentioned that these two cases, depending on the literature, are sometimes already classified as cross-talk or cross-regulation, as interactions take place between different pathways.

Given the large number of TCS present inside a single bacterial cell and their structural and functional similarities, a major question is the specificity of the performed signaling. On the one hand, the organism has to ensure the proper isolation of the single cascades from one another. This isolation prevents detrimental interactions between the different systems which could lead to a disturbance in information processing inside the cell. On the other hand, some degree of interactions between different pathways would enable cells to integrate information from different sources, similar to the mentioned ´many-to-one´ and ´one-to-many´ pathways. This could provide another layer of information processing on top of the single cascades.

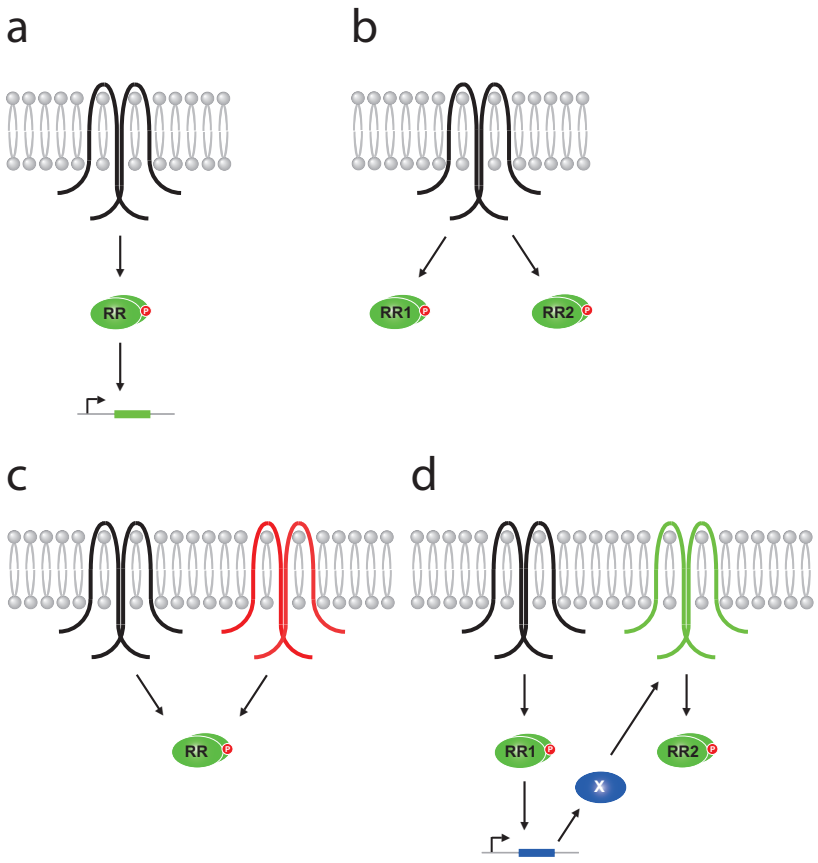

Figure 1.5: **Signaling pathway architectures.** (**a**) Prototypical TCS pathway architecture with one kinase acting on a single response regulator (**RR**). (**b**) One-to-many pathway; one histidine kinase phosphorylates two different RRs. (**c**) Many-to-one pathway; different histidine kinases phosphorylate the same RR. (**d**) Connector-mediated pathway. One two-component system regulates expression of an auxiliary protein (**X**), which in turn regulates another two-component system. (modified after [75])

1.3.1 Signaling specificity

Two-component systems exhibit different properties to ensure specificity in signaling. Sensor kinases for example have *in vitro* the intrinsic ability to distinguish between cognate and non-cognate substrates. Phosphorylation of the cognate response regulator is thereby kinetically preferred compared to other proteins. For instance the *E. coli* kinase NtrB is more efficient in phoshorylating NtrC than the non-cognate kinase CheA [80], and the same was shown between EnvZ/CheA and OmpR [81]. Systematic studies performed on

TCS from *E. coli* and *C. crescentus* confirmed a strong *in vitro* preference of sensors for their cognate substrate [82, 83, 84]. For example the osmolarity sensor EnvZ is able to phosphorylate 16 different non-cognate regulators after a timespan of about 60 minutes. Nevertheless, transphosphorylation of the cognate regulator OmpR takes only 10 seconds, indicating a kinetic preference between the cognate components [82]. This holds also true for branched pathways were the kinase shows a similar affinity for both regulators compared to the non-cognates. In *B. subtilis* the sensor KinA exhibits a 50000 fold higher preference for the response regulator Spo0F compared to Spo0A [58, 85]. Taken together these results confirm that kinetic preference is a general feature for signaling specificity of two-component pathways in different organisms.

Another possibility to guarantee signaling specificity is the competition of response regulators for the kinase, where the cognate outcompetes the non-cognate regulator. For example the kinase VanS of the vancomycin resistance pathway of grampositive bacteria is able to phosphorylate PhoB, with an enhanced rate in the corresponding regulator knockout for VanR [86, 87]. This effect is even more pronounced in the double knockouts of the non-cognate proteins (kinase and regulator), and similar results were shown for CpxA/OmpR and EnvZ/CpxR [84, 88, 89]. This idea is supported by results showing the phosphorylation of regulators by the general phosphodonor acetyl-phosphate, which mostly occured in the sensor knockout, only [90]. It is assumed that the effect of minimizing cross-talk by response regulator competition is enhanced by the relative low abundance of kinases compared to regulators, with a ratio of about 1:30 [91, 92, 93, 94, 95]. This robustness was demonstrated experimentally for the *E. coli* TCS EnvZ/OmpR, PhoQP and CpxAR [92, 93, 95, 88]. Additional evidence for this response regulator competition came from experiments by Ninfa and colleagues, who showed increased cross talk from overexpressed NtrB on CheY in a CheA knockout strain [80].

The bifunctional property of some kinases also provides an effective mechanism against cross-talk. Those sensors work as phosphatases for the cognate regulator preventing unintended cross-phosphorylation. This was experimentally confirmed for the VanSR and PhoRB systems mentioned above [86, 87]. Additionally, it was shown that in absence of the bifunctional kinases cross-talk occured from CreC to PhoB and UhpB to NtrC/PhoR [96, 97, 98, 99]. Further support comes from computational studies which showed that bifunctional kinases are more efficient in the suppression of cross-talk than monofunctional ones [100]. Monofunctional kinases thereby compensate this lack in phosphatase activity by using additional phosphatases (e.g. CheZ in chemotaxis), which protect those pathways against detrimental cross-talk [78]. Additionally to intrinsic specifity, the maintainance of a high level of phosphorylation and dephosphorylation provides insensitivity to disturbances

from the outer environment [100, 88, 84].

In addition to biochemical parameters, signaling specificity is provided through structural protein features. Even though the interaction interface between sensors and regulators exhibit a high degree in structural conservation [24], the amino acid motifs between different systems are variable and mediate specificity [101]. This specificity is mediated through residues located in the cytoplasmic DHp domain of the kinase [102, 103, 104] and the REC domain of the regulator [105, 106, 107, 108, 109]. By exchanging these residues, specificity can be rewired to increase cross-talk to a different two-component system [104].

It should be mentioned that there is also an extrinsic property to ensure signaling specificity, which is spatial organization (for details see section 1.4) as it is accomplished in eukaryotes. For example the chemotaxis apparatus in *R. sphaeroides* is organized in two different kinds of clusters, avoiding the occurence of cross-talk by separate cellular localization [110], and the proteins involved in *C. crescentus* cell cycle regulation PleC and DivJK guarantee position dependent specificity [111, 112].

1.3.2 Cross-regulation and cross-talk

Some two-component systems undergo cross-regulation, which is executed through auxiliary proteins, linking the activities of two different pathways [113]. In this scheme, one TCS regulates expression of an auxiliary protein, which subsequently controls the activity of a second system on the kinase or regulator level (Figure 1.5d). Examples are the interactions of the Mg^{2+} sensing PhoQP paralogues with EvgAS in *E. coli* [114] or PmrBA from *Salmonella enterica* [115, 116]. Also *B. subtilis* uses auxiliary proteins for regulation. The competence response regulator ComA thereby activates synthesis of the phosphatase RapA, which results in down-regulation of the RR Spo0F. Thus, cells do not enter sporulation [117].Taken a step further, direct interactions between different pathways on different levels would allow even more sophisticated regulation inside microorganisms (Figure 1.6). There are different levels, where these interactions can take place: On the level of sensor kinases, either via heterodimerization or formation of higher-order signaling complexes (Figure 1.6a), cross-phosphorylation of a response regulator by a non-cognate kinase (Figure 1.6b), interactions between regulators, for instance via heterodimerization (Figure 1.6c) or on the promotor level through regulation by a non-cognate pathway (Figure 1.6d). The phenomenon of beneficial cross-interactions between different signaling systems is called cross-talk, and was first suggested by Hellingwerf and colleagues around fifteen years ago [118, 119]. They proposed that the redundancy in the design of different two-component systems and their modularity might lead to cross-talk between different pathways.

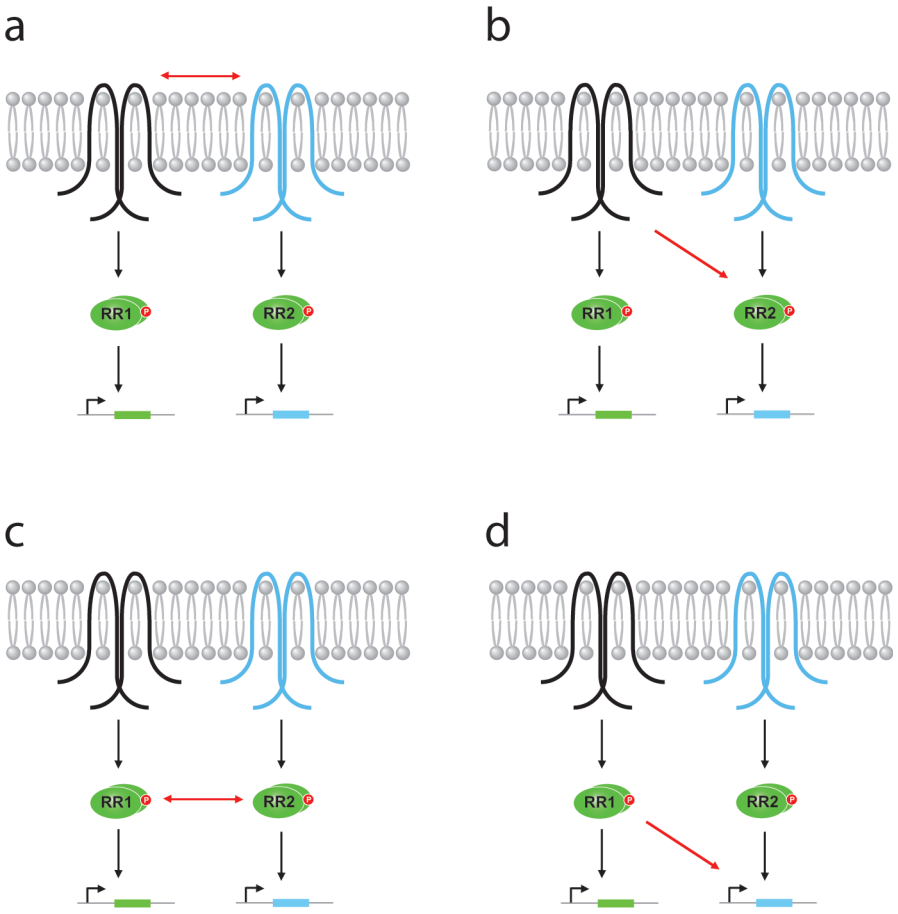

Figure 1.6: **Cross-talk on different pathway levels.**(**a**) Cross-talk between histidine kinases via complex formation or sensor heterodimerization. (**b**) Cross-phosphorylation of a non-cognate response regulator. (**RR**). (**c**) Cross-interactions between two individual response regulators via formation of heterodimers. (**d**) Cross-regulation of gene-expression via response regulator binding to a non-cognate promotor. Black arrows represent signal transmission within individual pathways, red arrows represent possible cross-talk.

Furthermore, they argued that bacteria have to respond to the variety of signals they receive from their environment [120] with an informed decision, forming a sort of ´neural network´. This could enable bacteria to develop a kind of ´learned behaviour´ [121] by using some sort of memory [122], as it is already described for bacterial chemotaxis pathways [123]. Neural networks are defined by four properties: (i) multiple systems have to operate in parallel, (ii) key network components have to perform logical operations, (iii) basic

elements are subject to auto-amplification and (iv) cross-talk can occur. Two-component systems exhibit most of the aforementioned properties. First, different TCS are simultaneously expressed in a single cell and work in parallel [124], the organization in signaling cascades is rather rare [125]. Second, response regulators have two different states (phosphorylated and unphosphorylated) during signal transduction, linking them to a binary (´digital´) operator with an ´on´- and ´off´- state [126]. Additionally, orphan proteins integrate and distribute signals from different information sources within the cell, working as ´hubs´ to perform logical operations between pathways [127]. Third, auto-amplification is a property which is exhibited in some TCS [121].

This leaves the fourth criteria of ´neural network´ , cross-talk. Generally, TCS are wired to trigger a specific response upon signal reception [128, 60, 15]. Nevertheless, in a variety of studies performed during the last years cross-talk was observed between different pathways. Ninfa and colleagues showed *in vitro* cross-talk between non-cognate partners, even though it was 2 to 4 orders of magnitude slower than the cognate phosphorylation reaction [80]. Different *in vivo* experiments exhibited occurence of cross-talk between different unrelated systems [80, 129, 130, 131, 132, 84], but it seems that it mostly occured after the introduction of genetic perturbations [94]. For example the nitrate/nitrite regulation from *E. coli* exhibits multiple layers of fine-tuned cross-talk for regulation [133]. Under anaerobic conditions, nitrate or nitrite is used as electron-acceptor instead of oxygen. Nitrate is sensed by the NarXL TCS, nitrite by the NarQP system. Besides to the linear signaling cascade, NarQ is able to phosphorylate the non cognate regulator NarL in presence of nitrite (Figure 1.6b), allowing a differential regulation dependent on the available nitrogen compounds. Additionally, NarL competes with NarP for an overlapping DNA binding site [134], adding a further layer of cross-talk to the circuit. For *B. subtilis*, Howell and colleagues were able to show cross-talk between the phosphate responsive sensor PhoR and the non-cognate regulator YycF [107, 135]. Systematic *in vitro* studies searching for cross-phosphorylation between sensor kinases and non-cognate response regulators were already performed for all TCS from *E. coli* [136]. Between all tested interactions, Yamamoto and colleagues were able to show $\sim$3 % of trans-phosphorylation between a kinase and a non-cognate response regulator.

Another example of physiologically relevant cross-talk was described in the pathogen *Pseudomonas aeruginosa* for the kinases RetS and GacS, modulating each others activity [137]. The two sensors thereby form a heterodimeric complex blocking the GacSA pathway which subsequently leads to acute virulence of *P. aeruginosa* (Figure 1.6a).

Another place where cross-talk could occur besides protein interactions is at the transcriptional level. This would allow the integration of signals sensed by different pathways

via the expression of a certain set of genes (Figure 1.6d). For example, in *S. enterica* the two response regulators PmrA and RcsB act on genes involved in regulation of the outer-membrane lipopolysaccharide (LPS) composition [138, 139]. Another case has been found in *E. coli*, where the two RR OmpR and CpxR directly regulate the same genes [140, 141].

Because the knowledge of signaling partners is important for understanding of the overall signaling netwerk architecture [142], several attempts have been made to predict candidates of cross-talking partners within the group of two-component proteins by using sequence data. The underlying principle is to identify amino acid residues within interaction domains of potential interacting protein pairs (in this case kinases and regulators). Li and colleagues searched for residues which are variable between paralogue proteins, but conserved between orthologues (for both HK and RR). Using that method they were able to identify residues that confer interaction specificity [143]. Based on amino acid alignments, Burger *et al.* rated the interaction possibility using a co-variation analysis algorithm [127]. They were able to reconstruct *in silico* the TCS pathways for all currently sequenced bacteria, proofing the feasibility of their attempt also for prediction of possible interaction partners. They were able to identify two different groups of TCS proteins, cognates and orphans which form rather isolated groups of signaling proteins. Both groups share the same evolutionary origin, but evolved independently on a shorter timescale [144]. Cognates represent the vast majority, and their characteristic is the organization of the two interation partners within one operon. Orphans represent proteins lying isolated from their interaction partner on the genome, and ∼10 % of them are so-called ´hubs´. They work as nodes in the signaling circuit that interact with multiple proteins and integrate and distribute signals. Furthermore, Burger and colleagues found out that occurence of cross-talk between cognates is low, but it increases with the number of pairs present in the organism. A more recent study rated the preference of directly interacting amino acid residues between TCS proteins which can be explained by biochemical interactions [142]. This work is again based on residue co-evolution and includes data from 769 sequenced bacterial genomes. Procaccini and co-workers predicted for 15-25 % of all TCS at least one of the proteins could participate in cross-talk. They tested their prediction using available experimental data sets and were able to confirm 2 out of 3 *in vivo* results from *B. subtilis* [135, 145] and 6 out of 7 from *C. crescentus* [102, 82]. For *E. coli* they identified a lower amount of cross-talk, namely between CitAB and DcuSR and between CusSR and YedVW. These predictions were in agreement with *in vitro* experiments performed earlier [136].

Taken together, these results highlight the potential of a certain degree of *in vivo* cross-talk, even though there is a high intrinsic specificity in the wiring of single signaling pathways. Nevertheless, a comprehensive general description of two-component pathway de-

signs seems to be difficult, as for every principle mentioned above only a few examples are described in detail [75].

1.4 Intracellular localization of signaling proteins

In recent years it became evident that also bacteria are more complex in respect to their cellular organization than the old view of simple ´bags of enzymes´ , and localization of cellular components plays a significant role in different processes [146]. Similar to eukaryotes, which use cellular compartimentalization or form scaffolding structures to bring signaling components together, bacteria make use of higher-order structures [147]. For the components of signaling pathways, distinct localization of proteins could ensure functionality of information processing by promoting enzymatic reactions at specific loci and isolate the components from detrimental interference with other pathways [148].

B. subtilis for example forms a high-order protein complex called the ´stressosome´, which localizes to distinct foci in the cytoplasm [149]. This complex integrates a variety of sensed cues to regulate subsequently ∼150 genes. The soil bacterium *Myxococcus xanthus* regulates its motility with regulator proteins specifically localized to the cell poles and the cell periphery [150, 151, 152]. Thereby the proteins AglZ, FrsZ and RomR control the direction of movement by regulating the action of type-IV-pili and the A-engine responsible for *M. xanthus´* motility [153, 152, 154].

One of the best studied example of spatial organization in prokaryotes is the chemotaxis apparatus of *E. coli*, a non-canonical two-component system. The sensory complexes are formed by MCPs, the kinase CheA and the adaptor protein CheW, and contain up to several thousand proteins per cluster [155, 156, 157]. They localize to distinct polar and lateral clusters at the cytoplasmic membrane [158, 159, 160], and enable the cell to transmit, amplify and integrate the sensed information. Additionally, clustering enhances the specificity and efficiency of signaling [161]. Such polar chemoreceptor clusters have also been described for a variety of other bacteria and archaea [162]. A bit more complex is the design of *R. sphaeroides´* chemotaxis apparatus, which contains two different chemotactic clusters, one at the poles and one at the cytoplasmic membrane at mid-cell [163]. Both systems have a different protein composition allowing a more elaborate processing of extracellular signals.

For canonical histidine kinases so far there are only a few studies describing their localization inside cells. Extensive studies have been performed on the kinases involved in the cell cycle regulation of *C. crescentus*, which provide a regulation cascade establishing the cellular asymmetry for differentiation into morphological different cell types [164, 111, 112].

Before cell division, the kinase DivJ and the kinase/phosphatase PleC are distributed to different cell poles, allowing different action on the response regulator DivK dependent on the spatial localization [165]. Additionally, the global regulator CtrA (located at the stalked pole) the ClpXP protease complex and the cyclic-di-GMP sensor PopA play a role in the cells differentiation process [166]. The information about the poles identity comes thereby from interactions with the pole-specific protein TipN and with MreB, the bacterial actin-homologue [167]. Polar kinase localization has also been observerd for cells which do not show morphological differentiation, for example for the two *E. coli* sensor kinases CitA and DcuS [168, 169]. They show distinct localization forming polar spots similar to those found for MCPs from chemotaxis [160]. Thereby, DcuS localization is independent from presence or absence of MCPs, indicating no direct connection of the two systems. DcuS spot formation is independent of the protein expression level, but seems to increase with the concentration of Fumarate, the stimulus of the sensor. The reason for this clustered localization remains unclear. As both CitA and DcuS are involved in metabolic processes for sensing of C_4-dicarboxylates [170, 171], a positive influence from clustering on the signal processing performance is not obvious for these systems. In *P. aeruginosa* polar localization of the histidine kinase PilS has been shown, which is involved in sensing required for type IV pilus synthesis [172]. A similar localization has been described for proteins involved in the c-di-GMP signaling cascade in *E. coli*, where localization provides a higher degree of specificity in infomation processing [8]. What the mechanism of the polar protein localization in bacteria is exactly remains elusive to date, but it seems that the different lipid composition at the cell poles and/or the changed membrane curvature play an important role[173, 174, 175].For response regulators of two-component systems very little specific localization has been found thus far. Sourjik and colleagues showed that the regulator CheY from *E. coli* chemotaxis co-localizes with the chemotaxis clusters [159]. It has been shown for EnvZ/OmpR, that for a sufficient high level of kinase expression the response regulator forms a complex with the sensor at the cell periphery [92, 176], and similar localization has been shown for the regulator PhoP [177]. However, the majority of regulators are thought to exhibit a homogenous cytoplasmic distribution pattern [178].

Even though there are some studies performed on the localization pattern of orthodox TCS components, a comprehensive characterization in a bacterial cell remains elusive.

1.5 Fluorescence microscopy

Fluorescence microscopy has become an important tool in modern cell and molecular biology, since it allows investigations of living systems through providing high spatial and temporal resolution [148]. It gives a powerful method to study the localization of cellular components and their dynamics *in vivo* on a single-cell level. Fluorescence microscopy relies on the usage of chromophores. These are molecules that are excitable with light of a certain wavelength, which induces spontaneous emission of light at a longer wavelength [179].

Such chromophores as fluorescent dyes are useful for the labelling of cellular components, but their application to bacterial systems is rather limited. Because of the low permeability of bacterial membranes the dye is not taken up into the cytoplasm. The labelling using immunofluorescence can only be performed on extracellular proteins or using permeabilized cells, making it not usable for intracellular applications. Quantom dots are another method for protein labelling, but their relatively large size exclude their usage from prokaryotes. For bacteria the method of choice to noninvasively label proteins is to fuse them to fluorescent proteins (FP).

1.5.1 Fluorescent proteins

Dependent on the spectral properties (´colour´) or other parameters like brightness or photostability, there is up to date a wide range of either natural occuring FPs like the green fluorescent protein GFP [180, 181], dsRed [182] or their artificially engineered variants [183, 184]. One major advantage is their non-cytotoxicity for prokaryotes, and that they are highly specific for protein labelling *in vivo*. Additionally, fusions to proteins of interest provide a readout for their localization and abundance inside cells as fluorescence intensity is a direct marker for the strength of protein expression [180]. This can furthermore be used to quantify the strength of promotor activities [185]. One main drawback of using FPs is the relatively large size of the formed β-barrel (2.4 by 4 nM), which might lead to steric hindrance within the labelled protein or interactions with other cellular components [184]. Another limitation is that distance of fluorophores lowers FRET efficiency (see below for details), which is to a certain degree the case for the two fluorescent proteins.

In this work different variations of FPs were used. After some initial tests of new YFP, CFP and mRFP variants [186, 187, 188, 189] in our FRET setup (see below and sections 2.12.3, 3.1), protein fusions to histidine kinases and response regulators were constructed using $\text{eyfp}^{\text{A206K}}$ and $\text{ecfp}^{\text{A206K}}$[190]. This variants harbour a point mutation at amino acid

position 206 changing Alanine to Lysine, which prevents dimerization of the fluorophores. This circumvents any artifacts due to their oligomeric state in the FRET measurements or the protein localization studies. The used promotor fusions from the *E. coli* promotor collection [185] contain the engineered gfpmut2 protein, a bright and fast folding green fluorescent protein optimized for flow cytometry applications [191].

1.5.2 Fluorescence Resonance Energy Transfer (FRET)

The underlying principle of FRET (Fluorescence or Förster Resonance Energy Transfer) [192] is a distance-dependent non-radiative energy transfer between two different fluorescent molecules, acting as donor and receptor, respectively (Figure 1.7a).

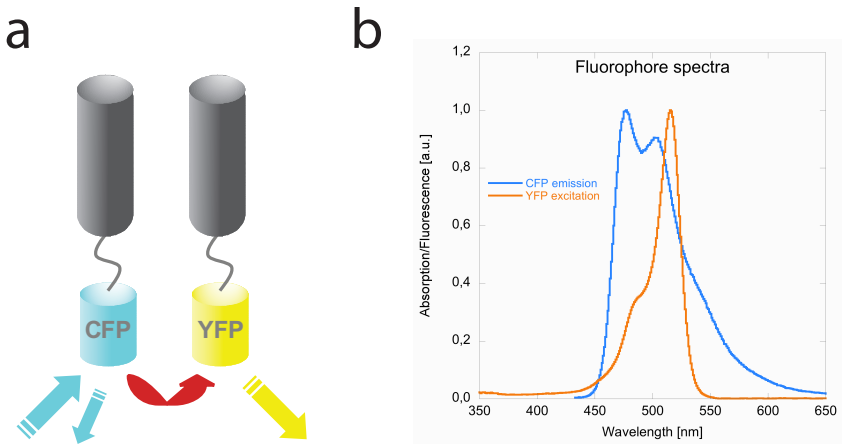

Figure 1.7: **FRET principles.** (**a**) Illustration showing FRET (red arrow) between two proteins labelled with YFP and CFP, respectively. (**b**) Curves showing the overlap between the CFP emission (blue line) and the YFP excitation (orange line) spectra. Data taken from the Tsien lab homepage (http://www.tsienlab.ucsd.edu/).

One requirement therefore is the overlap between the donor emission- and the acceptor excitation-spectrum as shown for YFP and CFP in Figure 1.7b.

FRET methods allow to investigate non-invasive interactions between fluorescently labeled proteins inside living cells [193]. The strength of FRET assays lies in the possibility to quantify (transient) *in vivo* interactions in real time, making it especially suitable to study protein-protein interactions or conformational changes of proteins involved in signal transduction networks [194, 148].

The efficiency of energy transfer between fluorescently labelled proteins organized in complexes depends on the distance between the two labelled molecules, and can be described as

$$E_{FRET} = \frac{R_0^6}{R^6 + R_0^6} \tag{1.1}$$

with R as distance between the centers of the used fluorophores and R_0 beeing the Förster radius [192]. At this distance the energy transfer between donor and acceptor has an efficiency of 50 %. R_0 thereby can be calculated using the overlap between the emission spectra of donor and acceptor, the orientation of the two fluorophores and the properties of the surrounding medium [195]. If the fluorophore is attached to a protein of interest using a flexible peptide linker (allowing its free rotation), the Förster radius R_0 is about 4.9 nm [196, 181]. This leads, taking the steep FRET dependence upon distance into account, to the conclusion that above a distance of about 10 nm no FRET can occur anymore [194]. Given this the occurence of false positive results using an *in vivo* FRET assay for protein-protein interactions are neglectable. Nevertheless, if for structural reasons the donor and acceptor fluorophore are more than 10 nm apart, false negative results might occur. To overcome this limitation it is advisable, if possible, to test combinations of different protein fusions, e.g. N- and C-terminal, in all possible combinations.

1.6 Aims of the current work

As the most important signal transduction pathways in prokaryotes and lower eukaryotes, two component signaling systems have been extensively investigated during the last thirty years. Members have been identified in nearly all bacterial and archaeal genomes, and a lot is known about the molecular details involved in signal transmission. Despite these progresses in the understanding of two-component systems, quite a few open questions still remain to be solved. For instance, to date little is known about the interconnection between different pathways inside a living bacterial cell. Additionally, a systematic study of spatial organization of the involved proteins is lacking.

To address these questions, we studied systematically *in vivo* the intracellular organization of proteins involved in two-component signaling pathways in *Escherichia coli*. Additionally, we were interested in possible interconnections between individual signal transduction cascades on different levels. Therefore we constructed a comprehensive library of histidine kinases and response regulators with fluorescent protein fusions. Furthermore, fluorescent transcriptional reporters of promotors regulated by two-component

systems have been used or constructed to investigate effects on gene expression. Testing the fluorescent fusions with such fluorescence techniques as imaging, flow cytometry, acceptor photobleaching and stimulus dependent FRET provided us with insights into the spatial organization and complex formations of the sensors. Furthermore, possible physical changes in response to various stimuli have been studied, and the effects of stimuli on the resulting transcriptional response were characterized. The obtained results provided new insights into spatial organization within and communication between different two-component systems in terms of information exchange or integration at different molecular levels. The 30 two-component systems present in *E. coli* represent most of the existing sensory kinase families. Hence, the results of this study broaden the understanding of cell signaling performed in other bacteria and even in lower eukaryotes outside the animal kingdom.

2 Materials and methods

2.1 Chemicals and consumables

All chemicals and consumables used in this work are listed in Table 6.6 in the Appendix.

2.1.1 Media and plates

Luria broth (LB) plates

10 g	Tryptone
5 g	Yeast extract
5 g	NaCl
15 g	Agar

Added ddH_2O up to a total volume of 1 L and adjusted to pH 7 using NaOH. Where appropriate, antibiotics were added to the following final concentrations: ampicillin 100 mg/mL, kanamycin 50 mg/mL and chloramphenicol 34 mg/mL.

LB media

10 g	Bacto tryptone
5 g	Bacto yeast extract
5 g	NaCl

Added ddH_2O up to a total volume of 1 L and adjusted to pH 7 using NaOH.

Tryptone broth (TB) media

10 g	Bacto tryptone
5 g	NaCl

Added ddH_2O up to a total volume of 1 L and adjusted to pH 7 using NaOH.

5x Minimal A stock solution

10 g	$(NH_4)_2SO_4$
45 g	KH_2PO_4
105 g	K_2HPO_4
5 g	Na-Citrate · H_2O

Added ddH_2O up to a total volume of 2 L and autoclaved.

Minimal A media

100 mL	5x Minimal A stock solution
0.5 mL	1 M $MgSO_4$
5 mL	20 % carbon source (glucose or glycerol)
25 mL	2 % Casaminoacids

Added ddH_2O up to a total volume of 500 mL.

2.1.2 Buffers and solutions

TAE buffer for DNA gel electrophoresis

242 g	Tris base
57.1 g	Glacial acetic acid
100 mL	0.5 M EDTA (pH 8)

Added ddH_2O up to a total volume of 1 L.

Tethering buffer

100 mL	0.1 M KPO_4
200 µL	0.5 M EDTA
13.4 mL	5 M NaCl
100 µL	10 M Methionine
100 µL	10 M Lactic acid

Added ddH_2O up to a total volume of 1 L and adjusted to pH 7 using NaOH.

Phosphate buffer

100 mL	0.1 M KPO_4
13.4 mL	5 M NaCl
100 µL	10 M Lactic acid

Added ddH_2O up to a total volume of 1 L and adjusted to pH 7 using NaOH.

6x DNA gel loading buffer

30 % (v/v)	Glycerol
0.25 % (w/v)	Bromophenol blue
0.25 % (w/v)	Xylene cyanol

4x SDS Laemmli buffer

8 %	SDS
40 %	Glycerol
20 %	β-mercaptoethanol
0.008 %	Bromphenol blue
0.34 M	Tris

Adjust pH to 6.8.

10x SDS gel running buffer

144.2 g	Glycine
30.3 g	Tris base
10 g	SDS

Added ddH_2O up to a total volume of 1 L.

12 % SDS resolving gel

1.7 mL	ddH_2O
2 mL	30 % Acrylamide mix
1.3 mL	1.5 M Tris (pH 8.8)
50 µL	10 % SDS
50 µL	10 % APS
2 µL	TEMED

5 % SDS stacking gel

0.68 mL	ddH_2O
0.17 mL	30 % Acrylamide mix
0.13 mL	1.5 M Tris (pH 6.8)
10 µL	10 % SDS
10 µL	10 % APS
1 µL	TEMED

Western blot transfer buffer

2.9 g	Glycine
5.8 g	Tris base
3.8 g	SDS
200 mL	Methanol

Added ddH_2O up to a total volume of 1 L.

10x TBS buffer

88 g	NaCl
12.1 g	Tris base

Added ddH_2O up to a total volume of 1 L and adjusted pH to 7.4.

1 kb plus DNA ladder

20 µL	DNA ladder stock (Invitrogen)
40 µL	10x DNA gel loading buffer
180 µL	ddH_2O

Antibiotics

Ampicillin	100 mg/mL in ddH_2O
Chloramphenicol	34 mg/mL in 70 % Ethanol
Kanamycin	50 mg/mL in ddH_2O

Inducers

L-arabinose	10 % in ddH_2O
Isopropyl-β-D-thiogalactopyranosid (IPTG)	0.1 M in ddH_2O

TSS solution

5 g	Polyethyleneglycol (PEG) 8000
0.3 g	$MgCl_2 \cdot H_2O$
2.5 mL	DMSO

Added LB medium up to a total volume of 50 mL and filter sterilized.

2.1.3 Reaction kits

- NucleoSpin Plasmid Kit, Macherey-Nagel, Düren
- QIAprep Spin Miniprep Kit 250, Qiagen, Hilden
- QIAquick Gel Extraction Kit, Qiagen, Hilden

Kits were used according to the manufacturer´s protocol.

2.1.4 Antibodies

For analysis of protein degradation using immunoblotting GFP-specific monoclonal mouse antibody JL-8 (BD Biosciences, Heidelberg) and fluorescently labelled anti-mouse IgG goat antibody IRDye™700DX (Rockland) were used as primary and secondary antibody, respectively.

2.2 Bacterial strains

Table 6.5 in Appendix shows a list of all bacterial strains used in this study. All strains are derivatives of the *Escherichia coli* K-12 strains MG 1655 [11] or BW25113 [197] in case of the Keio collection, where strains containing knockouts of either the kinase or response regulator were obtained from [198]. All knockout strains were tested using PCR for correct insertion of the kanamycin cassette using gene-specific primers (see Table 6.3). Where needed, the integrated kan-cassette was removed using the plasmid pCP20 [199]. This plasmid shows temperature-sensitive replication and thermal induction of FLP synthesis.

Cells were co-transformed with pCP20 and grown over night at 30 °C on a LB plate with ampicillin to induce FLP synthesis, leading to a flipout of the kan-cassette. To remove the plasmid, cells were incubated on LB plates at least two times over night at 42 °C. Selection for positive clones (e.g. loss of kanamycin resistance) finally was performed using different LB plates containing different antibiotics at 37 °C over night.

2.3 Plasmids

Table 6.1 in Appendix shows a list of all plasmids used in this study.

pES plasmids harbouring fluorescent protein fusions were constructed during this study using standard molecular cloning techniques described as below (for details see section 3.2). PCR products were cloned into either pDK112 (YFP fusions) or pDK113 (CFP fusions) vectors creating an C-terminal tagged fusion protein. For both plasmids a CCATGGAATTCGAGCTCGGATCCGGAGGTGGA sequence is placed in front of the gene coding for monomeric eyfp^{A206K} (pDK112) or ecfp^{A206K} (pDK113) [190], which allows cloning using the restriction sites *Nco*I and *Bam*HI and encodes for a GSGGG linker in front of the fluorophore. CFP fusions were subsequently transferred into the pBAD33 expression plasmid [200] using restriction sites *Spe*I (compatible to *Xba*I) and *Hind*III. For the fluorescent protein test, additionally CheY-FP fusions were constructed using fusion PCR as described in Sourjik and Berg 2000 [159]. YPet/CyPet [189], Venus/Cerulean [186, 187] and mCherry [188] were used as fluorophores fused to CheY.

pVS, pAM, pDK and pAE plasmids were a personal gift from Victor Sourjik, Anette Müller, David Kentner and Andreas Ernst, respectively (lab stocks). Plasmids pCP20 and pACBSR were taken from the lab stock. Promotor GFP fusions were obtained from the *E. coli* Promotor Collection [185]. The modified pKD13 plasmid for chromosomal YFP-fusions was a personal gift from Juliane Winkler and Axel Mogk.

2.4 Primers

Table 6.3 in Appendix shows a list of all primers used during this study. All primers were synthesized at MWG Biotech (Martinsried, Germany). VIC and DK primers were a personal gift from Victor Sourjik and David Kentner, respectively (lab stocks).

2.5 Molecular cloning

2.5.1 Polymerase Chain Reaction (PCR)

5 µL	Genomic template DNA*
8 µL	10x PCR buffer
0.3 µL	dNTP Stock (1.25 mM)
0.3 µL	sense primer
0.3 µL	reverse primer
36.1 µL	polymerase
add to 50 µL	ddH_2O

* For amplification of wildtype genes cells of a single colony (from a freshly streaked LB-plate) were used as template DNA.

PCR cycle:

5 min	95 °C	
30 sec	95 °C	25 cycles
45 sec	55 °C (variable, depending on melting temperature of used primers)	
1 min	72 °C (variable, depending on length of fragment and used polymerase)	
10 min	72 °C	

PCR reactions were performed using T gradient and T professional thermocycler (Biometra). Resulting fragments were separated and analyzed by electrophoresis using a 1 % agarose gel consisting of 0.5 g agarose in 50 mL TAE buffer and 0.5 µL Ethidium bromide. Gel extraction and PCR purification was carried out using the QIAquick Kit (listed in 2.1.2).

2.5.2 Restriction digest

Enzymes used for restriction digests were *Afl*II, *Afl*III, *Bam*HI, *Bgl*II, *Bsp*HI, *Eco*RI, *Eco*RV, *Hind*III, *Hpa*I, *Kpn*I, *Nco*I, *Nde*I, *Nhe*I, *Spe*I, *Xba*I and *Xho*I from Fermentas or New England Biolabs.

Preparative restriction digest was performed using

10 µL	Template DNA
3 µL	10x Restriction buffer
1 µL	of each restriction enzyme (if same activity in double digestion)
15 µL	ddH_2O

Mixture was incubated for 2-3 h at 37 °C.

Analytical restriction digest was performed using

5 µL	Template DNA
2 µL	10x Restriction buffer
0.5 µL	of each restriction enzyme (if same activity in double digestion)
12 µL	ddH_2O

Mixture was incubated for 1-2 h at 37 °C.

2.5.3 Ligation

Ligation of DNA fragments was performed using enzymes from Fermentas or New England Biolabs using the following protocol:

3-5 µL	Insert DNA
1 µL	Vector DNA
2 µL	5x ligation buffer
1 µL	T4 DNA ligase
1-3 µL	ddH_2O

Mixture was incubated either over night at 16 °C or for 10 min at RT followed by 16 h at 4 °C.

2.5.4 Competent cells

For producing competent cells, three different procedures were used during this work: the "classical" chemical approach, a slight variation of this method for electrocompetent cells and the one-step method (see section 2.5.5) developed by Chung and co-workers [201].

For the chemical method, 1 mL cells of an LB overnight culture were diluted into 100 mL fresh LB media and grown at 37 °C to an OD_{600} = 0.7. After harvesting the cells for 5 min at 4000 rpm, the pellet was resuspended in 25 mL chilled 0.1 M $MgCl_2$ and incubated on ice for 30 min. In the next step the cells were centrifugated 5 min at 4000 rpm and the pellet was resuspended in 50 mL ice-cold 0.1 M $CaCl_2$, centrifugation was performed again. Next cells were resuspended in 3 mL 0.1 M $CaCl_2$+18 % glycerol and incubated at 4 °C for two hours. Finally competent cells were aliquoted and frozen at -80 °C.

To produce competent *E. coli* cells for electroporation, first cells were transformed with the plasmid pKD46, harbouring the λ-red genes necessary for homologues recombination [197] and selected on solid LB+Amp plates over night. From a single colony, 5 mL LB+Amp overnight culture were inoculated and grown at 30 °C. 500 mL LB+Amp were inoculated using 5 mL overnight culture and shaken at 30 °C to an OD_{600} = 0.7. Cells were incubated on ice for 30 minutes. After harvesting the cells for 20 min at 4 °C and 2500 rpm, the pellet was resuspended in 500 mL 10 % glycerol. This step was repeated twice using 250 mL and 100 ml of 10 % glycerol for resuspending the cells, respectively. Finally, the pellet was resuspended in 3 mL 10 % glycerol and aliquoted to samples of 100 µL. Aliquots were immediately shock-frozen in liquid nitrogen and stored at -80 °C until their usage for electroporation.

2.5.5 One-step preparation of competent cells

Chung *et al.* [201] invented a method to make bacterial cells competent without the need of multiple washing and resuspending steps as performed in the "classical" approach. They developed a special transformation and storage solution (TSS), which allows to combine the chemical treatment of the cells for competence and transformation. Given this, the method is much faster to apply and especially feasible if only a small amount of competent cells is needed. In this work, the method was mainly applied to transform DNA into strains from the Keio collection [198].

1 mL cells of a LB overnight culture were diluted in 10 mL fresh LB medium an grown at 37 °C to an OD_{600} = 0.3-0.4. 1 mL of the culture was transferred into a chilled reaction tube and harvested using a table top centrifuge at 8000 rpm for 1 minute. The supernatant was removed and the pellet was resuspended in 100 µL ice-cold TSS using the pipet-tip. 1-2 µL plasmid DNA was added and gently mixed using the pipet-tip. Cells were stored on ice for 30-60 minutes. Then 900 µL LB were added and the suspension was incubated at 37 °C and 600 rpm for 1 hour. Finally, cells were harvested at 8000 rpm for 1 min,

the supernatant was reduced to 100 µL, the pellet resuspended and the volume plated on LB agar plates (with antibiotics where appropriate). Plates were incubated over night at 37 °C.

2.5.6 Transformation of chemical competent cells

For transformation, 1-2 µL of plasmid DNA and 50 µL of thawed competent cells were briefly mixed using the pipet-tip and incubated at 4 °C for 30 min. After applying a heat shock at 42 °C for 45 sec, cells were stored on ice again for another 10 min. Subsequently 1 mL LB medium was added and cells were shaken at 650 rpm and 37 °C for 45-60 min. After a centrifugation step at 8000 rpm for 1 minute, the supernatant was reduced to 100 µL, the pellet was resuspended and plated on LB agar plates (with antibiotics where appropriate). Plates were incubated over night at 37 °C.

2.5.7 Transformation using electroporation

Before performing transformation, electroporation cuvettes were stored on ice and LB media was heated to 37 °C. 100 µL of in ice thawed electrocompetent cells was mixed with 100-200 ng of linearized DNA and gently mixed using the pipet tip. The mixture was transferred into the cuvettes and they were dryed before loading into the electroporator. The electric shock was applied with a current of 2.5 kV for 5.2 ms and immediately afterwards 1 mL of pre-warmed LB was added to the cells. The solution was incubated at 37 °C and 350 rpm for 1 hour and plated on LB+kan plates for selection purposes. Plates were incubated at 37 °C over night.

2.6 Cloning by homologues recombination

To determine the native protein copy number of histidine kinases, chromosomal insertions of a gene sequence encoding YFP were constructed. These insertions were designed as shown in Figure 2.1, leading to a sensor-YFP fusion which is under control of the native promotor. The used method is a variation of the standard protocol for homologues recombination in *E. coli* [197], so called “gene gorging” [202]. A schematic representation is shown in Figure 2.1. The first step is to modify the plasmid pKD13 by introducing gene regions homologues to sites flanking the desired insertion locus on the chromosome.

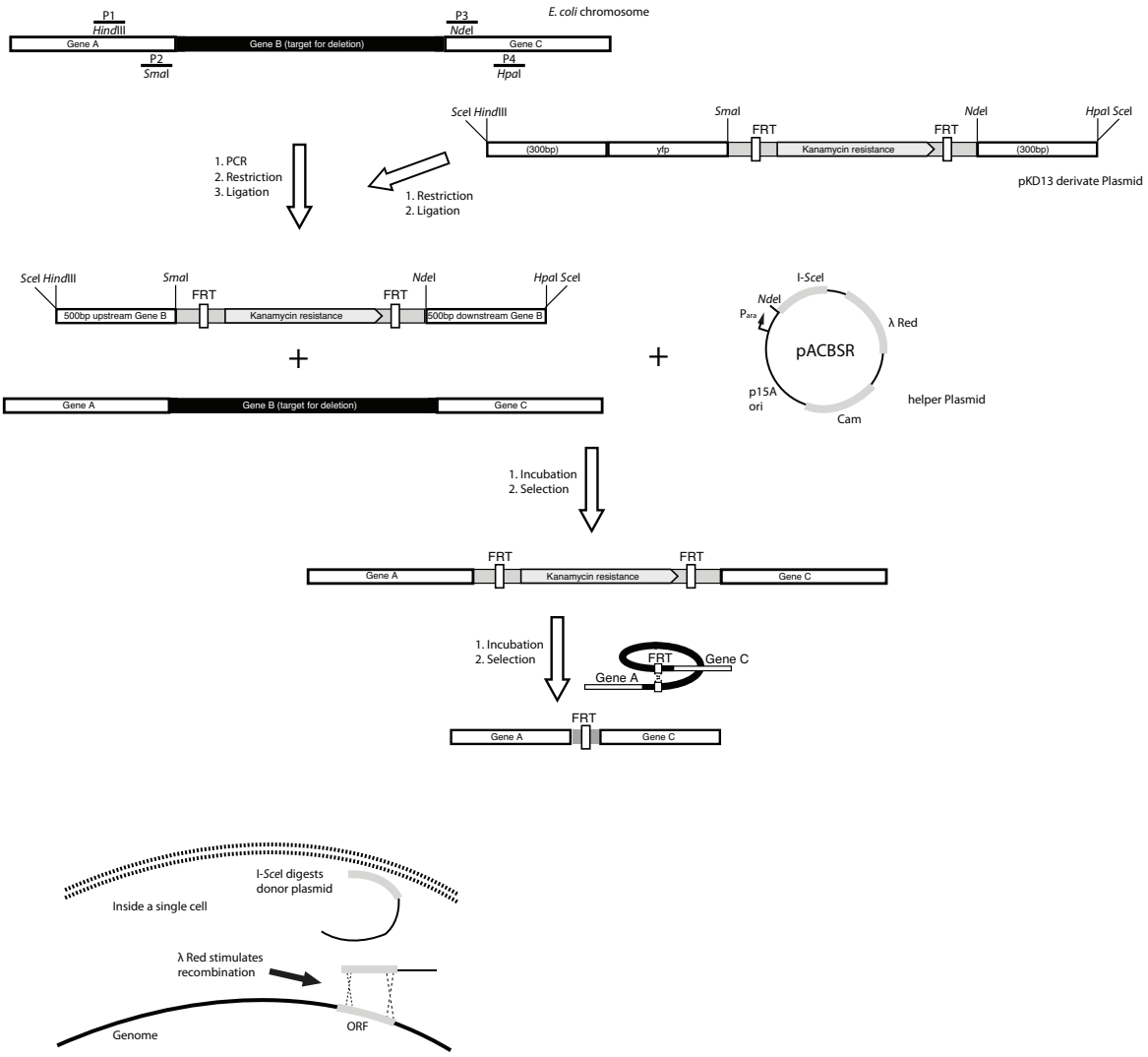

Figure 2.1: **Scheme "gene gorging" method.** Detailed methodology is described in the main text. **P1-P4**: Primer for homology amplification. **FRT**: Flp recombination target sites. (modified after [202, 198])

These 300-500 basepairs long regions were amplified using PCR and inserted into the plasmid using restriction endonucleases. The resulting plasmid was co-transformed with the pACBSR helper plasmid into wt cells using the TSS protocol and grown over night using LB+CAM+Kan plates. Transformants were incubated 1 mL of LB+CAM+Kan with 10 µL of arabinose (20 % stock solution) for 9 h at 37 °C. During this step the I-*Sce*I endonuclease and the λ-Red enzymes are expressed from the helper plasmid and performed *in vivo* linearization and final chromosomal insertion of the gene of interest. Positives

were selected on LB plates with different antibiotics and screened for $kan^+/cam^-/kan^-$-clones, which only harbour the chromosomal kan cassette. After co-transformation of the resulting strains with the pCP20 plasmid (TSS protocol) and incubation on LB plates at 30 °C (removal of the kan-cassette), clones were purified from the pCP20 plasmid by three rounds of selection on LB plates without antibiotics at 42 °C. The gene gorging method did not worked in our hands as described, the *in vivo* insertion failed several times. Alternatively, we co-transformed the digested homology plasmid DNA into cells carrying the pKD46 helper plasmid using electroporation. pKD46 carries the λ-Red genes homologues recombination under control of an arabinose inducible promotor.

2.7 Frozen cell stocks

For long-term storage, cells were inoculated in 5 mL TB medium (plus antibiotics were appropriate) and grown at 37 °C on a rotary shaker for 16 h. Cells were harvested at 4000 rpm for 7 minutes and resuspended in 1 mL TB+18 % glycerol. The stocks were briefly stored on ice and frozen at -80 °C.

2.8 Protein degradation analysis

To test the stability of the constructed protein-YFP fusions and identify possible degradation they were tested using SDS-PAGE and immunoblotting [203, 204]. The used SDS gel concentrations were 5 % and 12 % for the stacking and resolving gel, respectively.

Protein samples were expressed under the same conditions as used for FRET microscopy, and 1 mL culture was harvested and immediately shock-frozen in liquid nitrogen. The cell pellet was resuspended in 85 µL 3x Laemmli buffer and 165 µL H_2O, boiled at 95 °C for 5 minutes, briefly vortexed and boiled for another 5 minutes. The solution was centrifuged 1 minute at 8000 rpm and subsequently 10-15 µL of sample were loaded onto the SDS gel for separation. 3 µL of protein marker (Pageruler prestained protein ladder, Fermentas) was used. Electrophoresis was performed at 150 V (Biorad equipment), and subsequently samples were transferred onto a Hybond-ECL nitrocellulose membrane with 0.22 µM pore size (Amersham Biosciences) using a Biometra semi-dry blotting device. Electrophoresis and immunoblotting was performed according to the manufacturer´s instructions. Membranes were blocked and hybridized as described before [159]. Used antibodies were a GFP-specific primary monoclonal mouse antibody (JL-8, BD Biosciences;

dilution 1:5000) and a fluorescently labelled secondary anti-mouse IgG goat antibody (IRDye™700DX, Rockland; dilution 1:10000). Immunoblot signals were detected using an infrared LI-COR scanner (Odyssey). The amount of protein degradation was quantified using the gel analysis function of the public domain software ImageJ 1.40g (Wayne Rasband, http://rsb.info.nih.gov/ij/).

2.9 Bacterial growth conditions

Cells were grown in either Tryptone broth (TB), Luria broth (LB) or minimal A medium [205]. Minimal A medium was supplemented with 0.1 % (w/v) casamino acids, 1 mM $MgSO_4$ and 0.2 % (w/v) glucose or glycerol as carbon source, respectively.

For FRET and FACS experiments cells were grown in TB in a rotary shaker at 34 °C and 275 rpm as described before [159]. Antibiotics ampicillin, kanamycin and chloramphenicol were added to final concentrations of 100 mg/ml, 35 mg/ml and 50 mg/ml, respectively. All overnight cultures were diluted 1:100 and grown until OD_{600} of 0.4–0.5, when appropriate in the presence of antibiotics and isopropyl b-D-thiogalactoside (IPTG) or arabinose as inducer. Cells were harvested using centrifugation at 4000 rpm for 5 min, washed and resuspended in half of the volume phosphate buffer.

Cells for imaging experiments were grown in either LB, TB or minimal A medium and harvested and washed as described before (without final concentration step).

Cultures for promotor activation experiments were grown in minimal A medium as described before, and the stimulus was added to the shaking liquid culture 30-45 minutes before harvesting.

Before all measurements, samples were stored at 6 °C for about 30 minutes to stop further cell growth and protein expression.

2.10 Quantification of protein levels

To determine the mean expression levels of our protein-YFP reporter fusions, we performed flow cytometry experiments as described earlier [206, 207]. Measurements were performed on a FACScan (BD Biosciences) equipped with a 488-nm argon laser. FACScan data were analysed using the CellQuest™ Pro 4.0.1 software (BD Biosciences). In general, between 10000 and 100000 cells were measured per sample and at least one replication in a biological independent experiment was performed. Expression of the constructed CFP fusions was estimated using fluorescence imaging as it was described earlier [207]. Therefore, the

acquired pictures were quantified by measuring the grey values using the public domain software ImageJ version 1.40g (Wayne Rasband, http://rsb.info.nih.gov/ij/). The derived intensities from flow cytometry and imaging were recalculated into absolute protein numbers using a calibration with purified YFP and CFP proteins as it was described previously [207]. In all subsequent experiments, expression levels of protein fusions were adjusted to a few thousand copies per cell if possible.

2.11 Promotor reporter assay

For most of the investigated TCS no phenotypic readout is available. To verify functionality, we performed an assay using promotor activities as indicator for the presence of upstream signaling events. First, we identified one or few promotors for every TCS, which are reported to be a downstream targets of the signaling cascade. For all chosen reporters either transcriptional GFP fusions from the plasmid based GFP-promotor collection [185] were taken, or we constructed them in a similar fashion using molecular cloning. Wildtype and certain knockout cells were transformed with the promotor reporters and measured using flow cytometry (for details see section 2.10).

2.12 Fluorescence microscopy

2.12.1 Imaging

For imaging, bacteria were applied to a thin agarose pad (1 % agarose in tethering buffer) placed on a glass slide. Fluorescence imaging was performed on a Zeiss AxioImager microscope equipped with a Zeiss α Plan Fluor 100× 1.45 oil immersion objective, HE YFP (Excitation BP 500/25; Emission BP 535/30) and HE CFP (Excitation BP 436/25; Emission BP 480/40) filter sets and a EXFO 120 illumination system (Xcite). Pictures were acquired using an ORCA AG CCD camera (Hamamatsu). Each experiment was performed in duplicate on biological independent replicates.

2.12.2 Acceptor photobleaching FRET

Figure 2.2 shows the used microscopy setup for *in vivo* FRET applications. Acceptor photobleaching FRET measurements (Figure 2.2a) were performed using a custom-modified Zeiss Axiovert 200 microscope as described previously [207]. 1 mL of cells expressing fluorescent protein fusions were concentrated about twentyfold using centrifugation and applied to a thin agarose pad (1 % agarose in tethering buffer) placed on a glass slide.

Excitation light from a 75 XBO lamp was attenuated by a neutral-density filter (ND), passed through a 436/20 band-pass (BP) filter, a 495DCSP dichroic mirror and was reflected onto the sample by a Z440/532 dual-band beamsplitter (transmission 465-500 and 550-640 nm; reflexion 425-445 and 532 nm). YFP bleaching was performed using a 20 sec pulse from a 532 nm diode laser (Rapp OptoElectronic), which was reflected onto the sample by the dichroic mirror. The bleached area was narrowed using a diaphragm. CFP emission passed through a BP 485/40 filter and was measured using a H7421-40 photomultiplier (Hamamatsu). For each measured time point, photons per second were counted over 0.5 s using a PCI-6034E board (National Instruments). The photomultiplier was controlled using a custom-written routine for LabView 7.1 (National Instruments). CFP emission was recorded before and after YFP bleaching, and FRET was calculated using Equation 2.4.

2.12.3 Stimulus dependent FRET

The used microscopy setup is shown in Figure 2.2b. Stimulus-dependent FRET measurements were performed on a custom-modified Zeiss Axiovert 200 microscope as described previously [207]. 1 mL of cells expressing fluorescent protein fusions were concentrated about twentyfold using centrifugation and attached to a coverslip coated with poly-L-lysine. After 15 min of attachment, the coverslip was placed into a custom made flow chamber (ZMBH inhouse facility) connected to a syringe pump (Harvard Apparatus), which allowed incubation of cells under a constant flow of phosphate buffer (300 mL/min). Excitation light passed through a BP 436/20 filter and was reflected by a 455 dichroic mirror. Emission from about 500 cells passed through a 455 DC mirror and was split by a 515 dichroic mirror into two signals. The signals passed through a BP 485/40 filter and a BP 535/30 filter for cyan and yellow, respectively. Data aquisition was performed using a H7421-40 photomultiplier (Hamamatsu) for each channel. Photons per second were counted using a PCI-6034E board (National Instruments), the photomultiplier were controlled using a custom-written routine for LabView 7.1 (National Instruments). After establishment of a stable YFP/CFP ratio (base line), the reservoirs with solutions of stimuli or with phosphate buffer were added and removed. and the change in YFP/CFP ratio was monitored for about 100 sec. FRET was calculated from changes of YFP/CFP ratio by Equation 2.6.

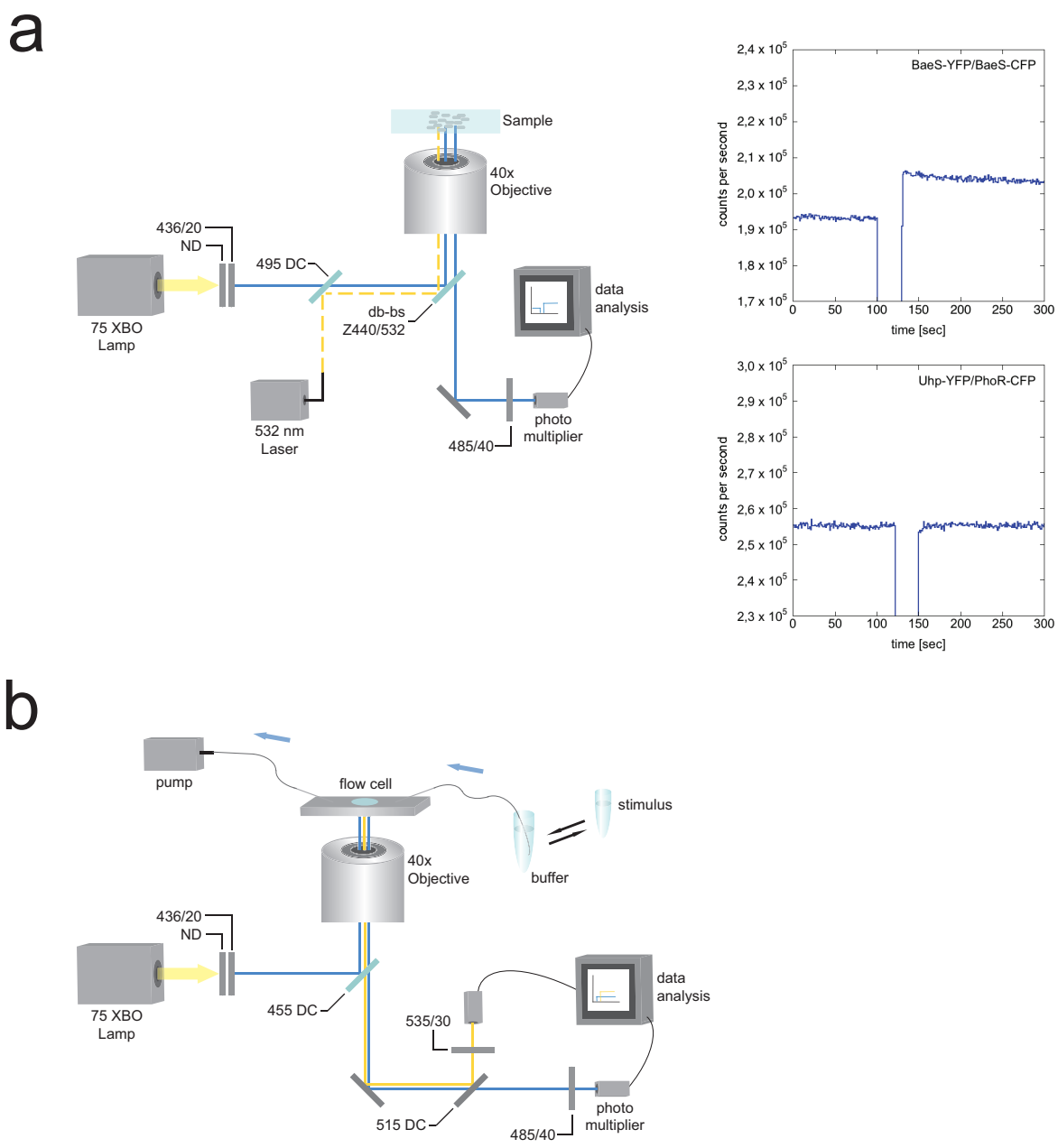

Figure 2.2: **Microscopy setup for *in vivo* FRET applications.** **(a)** Setup for acceptor photobleaching FRET measurements. **Insets**: Resulting curves from a typical experiment representing change in CFP signal for interacting proteins (upper panel) and no change for non-interacting proteins (lower panel). **(b)** Setup for stimulus dependent FRET measurements. Numbers describe used filters with wavelength/bandwith. Details are described in the main text.

2.13 Data analysis

All experiments were performed at least in two biological replicates (independent samples from different days). The resulting values x were calculated to derive an arithmetic mean $\overline{x}$ using

$$\overline{x} = \frac{1}{n}\sum_{i=1}^{n} x_i \tag{2.1}$$

The deviation between different measurements was determined calculating the standard error $s_{\overline{x}}$ using

$$s_{\overline{x}} = \frac{s}{\sqrt{n}} \tag{2.2}$$

with s being the standard deviation defined as

$$s := \sqrt{s^2} \tag{2.3}$$

Analysis of acceptor photobleaching and stimulus dependent FRET experiments is discussed in detail in the article from Sourjik and colleagues [194]. Based on that we define the FRET efficiency E_{FRET} measured in acceptor photobleaching measurements

$$E_{FRET} = \frac{\Delta C}{C_0} \tag{2.4}$$

as the fractional change in CFP fluorescence. ΔC describes the change in fluorescence due to the energy transfer to the acceptor, C_0 the CFP fluorescence without FRET.

To describe stimulus dependent FRET measurements, the steady state ratio between the two fluorophores is given as

$$\Delta R = \frac{YFP}{CFP} \tag{2.5}$$

Dependence on stimulus concentration (dose response curve) is calculated using

$$\Delta R = R_B - R_0 - \Delta R_S \tag{2.6}$$

with R_B and R_A being the fluorescence ratio without and with stimulus, respectively. ΔR_S represents the difference between the ratios.

The resulting values are fitted using a Hill equation

$$FRET([L]) = m_1 \cdot \left(\frac{m_0^{m_2}}{m_0^{m_2} + m_3^{m_2}} \right) \tag{2.7}$$

with m_0 as stimulus concentration, m_1 as FRET amplitude, m_2 being the Hill coefficient and m_3 being $K_{1/2}$, the stimulus concentration at the half maximum response. To fit the measurements in Figure 3.9b, m_1 to m_3 were set 1.

2.14 Software

The following software tools were used during this study:

Axiovision (Version 4.7)	Zeiss, Jena
CodonCode Aligner (Version 3.0.3)	CodonCode Corporation, USA
Cytoscape (Version 2.8.2)	[REF Smoot 2011]
DNA Strider (Version 1.3)	Commisariat a l´Energie Atomique, FRA
EnzymeX (Version 3)	Mekentosj B.V., NED
Excel 2008 for Mac (Version 12.2.3)	Microsoft Corporation, USA
Illustrator (Version CS 3)	Adobe Systems, USA
ImageJ (Version 1.38f)	W. Rasband, National Institute of Health, USA http://rsb.info.nih.gov/ij/index.html
KaleidaGraph (Version 4.03)	Synergy Software, USA
LabView (Version 7.1)	National Instruments, USA
LyX (Version 2.0.1)	GU General public license http://www.lyx.org
Papers (Version 1.9)	Mekentosj B.V., NED

3 Results

3.1 Fluorescent reporter protein test

To characterize protein-protein interactions *in vivo*, we used a FRET based microscopy setup. To investigate proteins using this method, they have to be fused to fluorescent proteins of two different colours, which have an overlap in their emission and excitation spectrum, respectively (see chapter 1.5 for details). So far, the commonly used pair was YFP and CFP [196]. As improved FPs were developed during the last years, we tested some different pairs in the yellow/cyan and red/yellow range for better FRET properties. The used setup is similar to the one described in Sourjik *et al.* from 2002, with donor and acceptor fusions made to the chemotaxis proteins CheY and CheZ, respectively.

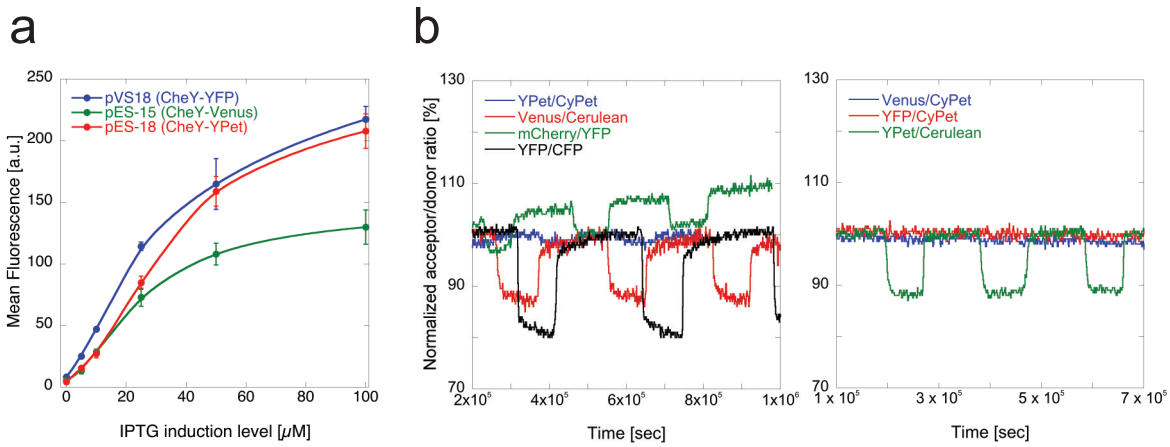

Figure 3.1: **Comparison of fluorescent protein pairs for FRET applications. (a)** FACS measurements showing fluorescence intensity dependent on protein expression for yellow CheY-fluorophore fusions. Error bars represent standard errors. **(b)** Stimulus dependent FRET measurements for different FRET-pair combinations (yellow/cyan and red/yellow) fused to CheY and CheZ, respectively. Upon stimulation of the FRET strain using 300 µM of chemoattractant serine, the FRET ratio decreases due to changes in CheY/CheZ interactions. Experiments were performed using fusions expressed from plasmids in strain LL5 at induction levels of 50 µM IPTG and 0.1 % arabinose.

These two proteins provide a readout of receptor activity and can be stimulated using chemoattractants. After addition of the chemoattractant serine, the number of CheYZ complexes decreases and leads to a decrease in FRET ratio. We tested the two yellow/cyan pairs Venus/Cerulean [186, 187] and YPet/CyPet [189], with the latter one optimized for applications in microbial systems. Additionally, the red and yellow pair YFP/mCherry [188] was investigated, with YFP being the donor molecule. Figure 3.1a shows the brightness-comparison of yellow fluorescent proteins at different expression levels. The YFP fusion exhibits the highest fluorescence over the whole expression range, while CheY-Venus is less strong in fluorescence (about 50 % of the YFP signal) for all tested expression levels. YPet shows a different behaviour with low fluorescence similar to Venus at lower and strong fluorescence nearly equal to YFP at higher expressions levels. Notably, this behaviour seems to be in contradiction to the results reporting Venus to be as bright as YFP and YPet being 60 % brighter than YFP [183].

Figure 3.1b shows the different FRET pairs in the stimulus dependent FRET setup, either as cognate or non-cognate pairs. Results are summarized in Table 3.1.

Table 3.1: **Comparison FRET pairs for FRET-ratio change.**

FRET pair	change in FRET-ratio upon stimulation
YFP/CFP	20 %
Venus/Cerulean	12 %
YPet/Cerulean	12 %
mCherry/YFP	5 %
YPet/CyPet	2 %
YFP/CyPet	∼1 %
Venus/CyPet	∼1 %

The pair YFP/CFP shows the highest change in FRET ratio of about 20 %. All other combinations tested displayed a change in ratio below 12 %. Among all tested combinations, the pair YPet/CyPet was documented to be optimized for FRET applications [189]. In our setup, this seems not to be the case.

As the FRET pair YFP/CFP worked best in the *in vivo* FRET setup, the plasmid based fusion library of all two-component proteins was constructed using these two fluorophores.

3.2 Plasmid library

To co-express two proteins independently in *E. coli* cells, we constructed a comprehensive vector based library of kinases and response regulators fused to the fluorescent proteins YFP and CFP. The tag was placed at the C-terminus of the proteins, connected with a linker containing five amino acids (GSGGG) allowing free rotation and folding of the fluorophore. For the sensor kinases, this position was chosen as the N-terminal location of the fluorophore would hinder the proper insertion into the cytoplasmic membrane. For the response reglators, the position of the tag is not that crucial, as they are relatively small cytoplasmic proteins.

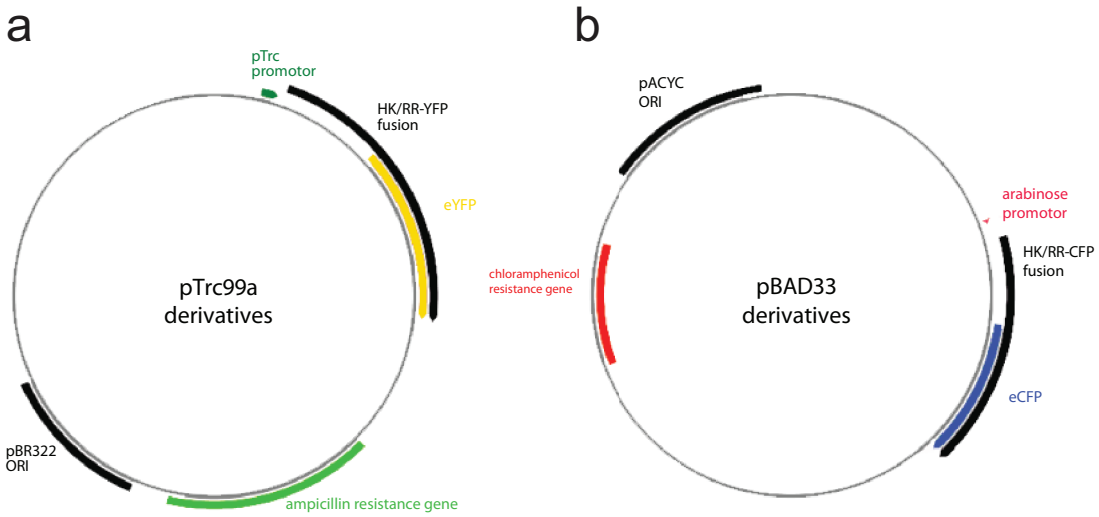

Figure 3.2: **Vector maps of the constructed expression plasmid library.** (**a**) Map of pTrc derivatives for expression of protein-YFP fusions under control of an IPTG inducible promotor. (**b**) Map of pBAD33 derivatives for expression of protein-CFP fusions under control of an arabinose inducible promotor. Arc segments are not scaled to gene length. **ORI**: origin of replication. Maps were generated using PlasMapper [208].

All constructed plasmids are derivatives of the two expression vectors pTrc99a and pBAD33 [209, 200], and a schematic representation of the resulting constructs is shown in Figure 3.2. pTrc derivates harbour an IPTG inducible pTrc promotor and a pBR322 origin of replication (ORI). For selection purposes the plasmids includes an ampecillin resistance marker. To simultaneously express a second protein, we constructed pBAD33 derivates harbouring a compatible pACYC184 ORI and an arabinose inducible pBAD promotor.

The selection marker for these vectors is chloramphenicol. The combination of both vectors allow independent expression and tight regulation of two different proteins in the same cell.

Out of the 28 histidine kinases present in *E. coli*, we made YFP and CFP fusions to 27 of them under control of a pTrc promotor. Only *kdpD-cfp* was not constructed as cloning failed in several attempts. With the exception of *evgS*, *kdpD*, *lytS* and *rcsC*, where again several attempts of molecular cloning were not successful, we constructed 24 kinase-*cfp* fusions under control of a pBAD promotor. For the response regulators we focused on fusions to YFP on pTrc plasmids, as for the kinases compatible plasmids encoding CFP fusions are available. Out of the 30 response regulators we made 26 protein fusions, only *atoC*, *hydG*, *lytR* and *yfhA* have not been included due to cloning problems. We left out the non-canonical two-component proteins CheA and CheY from our library, as they have not been included in our studies.

3.3 Protein expression levels and stability

The protein-YFP fusions were tested upon the amount of protein degradation inside the cells using SDS-PAGE and immunoblotting with an anti-GFP antibody. Fusions were expressed in wildtype MG1655 cells from plasmids under the same conditions used in the FRET setups. Figure 3.3 shows the immunoblots for the sensor kinase and response regulator YFP-fusions. The intensities of protein bands were quantified using the software ImageJ as described in chapter 2.8 to determine the amount of protein degradation compared to the total protein expression. The results are shown in Table 3.2.

The majority of sensor fusions were expressed as full length proteins with a stability between 46 and 100 % of total protein. The three fusions ArcB, NtrB and RstB showed a degradation rate of more than 60 %. ArcB-YFP exhibited a major degradation product with a molecular weight of approximately 40 kDa, NtrB-YFP was degraded in multiple fragments between 100 and 25 kDa. RstB-YFP only shows the 26 kDa band corresponding to free YFP. This can be explained by a clip-off of the fluorophore. Subsequently these three fusions were not used in further experiments. Fluorescent protein fusions to the response regulator proteins exhibited a stability of at least 67 % of full length protein for all tested reporters, enabling their usage in the subsequent *in vivo* studies.

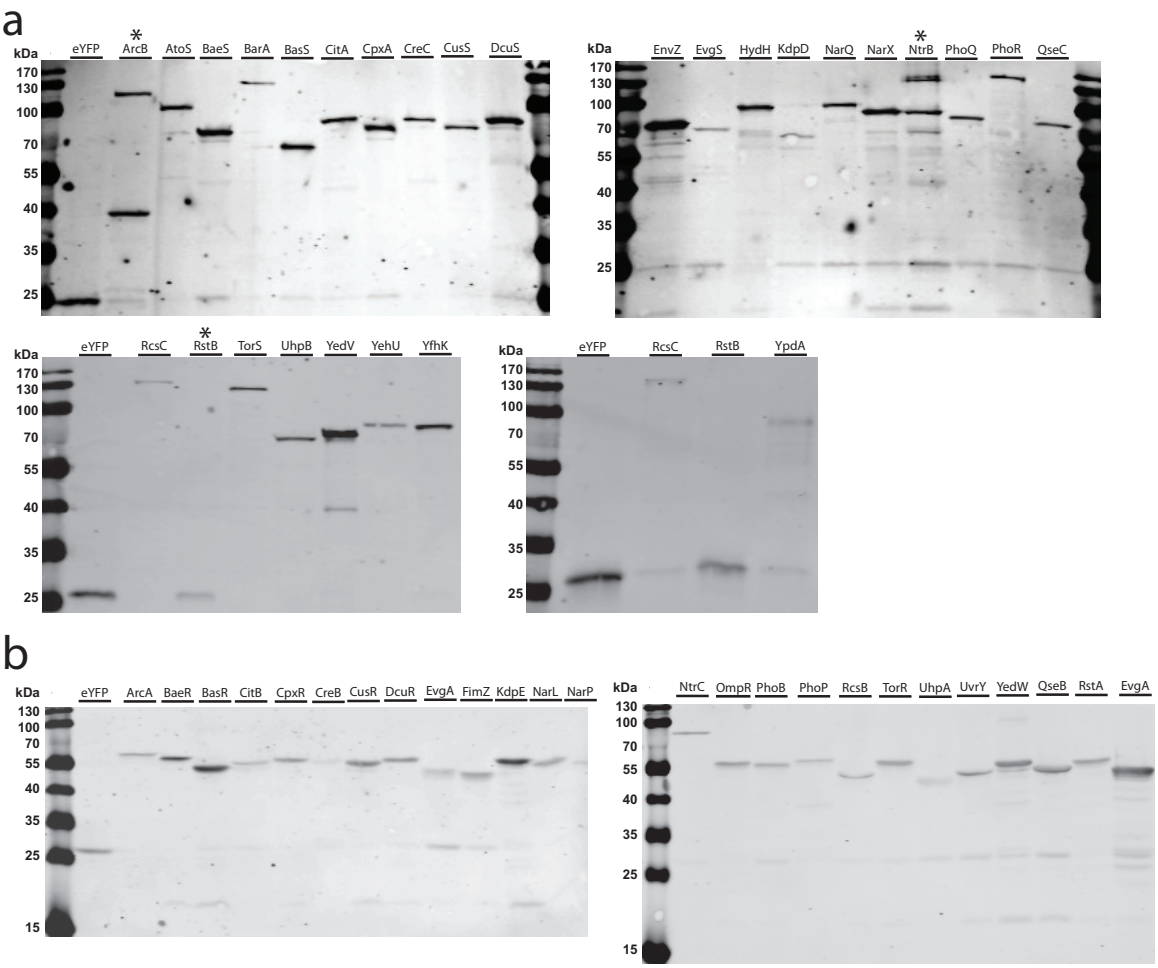

Figure 3.3: **Immunoblots depicting histidine kinase (a) and response regulator (b) degradation.** Kinase-YFP fusions were tested for the amount of protein degradation using an anti-GFP antibody. eYFP lanes were added as control. Fusions were expressed from plasmids in MG1655 wildtype cells. Numbers represent the size of molecular weight marker bands in kDa. Fusions exhibiting large amount of degradation are labelled by an asterisk.

Table 3.2: **Fractional degradation of kinase- and regulator-YFP fusions.** Numbers represent percentage of protein degradation for fusions expressed in MG1655 wildtype cells. Fusions exhibiting a degradation rate $\geq$ 60 % are displayed in bold.

Kinases

Fusion	Amount of degradation	Fusion	Amount of degradation
ArcB	**0.96**	NarQ	0.27
AtoS	0.08	NarX	0.25
BaeS	0.20	**NtrB**	**0.66**
BarA	0.20	PhoQ	0.28
BasS	0.10	PhoR	0.32
CitA	0.02	QseC	0.28
CpxA	0.11	RcsC	0.44
CreC	0.02	**RstB**	**1.00**
CusS	0.00	TorS	0.00
DcuS	0.15	UhpB	0.00
EnvZ	0.30	YedV	0.54
EvgS	0.46	YehU	0.00
HydH	0.20	YfhK	0.00
KdpD	0.43	YpdA	0.45

Regulators

Fusion	Amount of degradation	Fusion	Amount of degradation
ArcA	0.02	NarP	0.14
BaeR	0.03	NtrC	0.12
BasR	0.07	OmpR	0.11
CitB	0.11	PhoB	0.21
CpxR	0.07	PhoP	0.19
CreB	0.43	QseB	0.24
CusR	0.13	RcsB	0.16
DcuR	0.10	RstA	0.07
EvgA	0.42	TorR	0.10
FimZ	0.12	UhpA	0.11
KdpE	0.21	UvrY	0.36
NarL	0.02	YedW	0.23

To determine the copy number of proteins under our experimental conditions, FACS analyses was performed on the YFP fusions. The resulting copy numbers for the majority of all *E. coli* TCS components are shown in Figure 3.4. Protein expression in the FACS experiments was not induced using IPTG, the protein expression is due to the leakyness of the pTrc promotor. The measured numbers represent thereby the number of protein fusions additionally to the native unlabeled proteins. Results showed a large copy number distribution between the different sensors and regulators, spanning four and five orders of magnitude, respectively. Between the kinases, KdpD and QseC showed the highest expression level with approximately 24000 and 22000 copies, respectively. In contrast, EnvZ and YpdA exhibited the lowest number with 180 and 450 copies per cell, respectively. In case of the regulators, YedW shows the highest copy number with 154000 proteins/cell, and the lowest expression was measured for CreB with 315 copies per cell. Our measured copy numbers display a large distribution compared to the values available in literature, reporting about 100 copies of sensors and 3000 copies of regulators per cell and assuming these numbers for all existing systems [91, 93, 94].

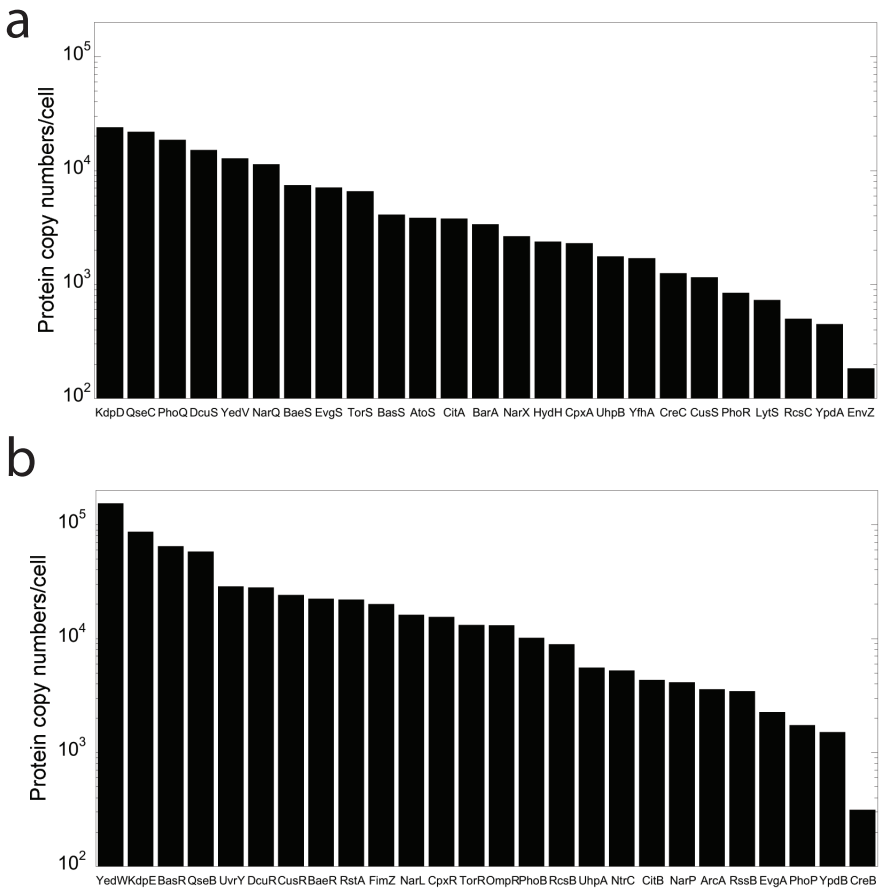

Figure 3.4: **Copy numbers of histidine kinases and response regulators.** FACS data showing the copy numbers of histidine kinase **(a)** and response regulator **(b)** YFP-fusions expressed from pTrc plasmids without induction in MG1655 wildtype cells. Absolute protein numbers were determined after FACS calibration (see section 2.10 for details).

To deduce the range of overexpression for sensors expressed from our plasmids, representative protein fusions were inserted into the bacterial chromosome to determine the native protein expression levels under control of the native promotors. A C-terminal in-frame insertion of YFP allowed quantification of the expression levels. The determined values and (for comparison) the correspondent numbers of plasmid expression are shown in Table 3.3.

The derived values for the three kinases BaeS, CitA and CusS display a copy number between 300 and 600 sensors per cell under the native promotor. Comparing these results with the plasmid based sensor expression, we estimate an overexpression rate of our fusions between 3.5 and 13 fold compared to the chromosomal (native) expression levels.

Table 3.3: **Comparison between chromosomal and plasmid based expression.** Absolute numbers were determined using FACS analysis after calibration (see section 2.10 for details). Variations represent standard errors.

	Copy number	
Kinase fusion	plasmid	chromosome
BaeS	4114 ± 341	320 ± 89
CitA	3777 ± 1171	634 ± 191
CusS	1159 ± 290	334 ± 113

3.4 Sensor and regulator localization

Intracellular localization of sensor kinases was investigated using fluorescence microscopy imaging. The different sensors were either expressed as YFP- or CFP-fusions (to derive the lowes possible copy number), and the used conditions and copy numbers are summarized in Table 3.4. Figure 3.5 shows representive pictures for all HKs which were expressed as full-length fusions (see Table 3.2 for details).

The sensor´s localization pattern can be classified in three different classes: homogenous localization around the cell periphery (Figure 3.5a), distinct localization pattern (Figure 3.5b) and intermediate punctuated distribution (Figure 3.5c). To determine possible differences in protein localization dependent on presence of wildtype proteins or nutrient source (influence of catabolite repression), localization was additionally tested under different growth conditions. The results are summarized in Table 3.5. Localization pattern shown in Figure 3.5a was exhibited by the sensors AtoS, BasS, CreC, DcuS, KdpD, NarX, QseC and YedV, and it was visible at all tested expression levels and growth conditions. Two kinases, EvgS and TorS, showed a specific cluster formation predominantly occuring at the cell poles (Figure 3.5b).The remaining sensors showed a milder tendency to form clusters and exhibited an intermediate punctuated kinase distribution shown in Figure 3.5c. This pattern was only visible at lower expression levels, changing into a homogenous localization with increased protein numbers. Some of the histidine kinases showed in-deed a different localization dependent on the applied growth conditions, with a higher tendency for cluster formation in rich medium compared to TB or Minimal A (Table 3.5). The presence of wildtype protein seems not to affect the localization pattern, as there was no difference visible between results obtained in wildtype or the corresponding kinase knockout.

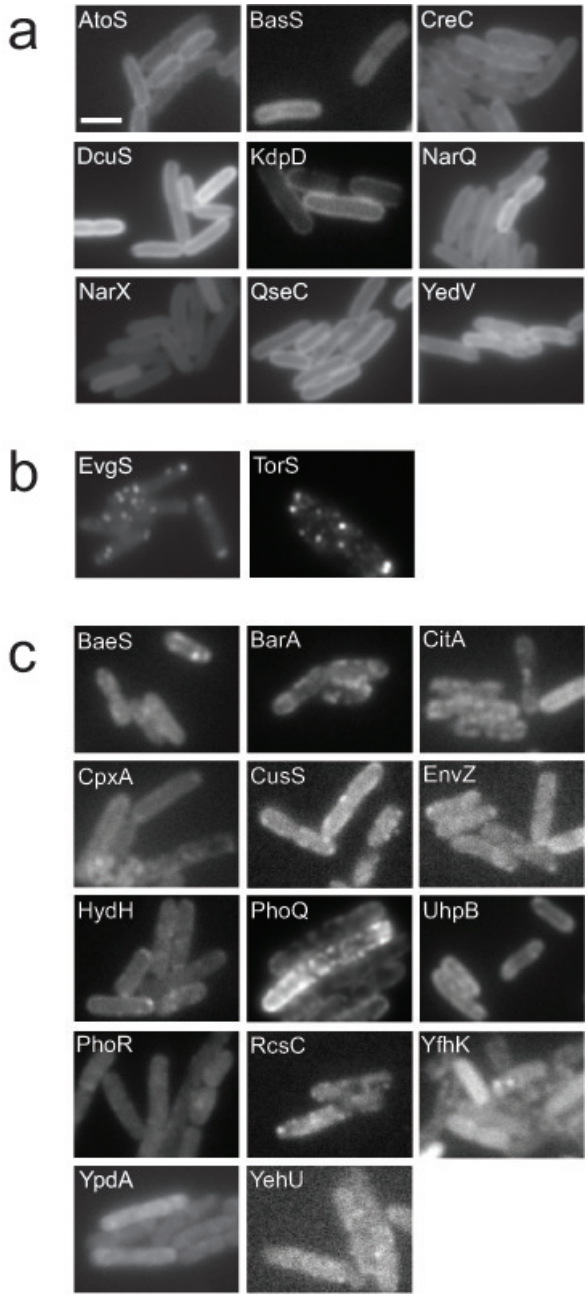

Figure 3.5: **Cellular localization of histidine kinases.** Fluorescence microscopy snapshots showing intracellular localization of kinase-YFP fusions. **(a)** Homogenous localization at the cell periphery. **(b)** Pattern of distinct protein localization. **(c)** Intermediate protein localization. Proteins were expressed from plasmids in MG1655 wildtype cells. Copy numbers for the different fusions are shown in Table 3.4. Scale bar: 2 µM.

Table 3.4: **Imaging conditions histidine kinase localization.** Copy numbers are measured as described in Section 2.10.

His-kinase	imaged as YFP	imaged as CFP	induction level	copies per cell
AtoS	x		0 µM IPTG	3800
BaeS		x	0.005% Ara	8200
BarA		x	0.01% Ara	1400
BasS	x		0 µM IPTG	4100
CitA	x		0 µM IPTG	3700
CpxA	x		0 µM IPTG	2300
CreC	x		7 µM IPTG	2000
CusS	x		30 µM IPTG	2000
DcuS		x	0.005% Ara	7600
EnvZ	x		30 µM IPTG	1800
EvgS	x		0 µM IPTG	7100
HydH	x		3.5 µM IPTG	2400
KdpD	x		0 µM IPTG	24000
NarQ	x		0 µM IPTG	11300
NarX	x		0 µM IPTG	2700
PhoQ		x	0.0001% Ara	21000
PhoR	x		9 µM IPTG	2000
QseC		x	0.0001% Ara	15800
RcsC	x		30 µM IPTG	1800
TorS	x		0 µM IPTG	6500
UhpB	x		0 µM IPTG	1800
YedV	x		0 µM IPTG	12800
YehU	x		30 µM IPTG	2300
YfhK	x		5 µM IPTG	2000
YpdA	x		30 µM IPTG	1000

Additionally, we studied the intracellular localization of the majority of TCS response regulator proteins. A corresponding fluorescence image is shown in Figure 3.6. All response regulators exhibit a homogenous distribution in the cytoplasm similar to the on displayed for ArcA in Figure 3.6. In all cases, there was no specific localization pattern to spots or protein complexes visible. It should be mentioned that some of the fusions showing high expression levels (for example bright cells of BaeR or YpdB) exhibit dark spots at the cell poles. These spots represent most probably vacuoles or aggregates of nutrients or other substances.

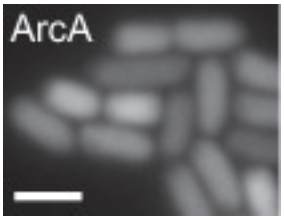

Figure 3.6: **Fluorescence microscopy snapshots showing intracellular localization of regulator-YFP fusions.** Proteins were expressed from plasmids in MG1655 wildtype cells without induction of protein expression. Scale bar: 2 µM.

Table 3.5: **Summary of HK localization for different growth conditions.** Sensor-YFP fusions were expressed from plasmids in MG1655 cells (**wt**) or in the corresponding deletion background (**ko**) from the Keio collection [REF Baba 2006]. Where possible, copy numbers were adjusted to about 2000 copies per cell.

	LB		TB		Gly/A	Gly+Stim/A	Glu/A	Glu/A-low
YFP-fusion	wt	ko	wt	ko	wt	wt	wt	wt
AtoS	M	M	M	n.d.	M	M	M	M
BaeS	M/A	M/A	M	M	M	M	M	M
BarA	M/A	n.d.	M/A	n.d.	M/A	n.a.	M/A	M/A
BasS	M	M	M	n.d.	M	M	M	M
CitA	M/A	M/A	M	M	M	M	M	M
CpxA	M/A	M/A	M	M	M	n.d.	M	M
CreC	M	M	M	M	M	M	M	M
CusS	M/A	M/A	n.d.	n.d.	M	M	M	M
DcuS	M	M	M	M	M	M	M	M
EnvZ	M/A	M/A	M	M	M	M	M	M
EvgS	M/A	n.d.	M/A	n.d.	M/A	n.a.	M/A	M/A
HydH	M/A	M/A	M	M	M/A	M	M	M/A
KdpD	M	n.d.	M	n.d.	M	M	M	M
NarQ	M	M	M	M	M	M	M	M
NarX	M	M	M	M	M	M	M	M
PhoQ	M/A	M/A	M	n.d.	M	M	M	M
PhoR	M/A	M/A	C	C	M/A	M	C	M/A
QseC	M	M	M	M	M	n.d.	M	M
RcsC	M/A	C	M	M	M/A	M/A	M/A	M/A
TorS	M/A	n.d.	M/A	n.d.	M/A	M/A	M/A	M/A
UhpB	M/A	M/A	M/A	M/A	M	M	M	M
YedV	M	M	M	n.d.	M	n.a.	M	M
YehU	M,M/A	n.d.	C	n.d.	M/A	n.a.	C	M/A
YfhK	M/A	M/A	M	n.d.	M/A	n.a.	M	M/A
YpdA	M/A	M/A	M	M	M/A	n.a.	M	M/A

A – minimal A medium; **Gly** – glycerol as carbon source; **Glu** – glucose as carbon source; **Stim** – Stimulus (see Table 3.12 for details)
Cellular distribution of the sensors was scored as follows:
M – homogenous membrane distribution; **M/A** – punctuate localization; **C** - homogenous cytoplasmic distribution;
n.d. – not determined; **n.a.** – not available/no stimulus known.

3.5 Kinase-kinase interactions

3.5.1 FRET screen on cognate sensor pairs

To test possible interactions between different two-component pathways on the sensor level, we performed a screen using an *in vivo* acceptor photobleaching FRET assay. For all following kinase-kinase FRET experiments, the copy numbers were adjusted as shown in Table 3.6. The results from the sensor screen are shown in Figure 3.7.

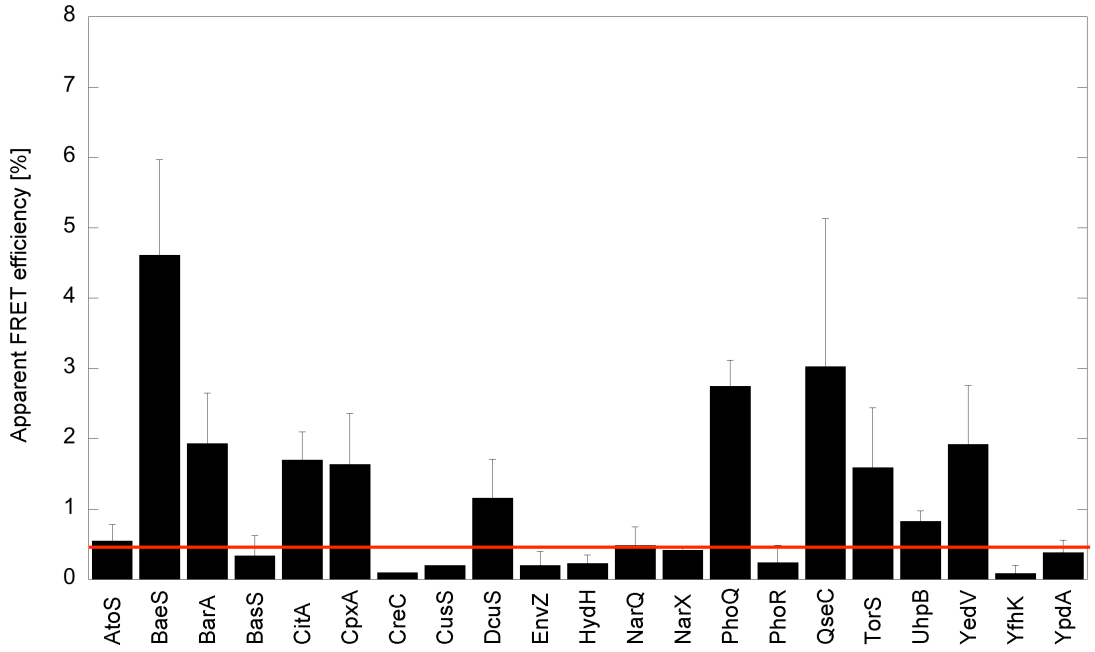

Figure 3.7: ***In vivo* bleach FRET investigation of kinase homodimers.** Protein interactions between sensor kinases of the same kind measured by acceptor photobleaching FRET. Red line represents 0.5 % scored as threshold for positive interactions. Fusions were expressed from plasmids in MG1655 wildtype background with copy numbers of about 2000 per fusion. Error bars represent standard errors.

Out of the 21 sensor kinases investigated, we could show interactions for 12 of them, namely AtoS, BaeS, BarA, CitA, CpxA, DcuS, NarQ, PhoQ, QseC, TorS, UhpB and YedV. All of them showed an increase in FRET ratio after photobleaching of more than 0.5 % (red line in Figure 3.7), which is scored as threshold for positive protein interactions. The strongest ratio change was measured for the three kinases BaeS (4.61 %), PhoQ (2.75 %) and QseC (3.03 %). Those three pairs are among the fusions exhibiting high copy numbers under our experimental conditions (Table 3.6), which might explain the relatively high

values of FRET ratio change due to a high probability of interactions inside the cell. The pairs showing a FRET value below 0.5 % are scored as non-interacting, which results from no energy transfer between the two fluorophores. The reason for this could be structural properties of the sensors, which separate the two C-terminal fluorophores to a distance greater than 10 nm.

Table 3.6: **Histidine kinase copy numbers for acceptor photobleaching experiments.** Copy numbers were determined as described in Section 2.10.

	copies per cell	
His-kinase	YFP fusion	CFP fusion
AtoS	3800	9000
BaeS	2800	8200
BarA	3000	1400
BasS	7500	4100
CitA	3000	3700
CpxA	3000	2300
CreC	2500	2000
CusS	1160	2000
DcuS	12000	7600
EnvZ	180	1800
HydH	3400	2400
NarQ	9000	11300
NarX	3000	2700
PhoQ	15000	21000
PhoR	3900	2000
QseC	18000	15800
TorS	6000	6500
UhpB	1700	1800
YedV	10000	12800
YfhK	1700	2000
YpdA	1900	1000

3.5.2 FRET measurements on kinase cross-talk

To elucidate possible interactions between sensor proteins of different kinds, we repeated the former screen by pairwise expressing kinase fusions in different combinations. The results are shown in Figure 3.8.

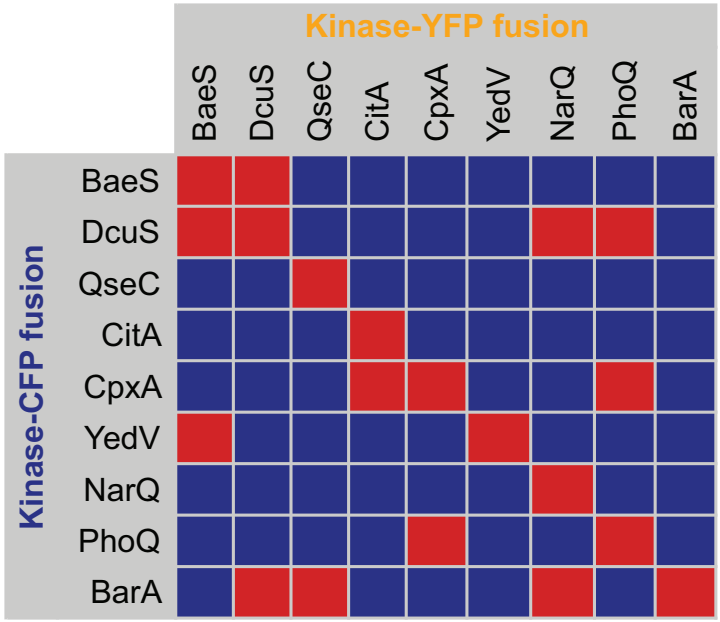

Figure 3.8: **Acceptor photobleaching screen between HK-YFP and -CFP fusions.** Heatmap represents measured interactions between histidine kinases of different kinds using FRET. Blue squares represent no interaction (change in FRET ratio < 0.5 %), red squares represent identified interactions (ratio change ≥ 0.5 %). Fusions were expressed from plasmids in MG1655 wildtype background. Copy numbers of kinase fusions are shown in Table 3.6.

The red diagonal line shown in the heatmap represents the interactions already shown in Figure 3.7, added to derive a comprehensive picture. Out of the measured combinations of different sensors, we identified in total 11 positives including two hits observed in both orientations, namely CpxA/PhoQ and BaeS/DcuS. This results in 9 identified protein hetero-interactions in total (BaeS/DcuS, BaeS/YedV, BarA/DcuS, BarA/NarQ, BarA/QseC, CitA/CpxA, CpxA/PhoQ DcuS/NarQ and DcuS/PhoQ), representing 12.5 % cross-talk among the pairs investigated. It should be mentioned that occurence of interactions in one orientation only most probably result from differences in the expression

levels between the two fusions (see Discussion for details).

3.5.3 Stimulus dependent FRET on cognate pairs

To derive informations about the dynamic range and sensitivity of kinase interactions, we performed stimulus dependent FRET measurements on different kinase-kinase pairs. The main focus was on the interacting candidates identified in Figure 3.8. An overview over the tested combinations is shown in Table 3.7.

Table 3.7: **Kinase-pairs tested in stimulus dependent FRET measurements.** +: combination responded to applied stimulus; -: combination did not respond.

cognate pairs

Kinase 1	Kinase 2	Stimulus	Response
BaeS	BaeS	$CuSO_4$	+
CitA	CitA	citrate	+
CpxA	CpxA	citrate, $MgSO_4$	-
CusS	CusS	$CuSO_4$	-
EnvZ	EnvZ	sucrose, KCl, NaCl	-
HydH	HydH	$ZnSO_4$, $PbCl_2$	-
NarX	NarX	$NaNO_2$, $NaNO_3$	-
PhoQ	PhoQ	$MgSO_4$, phosphate	-
TorS	TorS	TMANO	-

non-cognate pairs

Kinase 1	Kinase 2	Stimulus	Response
CitA	CpxA	citrate	+
CpxA	PhoQ	$MgSO_4$	+
BaeS	DcuS	fumarate, $CuSO_4$	-
BaeS	YedV	$ZnSO_4$	-
BarA	NarQ	$NaNO_2$, $NaNO_3$	-
DcuS	PhoQ	fumarate, $MgSO_4$	-
DcuS	NarQ	fumarate, $NaNO_2$, $NaNO_3$	-
DcuS	BarA	fumarate	-

Out of the 9 cognate kinase pairs tested, only BaeS and CitA showed change in FRET in reponse to their cognate stimulus. The other tested pairs did not exhibit any response

to the applied stimuli, which might be due to no occuring change in sensor confirmation upon stimulation (see discussion for details) or the ineffectiveness of the used substance. For the sensor BaeS, we were able to measure a stimulation dependent FRET response using $CuSO_4$ (Figure 3.9a).

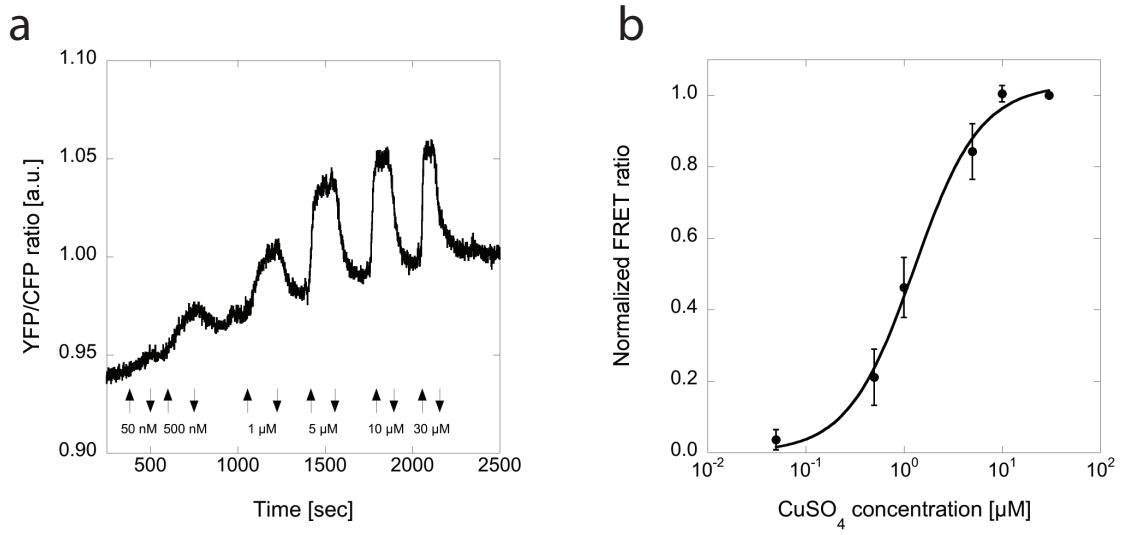

Figure 3.9: **Stimulation-induced conformational change for BaeS. (a)** FRET curve for BaeS-YFP/BaeS-CFP showing the change in YFP/CFP-ratio upon stimulation with $CuSO_4$. Arrows represent addition (↑) and removal (↓) of the stimulus; concentrations are indicated. **(b)** Dose-response curve for BaeS dimer calculated from measurements as shown in (a). Error bars represent standard errors. Values were fitted using a Hill equation (see Equation 2.7 for details).

Figure 3.9 shows the increasing change in YFP/CFP-ratio upon stimulation with increasing concentrations of $CuSO_4$, the substance sensed by the BaeSR system. The changes in ratio reflect a conformational change within a sensor dimer or between different sensors in a complex induced by the stimulus. The sensitivity of the FRET setup allows us to measure concentrations between 50 nM and 30 µM, whereas the ratio change saturates around a concentration of 10 µM $CuSO_4$. Figure 3.9b shows a dose response curve derived from FRET measurements as shown in panel a. The curve was fitted using Equation 2.7. Another described stimulus for the BaeSR system is indole, but application of this substance on the sensor pair did not show any change in the FRET-ratio.

With CitA, we identified another sensor responding in our stimulus dependent FRET setup upon application of the cognate chemical signal (Figure 3.10). CitA exhibits very weak changes in FRET ratio upon stimulation using citrate. Nevertheless, this seems to

be specific as the FRET ratio decreases upon stimulation, in contrast to an increase in ratio for unspecific interactions.

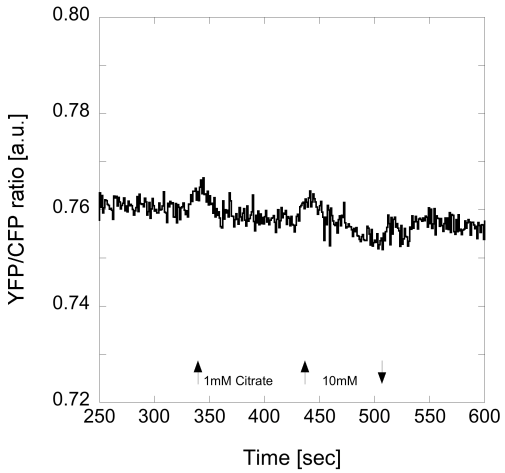

Figure 3.10: **Stimulation dependence of FRET for CitA.** Blue and orange curves show single fluorescence channels, black curve shows YFP/CFP-ratio change of CitA dimers as response to citrate. Arrows represent addition (↑) and removal (↓) of the stimulus. Citrate concentrations of 1 and 10 mM were used, applied without changing back to buffer.

3.5.4 Stimulus dependent FRET on kinase cross-talk

Given the possibility to use stimulus dependent FRET measurements to measure kinase-kinase interactions, we expanded our experiments on non-cognate pairs identified before (see Table 3.7 for details). Out of the 8 tested hetero-interactions we were able to measure stimulus dependence for CitA/CpxA and CpxA/PhoQ (Figure 3.11). Figure 3.11a shows the change in YFP/CFP-ratio for the non-cognate sensor pair CitA and CpxA. The applied stimulus is 10 mM Citrate, the substance detected by CitA. Figure 3.11b displays a FRET measurement for the sensor pair CpxA and PhoQ. We applied $MgSO_4$ in concentration between 30 µM and 100 mM sensed by PhoQ. The heteropair showed a specific response to the different concentrations of $MgSO_4$. For the kinase CpxA, only the unspecific stimulus pH is known. As pH changes intensities of YFP and CFP fluorescence, this was not applied in the FRET measurements.

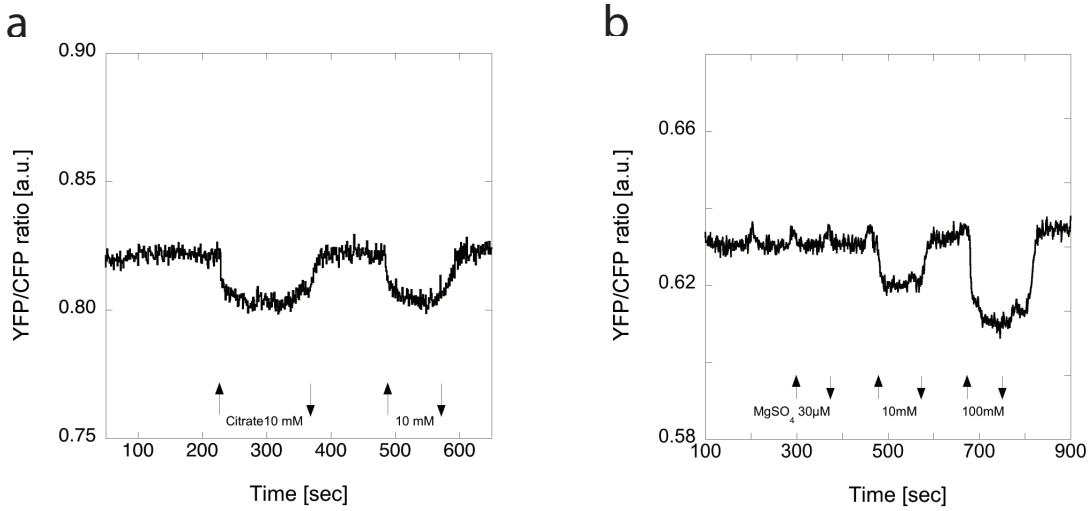

Figure 3.11: **Histidine kinase cross-talk. (a)** Stimulus dependent FRET between CitA and CpxA kinases. **(b)** FRET between CpxA and PhoQ kinases. Curves showing YFP/CFP-ratio change of dimers as response to a stimulus. Arrows represent addition (↑) and removal (↓) of the stimulus. Stimuli and concentrations are indicated.

3.6 Kinase-regulator interactions

3.6.1 Acceptor photobleaching FRET

To confirm interactions between sensor kinases and their cognate regulators we performed acceptor photobleaching FRET measurements on different HK-RR pairs. Additionally, we wanted to identify pairs we could assay with our stimulus-dependent FRET setup for further kinetic measurements. The identified pairs are listed in Table 3.8.

Table 3.8: **Kinase-regulator bleach FRET.** FRET efficiencies were determined using acceptor photobleaching. Majority of the pairs were tested in both orientations (HK-YFP/RR-CFP and HK-CFP/RR-YFP). -: no change on FRET efficiency; **n.d.**: not determined.

Sensor	Regulator	FRET efficiency	
		HK-YFP/RR-CFP	*HK-CFP/RR-YFP*
BaeS	BaeR	0.92 %	n.d.
BasS	BasR	1.08 %	1.30 %
CpxA	CpxR	n.d.	1.81 %
CreC	CreB	n.d.	-
CusS	CusR	n.d.	1.95 %
EnvZ	OmpR	0.49 %	2.33 %
PhoQ	PhoP	1.46 %	-
QseC	QseB	2.56 %	4.76 %
RstB	RstA	n.d.	-
YedV	YedW	2.01 %	9.35 %

Additionally we tested a set of non-cognate kinase-regulator pairs in the acceptor photobleaching setup to screen for possible interactions. Starting point were the identified interactions from the *in vitro* study performed by Yamamoto and colleagues [136] and computational predictions from the van Nimwegen group in Basel (Erik van Nimwegen, personal communication and [127]). The tested interaction set is shown in Table 3.9. All except one pair (YedV/CusR) are tested in the orientation HK-CFP/RR-YFP. This due to the leaky expression of the pTrc controlled YFP fusions. As regulators are more abundant than sensors, we assumed this orientation not to have any negative effects due to expression ratios (see Discussion for details).

Table 3.9: **FRET test on cross-talk HK-RR pairs identified *in vitro* and predicted.** Combinations are based on *in vitro* experiments [136] and computational predictions (Erik van Nimwegen, personal communication and [127]). Confirmed interactions using acceptor photobleaching FRET are shown in bold. All pairs, except were noted, are tested in the orientation HK-CFP/RR-YFP.

Sensor	Regulator	FRET efficiency	Sensor	Regulator	FRET efficiency
in vitro data			*computational predictions*		
BaeS	CheY	-[1]	**AtoS**	**CusR**	0.51 %
BaeS	RssB	-	BaeS	CpxR	-[1]
BarA	CusR	-	**BasS**	**QseB**	0.79 %
BarA	NarL	-	BasS	PhoP	-[1]
BarA	NarP	-	CpxA	OmpR	-[1]
CreC	PhoB	-	CreC	BasR	-[1]
CusS	PhoB	-	**CusS**	**YedW**	2.23 %
DcuS	CheY	-[1]	EnvZ	RstA	-
DcuS	CitB	-[1]	EnvZ	CpxR	-[1]
DcuS	PhoB	-	PhoQ	NtrC	-[1]
DcuS	RssB	-	QseC	CreB	-
EnvZ	CpxR	-[1]	RstB	OmpR	-[1]
EnvZ	PhoP	-	**YedV**	**CusR**	0.64 %[2]
HydH	RssB	-			
NtrB	CitB	-[1]			
NtrB	RssB	-			
PhoR	CpxR	-			
RstB	CpxR	-			
UhpB	**CitB**	6.61 %			
UhpB	CusR	-			
UhpB	**KdpE**	0.89 %			
UhpB	NarL	-			
UhpB	NarP	-			
UhpB	NtrC	-			
YedV	CusR	-			

-: no change in FRET efficiency

n.d.: not determined

[1]: confirmed in both orientations

[2]:measured in orientation HK-YFP/RR-CFP

Within the set of *in vitro* data we were able to identify positive interactions between the Kinase UhpB and the regulators KdpE (0.89 % change in FRET ratio) and CitB (6.61 %

change in FRET ratio), which are both significant. For the tested candidates from computational predictions, we measured a change in the FRET for the pairs AtoS/CusR (0.51 %), BasS/QseB (0.79 %), CusS/YedW (2.23 %) and YedV/CusR (0.64 %). Nevertheless, the vast majority of computational predictions or *in vitro* data did not show any cross-talk between the different proteins. The possible reasons for this might be the differences with the experimental setups used for the *in vitro* data (see discussion for details) and that predictions might not reflect the *in vivo* situation.

3.6.2 Stimulus dependent FRET

Focusing on those pairs where we identified an interaction in the acceptor photobleaching setup (see Table 3.8), we tested their responses using their cognate stimulus. The results are summarized in Table 3.10.

Table 3.10: **Kinase-regulator FRET upon stimulation.** Pairs were tested using kinase-CFP and regulator-YFP fusions. Copy numbers were adjusted to about 2000 sensor and 5000 regulator copies per cell, if possible. Fusions were expressed in wildtype MG1655 cells.

Sensor	Regulator	FRET response upon stimulation
		HK-CFP/RR-YFP
BaeS	BaeR	+
BasS	BasR	-
CusS	CusR	-
CpxA	CpxR	n.a.
DcuS	DcuR	-
EnvZ	OmpR	-
NarX	NarL	-
PhoQ	PhoP	-
QseC	QseB	-
RstB	RstA	-
TorS	TorR	-
UhpB	UhpA	-
YedV	YedW	n.a.

+: response upon stimulus; **-**: no response
n.a.: no stimulus known

Among the different TCS tested the majority did not show a response upon the certain stimulus. This is probably because of the orientation of the kinase and regulator fusions against each other, which separate YFP and CFP to a distance to far for FRET. Only for

one system (BaeS and BaeR) we where are able to measure stimulus dependent kinetics between sensor and regulator. Figure 3.12 shows the BaeS kinase and BaeR regulator, stimulated with 2 mM of the described stimulus indole.

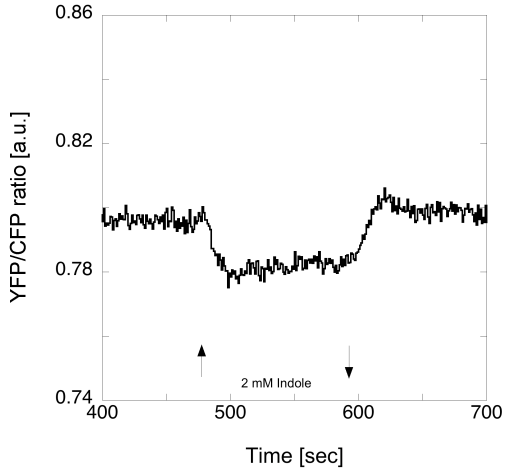

Figure 3.12: **Stimulus dependent FRET between BaeS and BaeR.** Curves showing sensor-regulator response to indole. Blue curve represents the YFP/CFP-ratio. Arrows represent addition (↑) and removal (↓) of the stimulus, concentrations are indicated.

The system shows a change in YFP/CFP-ratio, indicating a change in inter-protein interaction kinetics upon stimulation. The two proteins showed no response to stimulation using varying concentrations of $CuSO_4$, another stimulus of the system. This finding seems to be in contradiction to the results obtained for the BaeS sensor alone (see Figure 3.9), and the reason might be a different conformational mechanism for the sensing of indole and $CuSO_4$ (see discussion for details).

3.7 Promotor activation

3.7.1 Kinase overexpression screen

To test for possible influences of sensors on the downstream promotor activity, we expressed kinases without any stimulus in presence of promotor-GFP fusion plasmids [185]. These reporter plasmids harbour a gene coding for a fast folding GFP-variant under control of different *E. coli* promotors, and allows the measurement of changed GFP-fluorescence as readout of changed promotor activity. We focused on a subset of systems, where we identified interactions on the sensor level before (Figure 3.8). All kinases were induced with 10 µM IPTG in wildtype cells to achieve overexpression and strenghten their possible

effects. Dependent on the kinases there are three possible outcomes expected: no change in promotor activity, increased or decreased activity upon sensor expression. The results

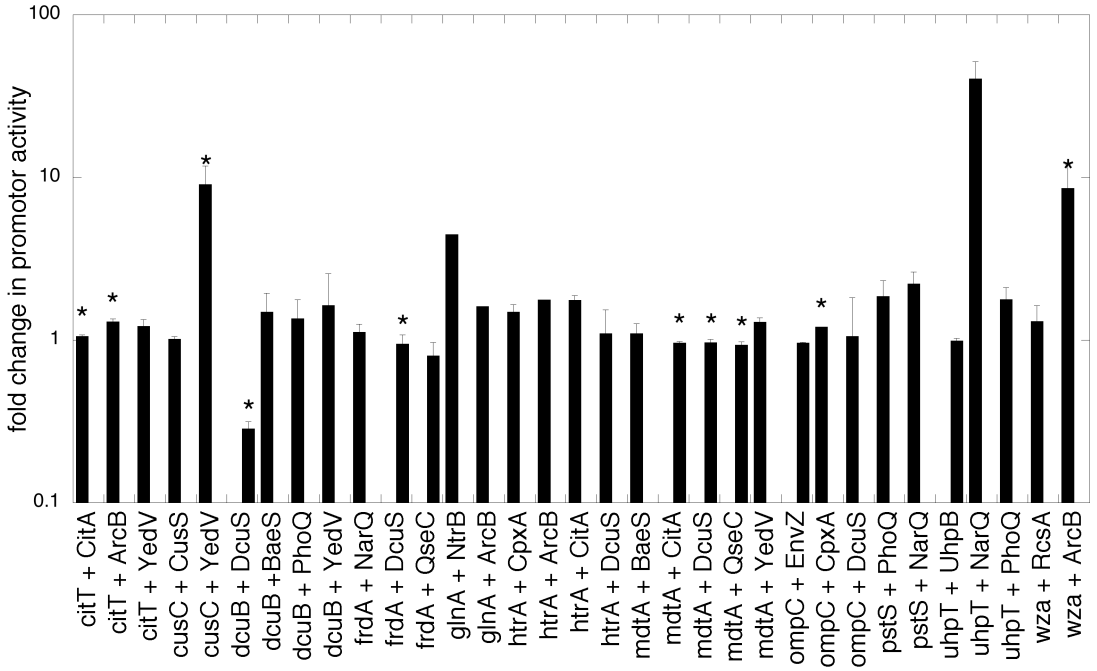

Figure 3.13: **Promotor activation upon histidine kinase overexpression.** Change in promotor activity upon overexpression of sensor kinase fusions. The first bar of each promotor represents the cognate kinase-promotor pair. All kinases were induced using 10 µM IPTG and expressed in wildtype MG1655 cells. Numbers are derived from promotor-GFP fusions measured by FACS. Values were normalized to the promotor activity in the absence of kinase-fusions. Error bars represent standard errors, asterisks indicate combinations with slower cell growth.

are shown in Figure 3.13. For the majority of the tested promotor fusions we were not able to see a strong effect upon kinase overexpression. This is possibly because sensor overexpression has no effect on the intrinsic kinase and/or phosphatase activity, which is changed by a cognate stimulus, only. Therefore, kinase overexpression is not leading to a difference in the regulator´s phosphorylation state, which would change the amount of regulators bound to promotors. Subsequently, there is no impact on the promotor activity detectable. Significant upregulation was seen for the four promotors *cusC* through YedV, *glnA* through NtrB, *uhpT* through NarQ and *wza* through ArcB. Significant downregulation was seen for the cognate pair *dcuB* and DcuS. Interestingly, all other of the cognate kinase-promotor pairs did not show any substantial effect on protein overexpression, which

might be due to the same lack of effects mentioned before.

3.7.2 Complementation of sensor-YFP fusions

To check the functionality of kinase-YFP fusions we performed complementation experiments. As in most of the cases sensor deletion exhibits no clear phenotype, we chose an assay providing a readout of promotor activity. We focused our experiments on the candidate systems identified in the kinase FRET screen (Figure 3.8). Where available (and the downstream promotor is known), we used GFP fusions from the *E. coli* promotor collection [185] and tested the change in promotor activity. Using FACS analysis we measured activity in the wildtype, the kinase knockout and the strain complemented with the corresponding kinase-fusion. Results for all tested promotors are summarized in Table 3.11 and positives are shown in Figure 3.14.

Table 3.11: **Promotor activity change upon kinase deletion and complementation.** Values are derived from promotor-GFP fusions using flow cytometry. Corresponding promotors are shown in brackets.

Kinase (Promotorfusion)	Complementation
CitA (*citT*)	n.e.
CpxA (*htrA*)	-
DcuS (*dcuB*)	+
EnvZ (*ompC*)	+
EnvZ (*pstS*)	n.e.
NarX (*fdnG*)	-
NarX (*frdA*)	n.e.
PhoQ (*phoA*)	-
PhoR (*phoA*)	+
QseC (*flhD*)	+
QseC (*fliA*)	+
QseC (*fliC*)	+
QseC (*motA*)	n.e.
RcsC (*rcsA*)	n.e.
RcsC (*wza*)	n.e.
UhpB (*uhpT*)	-

\+ - complementation; **-** - no complementation
n.e. - no effect of the knockout visible

In case of the four promotors *fdnG* (NarX), *htrA* (CpxA), *phoA* (PhoQ) and *uhpT* (UhpB), complemetation did not work as there is no effect on the promotor activity visible. For a group of promotors we do not even see a effect of the corresponding kinase knockout. Those include *citT* (CitA), *frdA* (NarX), *motA* (QseC), *pstS* (EnvZ) *rcsA* and *wza* (both RcsC).

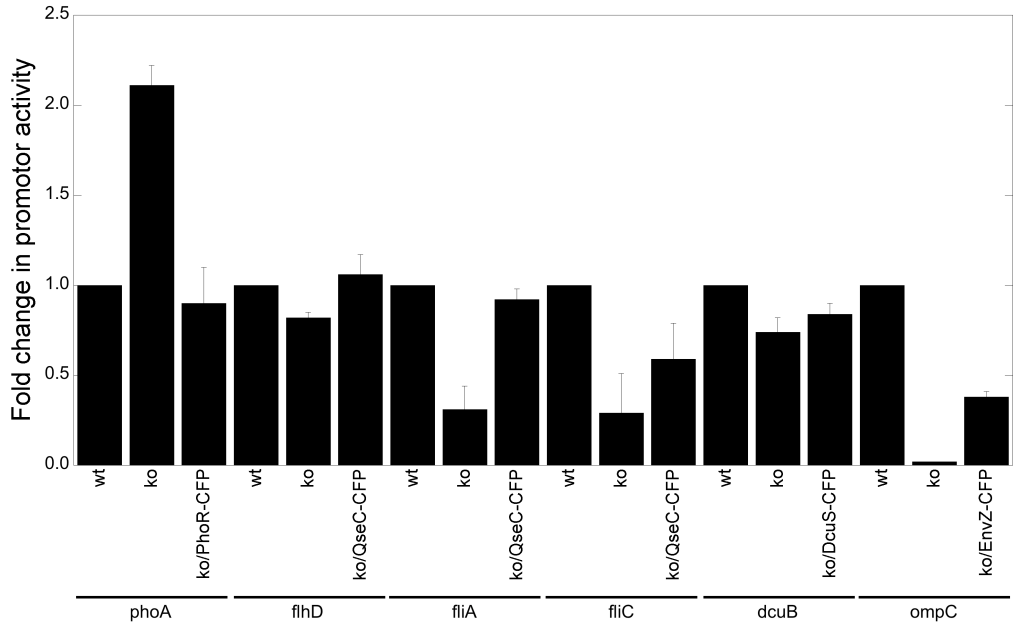

Figure 3.14: **FACS based complementation assay.** Change in promotor activity upon deletion (**ko**) and complementation (**ko/sensor fusion**) with sensor kinase fusions. Letters below lines represent promotor fusion. Values are derived from promotor-GFP fusions using FACS. Values were normalized to the wildtype (**wt**) promotor activity. Error bars represent standard errors.

YFP-fusions of the four sensors DcuS, EnvZ, PhoR and QseC are able to restore the promotor activity, at least partially. In these cases the obtained results indicate the (partial) functionality of the constructed protein fusions. For *flhD* (QseC) and *phoA* (PhoR) deletion of the sensor leads to an increase in promotor activity, which drops again upon addition of the cognate sensor. *dcuB* (DcuS), *fliA*, *fliC* (both QseC) and *ompC* (EnvZ) show an activity decrease in absence of the kinase, which (partially) increases again upon complementation with the kinase fusion.

3.7.3 Cross-activation of sensors on promotors

For those kinases performing cross-interaction in the acceptor photobleaching FRET assay (Figure 3.8), we were interested whether they also perform cross-talk on the promotor level. The detailed FACS results for the kinases that show a specific effect on non-cognate promotor activity is shown in Figure 3.15.

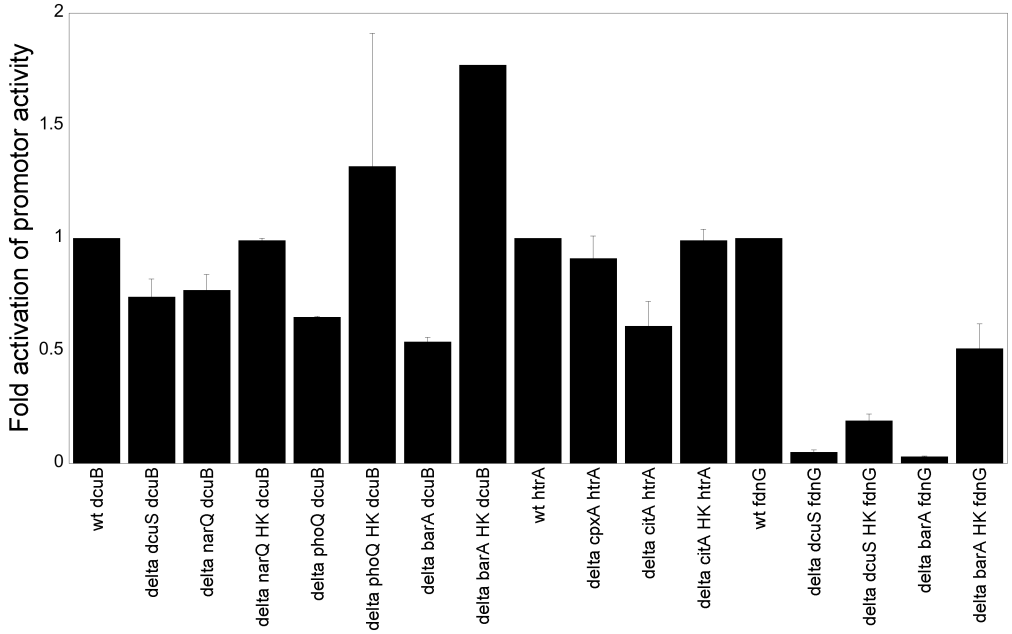

Figure 3.15: **Cross-talk effects on promotor level.** Change in promotor activity upon deletion (**ko**) of cognate and non-cognate sensor kinase fusions and complementation (**HK**) using the specific fusion protein. Values are derived from promotor-GFP fusions using FACS. Values were normalized to the wt promotor activity. Error bars represent standard errors.

The FACS results display an effect on the non-cognate promotors for the sensor pairs DcuS/NarQ (in both directions), DcuS/PhoQ, DcuS/BarA and CitA/CpxA. In all cases the promotor activity changes for if the proposed cross-talking kinase is knocked out. Additionally, complementation with this kinase fusion restores the promotor activity at least partially. This result confirms the physiological relevance of the kinase interactions we found in the FRET screen before.

3.7.4 Stimulus dependence of promotor activity

Table 3.12 shows a summary of stimuli for different two-component systems in *E. coli*. The listed substances have been reported in different experimental studies performed on

the different systems (for references see Table 3.12).The reported stimuli summarized in Table 3.12 were used to test their effect on promotors known to be downstream targets of two-component systems.

Table 3.12: **Stimuli of histidine kinases reported in literature.**

His-kinase	Reported stimulus	Literature experiment	Literature concentration	Effect on phosphorylation	Reference	Used concentration
ArcB	D-lactate	*in vitro*	10 mM	+	[210]	10 mM
AtoS	acetoacetate	*in vivo*	10 mM	+	[211]	10 µM
BaeS	indole	*in vivo*	2 mM	+	[212]	2 µM
	$CuSO_4$	*in vivo*	2 mM	+		5 mM
	$ZnSO_4$	*in vivo*	1 mM	+		200 µM
BasS	$FeSO_4$	*in vivo*	0.4 mM	+	[213]	500 µM
CitA	citrate	*in vivo*	20 mM	+	[169]	0.1-10 mM
CusS	$CuSO_4$	*in vivo*	1-2 mM	+	[214]	100 µM
DcuS	fumarate	*in vivo*	20 mM	+	[215]	2 mM
EnvZ	sucrose	*in vivo*	15 %	-	[176]	100 mM
	NaCl	*in vivo*	210 mM	-		500 mM
	KCl	n.d.	50-300 nM	n.d.		0.1-100 mM
HydH	$ZnCl_2$	*in vivo*	1 mM	+	[216]	1 mM ($ZnSO_4$)
NarQ	$NaNO_2$	n.d.	5 mM	n.d.	[133]	100 mM
	$NaNO_3$	*in vivo*	40 mM	-		100 mM
NarX	$NaNO_2$	n.d.	5 mM	n.d.	[133]	100 mM
	$NaNO_3$	*in vivo*	40 mM	-		100 mM
NtrB	α-ketoglutarate	*in vitro*	50 µM	+	[217]	0.03 µM
PhoQ	$MgCl_2$	*in vitro*	30 mM	-	[218]	500 mM ($MgSO_4$)
RstB	$MgCl_2$	n.d.	30 mM	n.d.	[218]	500 mM ($MgSO_4$)
TorS	trimethylamin-N-oxid	*in vitro*	10 mM	+	[219]	20 mM
UhpB	glucose-6-phosphate	*in vivo*	0.34 mM	+	[220]	0.04 µM

+: increase in kinase-regulator phophorylation; **-**: decrease in phosphorylation
n.d.: not determined in cited reference

Promotors were therefore identified using the EcoCyc database (http://EcoCyc.org/, [221]). Figure 3.16 shows the results of the performed FACS promotor activity screen.

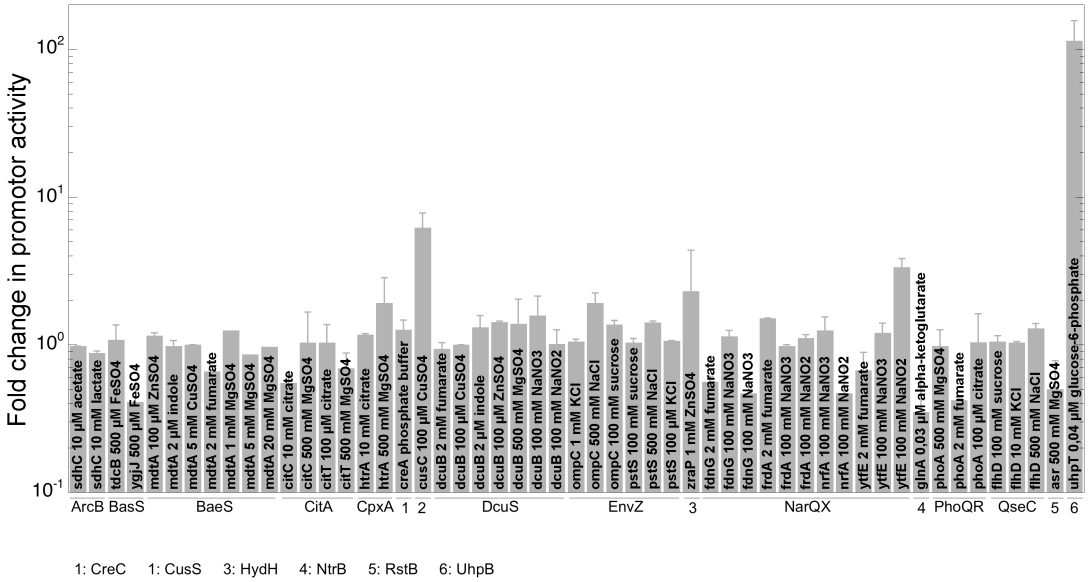

Figure 3.16: **FACS promotor stimulation screen.** Bars show the rate of change in promotor activity upon stimulation compared to the unstimulated state. Values were derived by FACS using GFP promotor reporter plasmids. Names of promotors, used stimuli and their concentrations are indicated inside the bars. Names below the x-axis indicate the corresponding sensor kinase(s). Error bars represent standard errors.

Among all tested reporter fusions we identified a couple of promotors which we could stimulate using the reported substance. The *uhpT* promotor (stimulated through UhpB with 0.04 µM glucose-6-phosphate) exhibits the highest change in activity with a 100 fold activation. Four promotors show a significant activation with an at least 2 fold increase in activity: *cusC* (through CusS, 100 µM $CuSO_4$), *ompC* (EnvZ, 500 mM NaCl) *ytfE* (NarQX, 100 mM $NaNO_2$) and *zraP* (HydH, 1 mM $ZnSO_4$). Six promotors exhibited a significant decrease in activity upon stimulation with a chemical cue, leading to a residual activity of about 50 %: *citC* (CitA, 10 mM Citrate), *fdnG* (NarQX, 100 mM $NaNO_3$ and 2 mM Fumarate), *glnA* (NtrB, 0.03 µM α-ketoglutarate), *nrfA* (NarQX, 100 mM $NaNO_2$), *phoA* (PhoQR, 2 mM Fumarate) and *ygjJ* (BasS, 500 µM $FeSO_4$). Compared to the results from complementation experiments (Figure 3.14), only *fdnG* and *phoA* showed a response to their stimulus. The other the complementing promotors did not show any change in gene expression upon stimulation. For all identified cases, these results provide us a downstream readout for a number of two-component pathways, allowing their further

characterization in for example stimulus dependent FRET experiments. Nevertheless, the majority of tested promotors did not show a significant response upon stimulation. The reason might be the application time of the stimulus, which was added to the liquid culture for 30-45 minutes. For some processes this might be too short to elicit a response. Another explanation could be that the documented stimuli have no effect on the two-component systems as reported before. In some cases, negative results might be due to the growth conditions, as we used minimal A medium and aerobic conditions for all samples. This might have a negative effect on the gene expression of some TCS proteins.

4 Discussion

Prokaryotes occupy all possible habitats in earths biosphere and developed several different ways of signal perception and transmission. Successful information processing allows for adaptation, maintenance of their viability, and the movement towards more favourable conditions. Two-component systems are the most widespread signaling pathways in prokaryotes and can be found in nearly all bacteria and archaea. The relatively simple layout of these systems and the modularity in their architecture makes them suitable to study basic principles of signal transduction. There is a high degree of homology between different systems and even organisms. A detailed understanding of the mechanisms of *E. coli´*s two-component systems will lead to a system-wide view of the cells signaling and information processing properties. Furthermore, given the high degree of homology between systems of different organisms, such analysis will shed light on signaling performed in other prokaryotes. This knowledge can be used to better understand processes involved in virulence or pathogenicity and to construct novel signaling circuits and genetic networks in synthetic biology or metabolic engineering.

4.1 Fluorescent protein reporter fusions

4.1.1 Test of fluorescent proteins

Before we started to construct a library of fluorescently labelled proteins for our experiments, we performed a set of preliminary tests on different fluorophores. As there has been much optimization on fluorescence proteins being performed during the last years, the aim was to identify a combination of two fluorophores that works best in imaging, flow cytometry and our *in vivo* FRET applications. As comparison to the well known FRET-pair eYFP and eCFP, we tested additionally YPet and Venus as yellow, CyPet and Cerulean as cyan and mCherry as red fluorophore, respectively. Criteria to be fulfilled for the chosen proteins were the following: (i) improved brightness or photostability compared to the established ones, (ii) no tendency to form dimers between two fluorophores

(iii) combinations with emission- and excitation-spectra allowing FRET and (iv) spectral properties fitting to the filter sets in the existing fluorescence microscopes.

For the yellow fluorescent proteins we performed flow cytometry measurements over a wide range of expression levels (Figure 3.1a). The goal of these experiments was to determine the brightness of different yellow fusions and to identify the protein best suited for imaging and flow cytometry applications. The best performance was exhibited by YFP, which showed the highest signals for all expression levels. The optimized proteins Venus and YPet displayed lower and similar fluorescence intensities compared to YFP, respectively. This contradicts the results reporting a brightness of Venus nearly identical to the one of YFP, and YPet being around 60 % brighter than YFP [183]. In this review the brightness has been calculated as product between the molar extinction coefficient and the quantum yield determined for the different proteins. In a comparison of relative whole cell fluorescence of YFP, Venus and YPet [189], YFP displays 76 % and YPet 49 % of Venus´ fluorescence. This difference might be due to a low expression level of the improved fluorophores under our conditions, which leads to a decreased fluorescence to background ratio. Taken together, YFP showed stronger (or similar at higher expression levels) brightness in our hands compared to YPet and Venus, respectively.

To identify the best combination for our *in vivo* FRET applications, we compared donor fusions made to CheY and acceptor fusions made to CheZ, respectively (Figure 3.1b and Table 3.1). The pairs were tested for their energy transfer efficiency, represented by a decrease in the FRET ratio upon stimulation of the chemotaxis pathway using the chemoattractant serine [196]. This decrease is due to a change in the interaction between CheY and CheZ, and provides a direct and quantitave readout of the pathway activity. As reference we measured the FRET change between CheY-YFP and CheZ-CFP, which was about 20 % between unstimulated and stimulated cells. All other tested combinations showed a change in ratio about or below 12 %. Nguyen and co-workers described their pair YPet/CyPet to be especially optimized for *in vivo* FRET applications in a bacterial expression system [189], a fact which we could not confirm in our setup. The reason for this difference remains unclear. One explanation might be the low expression level of our fusions under the used conditions as dicussed above. Additionally, the ratio between the donor and acceptor fluorophores might not be optimal, which results in a low FRET efficiency. In case of the non-cognate conbinations, additionally the fluorophore properties might not match to ensure an efficient energy transfer between protein.

Taken together, our preliminary experiments using flow cytometry and FRET identified YFP and CFP as the best candidates to be used in our setups. Therefore we made all protein fusions for the plasmid library using these two fluorophores.

4.1.2 Plasmid library of fluorescent labelled proteins

We constructed a comprehensive library of plasmids encoding histidine kinases and response regulators fused to either YFP or CFP, respectively. Out of the 28 histidine kinases present in *E. coli*, we made YFP and CFP fusions to 27 of them under control of a pTrc promotor and 24 kinase-*cfp* fusions under control of a pBAD promotor. The other kinases were not included as cloning failed in several attempts. For the 30 response regulators we made 26 protein fusions, the residual regulators have not been included due to cloning problems. We left out CheA and CheY from our library, because they are part of a non-canonical two-component system.

We tested the protein fusions for their full-length expression and the amount of protein degradation using SDS-PAGE and immunoblotting with an anti-GFP antibody (Figure 3.3 and Table 3.2). The majority of kinase fusions displayed protein degradation below 60 %; only three were excluded from further investigations because of extensive protein degration. A change in the linker sequence could probably solve the degradation problem in future experiments. The response regulator fusions were tested in a similar fashion (Table 3.2), all of them showed degradation below 33 %. This means that there was no limitation in using the regulator fusions in further experiments. Generally, the sensor kinases showed a higher amount of protein degradation in contrast to the response regulators. This was expected, given that for membrane proteins there is a much higher probability to interfere with proper folding by adding a fluorophore.

So far, only little is known about the copy numbers of two-component proteins in bacteria. There have been a few studies showing that kinases are in relative low abundance compared to regulators, with ratios between 1:30 or 1:50 [93, 95]. The total numbers have been estimated to 100 and 1000 copies for the sensors EnvZ and KdpD, respectively, and around 3500 for the regulators OmpR and KdpE [91, 93]. It has been suggested that the copy numbers derived for EnvZ and OmpR are representative for other two-component systems [94]. We constructed three chromosomal kinase-YFP fusions (to *baeS*, *citA* and *cusS*) to be able to estimate their native expression level. Under our conditions, the fusions exhibited copy numbers between 300 and 600 molecules per cell. This leads us to the conclusion that a number of 100 kinase copies per cell might be an underestimation, and this is further confirmed by the results derived from the plasmid based measurements discussed below.

To estimate the expression level of the plasmid based HK- and RR-fusions, we performed flow cytometry measurements using the YFP fusions. The motivation behind these experiments was to derive reliable copy numbers which allowed us to adjust the protein ratio in

our FRET experiments, especially for the sensor heterodimer experiments (Figure 3.8) and the kinase-regulator measurements (Section 3.6). Surprisingly, we found a copy number variation over four and five orders of magnitude for sensors and regulators, respectively (Figure 3.4). The total numbers are between 200 and 24000 sensors and between 300 and 154000 regulators per cell. Remarkably, all fusions were cloned under the same ribosome binding site and under control of the pTrc promotor. In addition, we did not use any inducer in all experiments, the protein expression is due to the leakyness of the pTrc promotor. We think the reasons for these variations are a different codon usage between the proteins, which leads to difference in gene expression. In addition, there might be formation of mRNA secondary structures or differences in translational efficiency between the proteins. leding to a variation in the protein copy numbers. Even though these numbers cannot be directly used to determine the native copy numbers, we assume that large differences between protein numbers might also occur for wildtype proteins. Additionally, as EnvZ exhibited the lowest value in our assay, we think that 100 sensors per cell might be a lower limit of sensor numbers for other two-component systems. We therefore adjusted the protein expression for our further experiments to about 2000 copies for the kinases and about 5000 copies for the regulators, except for a few constructs which showed already higher expression levels without induction. We assume that this corresponds to about 10 fold or less protein overexpression above the native level in our FRET assays. In this range, we can rule out false positive results because of random protein collisions or a high protein density inside the cytoplasmic membrane, which leads to unspecific FRET interactions.

4.2 Sensor localization

Distinct localization of cellular components plays a significant role in different processes. Similar to eukaryotes, in some cases bacteria make use of higher-order structures. Especially for components of signaling pathways, distinct protein localization could ensure functionality of information processing and isolation against interference with other pathways. This holds true even though clustering might not be obvious for proteins sensing environmental cues, which occur more or less homogenously distributed in the cell´s sorroundings. There are some studies performed on the localization of two-component signaling components in *E. coli* and other bacteria such as *C. crescentus* and *R. sphaeroides* [158, 162, 159, 92, 176, 163, 169, 111]. However, a comprehensive characterization of all TCS present in a bacterial cell remains elusive. We therefore performed fluorescence imaging experiments with YFP fusions to the sensor kinases and response regulators to identify their localization inside the cell (Section 1.4).

Figure 3.5 shows an overview of histidine kinase localization, and we found three different kinds of localization pattern. A group of nine sensors showed an uniform distribution around the cell periphery, indicating a homogenous insertion into the periplasmic membrane without any spatial preference to form higher order structures (Figure 3.5a). The distribution seems to be an intrinsic property of these sensors, as it was observed under a variety of different conditions we tested. The largest group of sensors showed a distribution which can be described as punctuated localization, representing a homogenous sensor arrangement with additional small clusters formed in the cytoplasmic membrane (Figure 3.5c and Table 3.5). Some of these kinases showed punctuated localization under all conditions tested, hinting at intrinsic protein properties responsible for the formation of higher-order clusters. The sensors BaeS, CitA, CpxA, CusS, EnvZ and PhoQ exhibited different localization dependent on growth medium. One explanation could be differences in media composition can effect localization. However, catabolite repression can be excluded in most cases, as minimal media samples containing glucose had no effect on localization compared to those containing glycerol. Another reason might be that protein expression was weaker in LB compared to other media due to faster cell growth. As proteins are less abundant, this could explain the spotted localization pattern in LB in contrast to a homogenous distribution in other media, where the sensor expression is higher. This seems to be true for CitA, CpxA and PhoQ. Another explanation might be the changed membrane composition upon different growth conditions. The formation of different lipid domains might favour clustering of some sensors into specific membrane compartments. The effect of stimulus on localization was only visible for two proteins, HydH and PhoR, suggesting that for the majority of sensors stimulation has no effect on the spatial organization. HydH and PhoR are involved in sensing of the bivalent cations Zn^{2+} and Mg^{2+}, respectively. An explanation might be a spatial coordination of different sensor dimers through the charge of these ions, which might induce the formation of clusters upon stimulation. In nearly all cases localization in wildtype and knockout cells were identical, suggesting that presence of the unlabeled sensor has no effect localization. The third localization pattern we observed for EvgS and TorS, both exhibit a pattern of distinct protein localization mainly at the cell poles (Figure 3.5b). The occurence of sensor clusters is independent of the experimental conditions (Table 3.5). Since dimerization mediated by the monomeric fluorophores is unlikely, localization seems to represent an intrinsic property of the proteins. This is confirmed by additional experiments from our colloborators in the Vaknin group. Using fluorescence polarization measurements on YFP labelled TorS and EvgS, they could show that both protein fusions exhibited low anisotropy values (Sommer *et al.*, in preparation and Ady Vaknin, personal communication). As fluorescence anisotropy is sensitive

to fluorophore distance and the occurence of homo-FRET reduces steady state anisotropy [222, 223], these results demonstrate a high affinity for molecular self-association for both sensors. Additionally, they could confirm specificity of TorS clustering performing co-localization studies with the cognate response regulator TorR and the periplasmic binding protein TorT, which showed specific clustered co-localization in presence of the kinase. To our knowledge, this localization pattern has not been reported so far in the literature. The next question is the physiological meaning behind this sensor complex formation. TorS senses trimethylamin-N-oxid (TMANO) and subsequently activates the *torCAD* operon, encoding the TMANO anaerobic respiration system [224]. TorS is a unorthodox kinase with a four-step phosphorelay to provide additional regulatory checkpoints [225], and is member of a sensor subfamily including EvgS, ArcB and BvgS from *Bordetella pertussis*. EvgS is involved in the acid and multidrug resistance of *E. coli*, but a specific stimulus is unknown to date [114]. Bock and co-workers showed that EvgS *in vitro* responds to oxidized ubiquinone-0, which is part of the electron transport chain [226]. ArcB and BvgS are involved in switching between anaerobic and aerobic conditions and in quinone signaling, respectively. Taken together, this might suggest co-localization of EvgS and TorS to components of the respiration chain localized in the cytoplasmic membrane, which we will try to varify in future experiments. Unfortunately, our ArcB-YFP fusion showed a strong amount of degradation (Table 3.2), thus it was not possible to test the localization pattern of another kinase in this subgroup. We were not able to reproduce the same localization pattern observed by Scheu and co-workers for DcuS and CitA, which showed polar spots distinct from chemotaxis receptor clusters [169]. In our hands, CitA formed small clusters distributed around the cell, which did not exclusively localize to the poles. A reason for this might be a difference in the background strain, which has an effect on the localization pattern. For DcuS we saw a homogenous localization around the cell periphery. In contrast, our collaborators saw the formation of polar regulator DcuB-YFP clusters in presence of the unlabeled kinase (A. Vaknin, personal communication). The explanation for this difference might be steric hindrance of the fused proteins due to the attached fluorophores, hindering the self-association of DcuS. Taken together, our results show that protein clustering is not only a property of protein complexes involved in cell motility [161], it can also occur in other signaling circuits regulating metabolic processes.

4.3 Protein interactions and promotor activation within pathways

Sensor histidine kinases are thought to form homodimers, which are facilitated through the cytoplasmic DHp domain located between the HAMP and CA domains. There were several studies performed *in vitro* which confirmed homodimerization by providing biochemical and structural data [39, 41, 42, 40, 43]. Noteworthy, this seems not to be the case for all existing two-component sensors, as there is at least one example of a monomeric sensor kinase present in *B. subtilis* [44].

4.3.1 Histidine kinase interactions

To verify homooligomerization for the different kinase fusions, we performed acceptor photobleaching FRET measurements on 21 different sensor pairs (Figure 3.7). We could identify a significant FRET signal for 12 of the measured pairs, which strongly indicates the formation of dimers or higher-order oligomers between the sensors. Currently, our setup does not provide a spatial resolution on the molecular level, and we cannot distinguish between the occurence of dimers or higher-order oligomers. To investigate this in more detail, we will perform co-localization experiments on the positives in future experiments. The identified interactions are likely to be specific, as we performed our experiments in wild-type strains with expression levels of several thousand copies per cell. Only above $\backsim$40000 copies sensors start to form unspecific interactions because of the density of proteins inserted into the membrane. This has been shown by our collaboration partner with titration experiments using fluorescence anisotropy measurements (A. Vaknin, personal communication). There were also 9 pairs exhibiting no change in FRET, which may be due to intrinsic structural properties of the proteins. Given the distance dependence of FRET, energy transfer can only occur for intermolecular distances below 10 nm [192]. Therefore, the two fluorophores might be too far apart for sensors exhibiting a large size, which prevents energy transfer between YFP and CFP. To circumvent false negative results, one possibility is to construct truncated sensor fusions, as it was successfully performed for the chemoreceptor Tar from *E. coli* chemotaxis [155, 207]. One drawback might be the loss of signaling functionality, as the DHp domain responsible for dimerization (and therefore the best target for labelling) lies N-terminal of the catalytic ATPase domain providing the phosphoryl group required for kinase autophosphorylation. Therefore, a C-terminal truncation may have a negative impact on the signaling properties, but could resolve the question about dimerization properties *in vivo*.

Next, we were interested in characterizing the kinetics of conformational changes of sensors taking place during signal transmission. Similar experiments have been performed extensively to characterize the signaling properties of chemoreceptors in *E. coli* [161, 194, 227]. To fit these measurements to our needs, there are a couple of requirements which have to be fulfilled by the systems we want to investigate. One prerequisite is a change in FRET signal in our acceptor photobleaching setup, showing the general functionality of the fusions. Another requirement is the availability of a defined stimulus for activating the systems, and for the simplest application this should be a non-toxic chemical. In addition, application of a stimulus has to induce a conformational change within the kinase dimer, which is large enough to have an impact on the energy transfer between the two fluorophores.

We tested a range of different kinases with a variety of stimuli documented to activate the individual systems (Table 3.7), and identified BaeS and CitA responding to their stimuli $CuSO_4$ and citrate, respectively. CitA showed a very weak response to 1 and 10 mM citrate (Figure 3.10), with the applied concentrations being in the order of magnitude of the literature value [169]. BaeS responded to different concentrations of $CuSO_4$ in a concentration dependent manner between 50 nM and 30 µM of stimulus (Figure 3.9). The clear response allowed us to measure a dose response curve of the BaeS sensor upon stimulation, which is depicted in Figure 3.9b. From the Hill-fit applied to the measured values, we could determine a $K_{1/2}$ for the conformational change of the kinase *in vivo* of about 1.2 µM. We detected a dynamic range of the signaling system between 10 nM and 10 µM. BaeS has been reported to react on 2 mM of $CuSO_4$in a β-galactosidase assay, an order of magnitude higher compared to our results [212]. A possible explanation might be the higher sensitivity of the confirmational change exhibited by BaeS compared to the donwnstream effect on gene regulation.

4.3.2 Sensor-response regulator interactions

In the next step we investigated interactions a step further in the signaling cascade, between histidine kinases and response regulators. We focused on a subset of ten pairs and we identified 8 kinase-regulator pairs which exhibited a change in FRET upon YFP bleaching (Table 3.8), confirming an interaction between the sensor and regulator *in vivo*. Most of these pairs displayed a change in FRET in both orientations (HK-YFP/RR-CFP and HK-CFP/RR-YFP), strenghtening the findings as specific interactions. As expected, almost all positives exhibited a FRET change of 1 % or more, which represents a strong interaction for the cognate pairs.

The 8 identified kinase-regulator pairs were subsequently tested for response to their reported stimuli, excluding CpxAR and YedVW, as they lack well defined stimuli [228, 229]. We identified only BaeS/BaeR responding to 2 mM of indole (Figure 3.12), all other systems displayed no response (Table 3.10). For BaeSR, further experiments are required to perform a similar characterization of concentration-dependent protein kinetics as performed for the sensor interactions discussed before (Figure 3.9). Surprisingly, we could not stimulate the interaction using $CuSO_4$ as in the stimulus dependent sensor measurements discussed before. Also applying indole as stimulus on the sensor did not show any effect on the kinetics. We do not have a good explanation for this difference in behaviour of the pathway between individual experiments. It is possible that the signaling mechanisms for copper and indole sensing are different, with distinct conformational changes of the kinase dependent on the applied substance.

4.3.3 Promotor activation upon stimulation

As the performed stimulus dependent FRET experiments showed no responses in most of the cases, we investigated the effect of sensor stimuli on the activity of TCS regulated promotors. We focused on the subset of positively tested TCS depicted in the heatmap (Figure 3.8) and investigated the promotor activation by using chemical stimuli reported for the single systems (Table 3.12). We identified a few examples where we could measure a significant change in promotor activity (Figure 3.16). An upregulation of at least twofold was detected for *cusC* (from CusSR pathway) in response to $CuSO_4$, for *ompC* (EnvZ/OmpR) responding to NaCl, for *ytfE* (NarXL) in response to $NaNO_2$ and for *zraP* (HydHG) increasing on $ZnSO_4$ application. For a set of six promotors we saw a significant decrease in promotor activity of about 50 %. These promotors include *citC* (from CitAB pathway) responding to citrate, *fdnG* (NarQP) responding to nitrate and fumarate, *glnA* (NtrB) responding to α-ketoglutarate, *nrfA* (NarQP) reacting on nitrite, *phoA* (PhoQP) on fumarate and *ygjJ* (BasSR) on ferric sulfate. For these systems we now have substances available which can be used to activate or inhibit the certain pathways, especially in further stimulus dependent FRET experiments to study pathway dynamics of two-component systems. Though, for the majority of investigated promotors, regulation was very weak and in the range of the background activity without stimulus. Other promotors which are reported to be activated or repressed by a certain pathway did not show any significant change in their activity. This can be explained by the applied substance not acting on the pathway as it was reported before, and would explain the negative responses in our stimulus-dependent FRET experiments. Another explanation might be the time scale of

the promotor response, with an application time between 30 and 45 minutes to the liquid culture was too short to trigger an intracellular response. In some cases, negative results might be due to the growth conditions. We incubated all samples aerobically in minimal A medium, which might have a negative effect on the gene expression of some TCS proteins.

4.4 Pathway interconnections and cross-talk

Given the structural and functional redundancies among individual two-component systems, the possibility of interconnections between different signaling pathways is an interesting question. A certain degree of cross-regulation between pathways would enable cells to integrate signals from various sources, providing another layer of information processing and a more sophisticated regulation of metabolic processes. There are some *in vivo* and *in vitro* studies reporting the occurence of cross-regulation between *E. coli* TCS pathways through auxiliary proteins [113, 114] and direct cross-talk [80, 134, 230, 136, 94]. However, a systematic *in vivo* screen has not been performed so far.

4.4.1 Cross-talk between histidine kinases

One possibility where cross-talk between two-component pathways can take place is on the level of histidine kinases. Therefore, we investigated the interactions between different sensors using our acceptor photobleaching FRET approach. We focused on the set of kinases which showed interactions in the dimer screen performed before (Figure 3.7). The results are depicted in Figure 3.8. We identified 9 hetero-interactions between different sensors, which represents 12.5 % of the tested combinations. The interacting sensor pairs are summarized in Figure 4.1a. It should be mentioned that some interactions were observed in one orientation, only. This most probably results from differences in the expression levels between the fusions. The FRET setup is sensitive to the YFP/CFP ratio, for an effective energy transfer between the fluorophores the number of YFP molecules should be in slight excess compared to CFP. Otherwise, FRET occurs less efficiently, which leads to false negative results. For the identified interactions there are several possible explanations. One is the formation of heterodimers between the different kinases. This is a real possibility given that sensors show a high degree of structural conservation [27], and heterodimerization has already been described for the two histidine kinases RetS and GacS from *P. aeruginosa* virulence regulation [137]. Another explanation would be the formation of higher-order complexes similar to the non-canonical two-component system in *E. coli* chemotaxis [161].

These complexes are multi-protein clusters including sensors and kinases which localize in distinct polar and lateral spots. In this case, identified interactions would represent clustered signaling complexes between different sensor homodimers. Even though we could not see a distinct localization pattern, we found for the pairs CpxA/CitA and CpxA/PhoQ a spotted localization indicating possible complex formation (Figure 3.5).

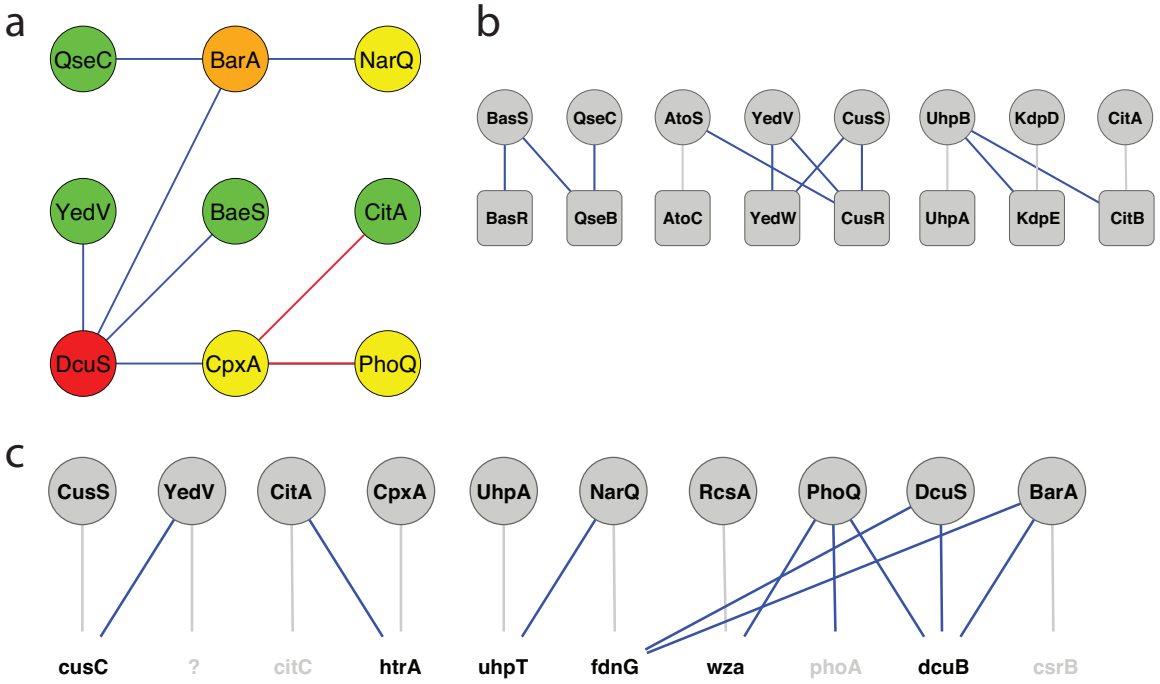

Figure 4.1: **Overview *in vivo* cross-talk between two-component systems.** (**a**) Cross-talk between different sensor kinases identified using acceptor photobleaching FRET. Node colour represents degree of interconnection, increasing from green to red. Blue edges show interactions, red edges represent interactions confirmed with stimulus dependent FRET. (**b**) Kinase-regulator cross-talk from acceptor photobleaching FRET experiments. Circles represent sensors, squares represent regulators. Blue edges show identified interactions. (**c**) Cross-talk on non-cognate promotors, determined by complementation and overexpression screens using flow cytometry. Circles represent sensors, letters represent promotors. Blue edges show identified (cross-)regulation. Networks were visualized using Cytoscape [231].

Noteworthy, we cannot distinguish between the formation of dimers or higher-order complexes in our setup due to the limitation in spatial resolution. To examine this further experiments are required, for example the investigation of co-localization between the different sensors. Where available or identified (Figure 3.16), we tested chemical stimuli on the sensor hetero-pairs established in the cross-talk screen. We found a response for

the two pairs CitA/CpxA and CpxA/PhoQ (Figure 3.11). In both cases, we did not use a stimulus for CpxA, as envelope protein misfolding is difficult to apply in a quantitative way and different pH values change fluorescence signals during our FRET measurements. Using citrate and $MgSO_4$, respectively, both pairs showed a specific response in sensor-sensor interactions (Figure 3.11b). It is not clear why the other pairs did not respond in our setup. Sensors might not perform a large conformational change upon stimulation which is required for FRET, or the reported stimuli may have no effects on the pathways (as discussed above).

As confirmation of the results from FRET experiments, we could verify the physiological relevance of sensor interactions in the case of DcuS/NarQ, DcuS/PhoQ, DcuS/BarA and CitA/CpxA (summarized in Figure 4.1c). We confirmed a significant effect on the non-cognate promotor activity in kinase knockouts (Figure 3.15), and after complementation with the kinase-fusion wildtype promotor activity recovered. These experiments will be expanded by testing cross-regulation on the promotor level using stimulation. The physiological meaning behind the identified interactions is not obvious for all pairs, as involved sensors react to a variety of signals (including bivalent cations, nitrate and nitrite, C_4-dicarboxylates, cell density, protein folding) or a defined stimulus is not known. However, for the kinases NarQ and DcuS an interconnection is plausible, as they regulate the *frd* operon encoding a fumarate reductase [230] and the fumarate respiratory gene *dcuB*, respectively[232]. Under anaerobic conditions, this might provide a mechanism for adjustment of the metabolism dependent on the availability of fumarate. CpxA and PhoQ regulate expression of the protein folding/degradation gene *htrA* and the *pag* operon for antimicrobial peptides, respectively [233, 234, 235]. Therefore, the physiological connection between the pathways despite their involvelment in stress response ist not clear .

Taken together, we were able to identify some interactions between pathways on the sensor level, which seem to be of physiological relevance. Nevertheless, there is a demand for further experiments to elucidate the detailed molecular mechanisms, and the remaining histidine kinases should be included to draw a comprehensive picture.

4.4.2 Cross-talk between sensors and response regulators

To extend our knowledge of the *E. coli* two-component network, we investigated cross-interactions between non-cognate histidine kinases and response regulators, which has been previously described *in vitro* for a few systems [80, 134, 230, 136, 94]. We chose a subset of sensor-regulator-pairs based on two available sources: identified proteins which performed cross-phosphorylation *in vitro* [136] and *in silico* predictions of interaction probabilites from

the van Nimwegen group ([127] and Erik van Nimwegen, personal communication). All combinations were tested in the orientation HK-CFP/RR-YFP, as CFP-fusion constructs are under control of a pBAD promotor, which enables tighter regulation of expression in contrast to the pTrc promotor controlling the YFP-constructs [200]. As regulators are more abundant compared to kinases, stronger leakiness in regulator-expression from the pTrc promotor should not have an impact on the FRET experiments favoured by the higher ratio of YFP to CFP.

Within the 38 interactions tested, we were able to identify six pairs exhibiting cross-talk between a kinase and a non-cognate regulator (summarized in Figure 4.1b). The reason for this small number of positives might be due to conceptual differences between the *in vitro* experiments/*in silico* predictions and our investigations. Yamamoto and co-workers used a phosphorylation assay with purified cytoplasmic kinase domains, only. As there is most likely an effect of the membrane on the sensor´s orientation, this might structurally inhibit cross-talk to non-cognate response regulators *in vivo*. In addition, the phosphorylation of purified proteins *in vitro* is probably more efficient compared to the one *in vivo*. The computational predictions rated the interaction probability between different TCS proteins, and are based on the co-variation of amino acids located in their interaction interfaces. The approach is therefore not able to depict the cellular environment in all details which might interfere with interactions.

For some identified cross-talk we have a possible physiological explanation. UhpB is a sensor for glucose-6-phosphate [220], and regulates the *uhpT* gene responsible for hexosephosphate uptake. CitB is involved in sensing of citrate and regulation of the *cit* operon for anaerobic citrate fermentation [236]. This connection might play a role in metabolic fine tuning dependent on the availability of energy sources under aerobic or anaerobic concditions. YedVW is a predicted two-component system, which function or stimuli are not well known, but may be involved in the *E. coli* metal homeostasis [136]. This is in agreement with our findings, showing an interconnection with the copper resistance system CusSR. We confirmed this pathway interconnection on the promotor level, as the YedV kinase has an influence on the *cusC* promotor (discussed below). In addition, the Vaknin group found that YedV responded to Cu^{2+} in their fluorescence anisotropy measurements (A. Vaknin, personal communication). Taken together, these results strongly suggests an interconnection between the two pathways, which provides a premise for further investigations.

4.4.3 Effects of cross-talk on gene expression

To verify and expand the list of cross-talking candidates identified in the FRET screens (Figure 3.8), we performed experiments involving the input and output of the pathways, i.e. sensor kinase and downstream promotor. We tested the effect of kinase overexpression on the activity of cognate and non-cognate promotors. These experiments are motivated by the sensor´s intrinsic kinase and phosphatase property [237]. Either these reactions can be increased by sensor overexpression, changing the ratio between kinase and regulator. Subsequently, this should lead to a change in transcriptional activity. This change in gene expression in dependence on phosphorylated RR concentration has been described earlier for various bacteria [79, 238, 239]. Additionally, it has been shown that the amount of cross-talk increases with sensor overexpression [80].

The results of kinase overexpression are depicted in Figure 3.13. We observed that, except the combinations DcuS/*dcuB* and NtrB/*glnA*, we could not detect any significant change in promotor activity upon overexpression of the cognate sensors as expected. The reason for this is probably the ratio between the sensor´s kinase and phosphatase activity, which might not change upon protein overexpression for some of the sensors. Additionally, the effects of kinase knockouts on promotor activity were stronger in contrast to kinase overexpression (Figure 3.15). Even though the cognate combinations did not show a general response, we identified three cases of non-cognate activation upon kinase overexpression (summarized in Figure 4.1c). YedV activated the *cusC* promotor from the copper resistance system CusSR [214], and relevance of this interaction could be confirmed by the HK-RR cross-talk results already discussed before. The strongest cross-activation was exhibited between NarQ from anaerobic respiration on *uhpT* from the glucose-6-phosphate sensing system UhpAB. This connection might reflect a metabolic fine-tuning dependent on the availability of oxygen. The promotor *wza* from the RcsAB system was strongly activated by PhoQ, but the physiological implication for this cross-talk between capsule synthesis and magnesium starvation pathways remains unclear.

5 Conclusion and outlook

The majority of prokaryotes use two-component signaling systems to sense a variety of intra- end extracellular signals. In this work we were able to characterize the spatial organization of sensor kinases and the interconnections between signaling pathways on different levels.

We found that most of the sensors exhibit a intrinsic tendency for cluster formation, which might provide a scaffold for information processing and insulates pathways against detrimental noise from other sources. For kinases, we could confirm the formation of sensor dimers or higher order oligomers *in vivo* for most of the two-component systems. For the sensor BaeS, we characterized the change of sensor confirmation upon stimulation. In addition, we identified two histidine kinases, TorS and EvgS, which exhibit a spotted localization pattern similar to those found for other multiprotein complexes like chemotaxis clusters. These results suggest the possibility, that clustering of histidine kinases can be beneficial not only for motility control, but plays moreover a role in the regulation of gene expression. Further experiments are required to uncover the nature of cluster formation in these cases. Co-localization studies on sensors will show if different kinases cluster into the same complexes, and the stability of kinase clusters will be investigated using FRAP (Fluorescence Recovery After Photobleaching) microscopy.

We found, at least within the tested pairs, a high degree of specificity between intracellular signaling circuits in *E. coli*, as it was already proposed in the literature. This is a necessity against detrimental interactions, interfering with proper signal transmission inside the cell. Nevertheless, we identified a few pathways exhibiting interconnections on the sensor level and between sensors and non-cognate regulators, providing an additional layer of information processing. Some of these pathway interconnections seem to be physiologically meaningful as we could show effects on the level of gene expression. For other systems, these experiments will be expanded with tests of cross-regulation on the promotor level using kinase knockouts and/or pathway stimulation. In addition, the screens for kinase-kinase and kinase-regulator inteactions will be expanded on all two-component system to draw a comprehensive picture of *E. coli* signaling.

6 Publications

Some of the results presented in this work are in preparation for article submission or have been presented during scientific meetings:

Publications

Sommer E, Koler M, Sourjik V, Vaknin A. Cellular organization of sensory histidine kinases in *Escherichia coli*. *In preparation*

Additional publications

Kuhn P, Weiche B, Sturm L, **Sommer E**, Drepper F, Warscheid B, Sourjik V, Koch HG. The bacterial SRP receptor, SecA and the ribosome use overlapping binding sites on the SecY translocon (2011) Traffic, 12: 563-578

Oral presentations

03/2011 VAAM Annual meeting, Karlsruhe, Germany. "Physical organization and interactions between sensory histidine kinases in *E. coli*."

Poster presentations

08/2011 DECHEMA/VAAM Summer School Biotransformations 2011, Bad Herrenalb, Germany. "Physical organization and interactions between sensory histidine kinases in *E. coli*."

03/2010 VAAM Annual meeting, Hannover, Germany. "Analysis of the two-component network in *E. coli*."

01/2010 Gordon Conference Sensory Transduction in Microorganisms, Ventura Beach, USA. "Analysis of the two-component network in *E. coli*."

03/2009 VAAM Annual meeting, Bochum, Germany. "*In vivo* study of the two-component signaling network in *E. coli*."

01/2009 Conference on Bacterial Locomotion and Signal Transduction, Cuernavaca, Mexico. "*In vivo* study of the two-component signaling network in *E. coli*."

List of Figures

List of Tables

Bibliography

[1] Polz, M.; Hunt, D. *Philosophical Transactions of the Royal Society* **2006**, *361*, 2009–2021.

[2] Whitman, W. B.; Coleman, D. C.; Wiebe, W. J. *Proc Natl Acad Sci USA* **1998**, *95*, 6578–83.

[3] Schloss, P. D.; Handelsman, J. *Microbiol Mol Biol Rev* **2004**, *68*, 686–91.

[4] Krämer, R.; Jung, K. *Bacterial Signaling*, 1st ed.; Wiley-VCH, 2010.

[5] Ulrich, L. E.; Koonin, E. V.; Zhulin, I. B. *Trends Microbiol* **2005**, *13*, 52–6.

[6] Deutscher, J.; Francke, C.; Postma, P. W. *Microbiol Mol Biol Rev* **2006**, *70*, 939–1031.

[7] Camilli, A.; Bassler, B. L. *Science* **2006**, *311*, 1113–6.

[8] Hengge, R. *Nat Rev Micro* **2009**, *7*, 263–73.

[9] Ng, W.-L.; Bassler, B. L. *Annu Rev Genet* **2009**, *43*, 197–222.

[10] Escherich, T. *Dtsch med Wochenschr* **1898**.

[11] Blattner, F. R.; Plunkett, G.; Bloch, C. A.; Perna, N. T.; Burland, V.; Riley, M.; Collado-Vides, J.; Glasner, J. D.; Rode, C. K.; Mayhew, G. F.; Gregor, J.; Davis, N. W.; Kirkpatrick, H. A.; Goeden, M. A.; Rose, D. J.; Mau, B.; Shao, Y. *Science* **1997**, *277*, 1453–62.

[12] Ulrich, L. E.; Zhulin, I. B. *Nucleic Acids Research* **2010**, *38*, D401–7.

[13] Stock, A. M.; Robinson, V. L.; Goudreau, P. N. *Annu Rev Biochem* **2000**, *69*, 183–215.

[14] Mizuno, T. *Biosci Biotechnol Biochem* **2005**, *69*, 2263–76.

[15] Mizuno, T. *DNA Research* **1997**, *4*, 161–8.

[16] Galperin, M. Y. *BMC Microbiol* **2005**, *5*, 35.

[17] Wolanin, P. M.; Thomason, P. A.; Stock, J. B. *Genome Biol* **2002**, *3*, REVIEWS3013.

[18] The C. elegans Sequencing Consortium *Science* **1998**, *282*, 2012–8.

[19] Adams, M. D.; Celniker, S. E.; Holt, R. A.; Evans, C. A.; et al. *Science* **2000**, *287*, 2185–95.

[20] Lander, E. S.; International Human Genome Sequencing Consortium *Nature* **2001**, *409*, 860–921.

[21] Barrett, J. F.; Hoch, J. A. *Antimicrob Agents Chemother* **1998**, *42*, 1529–36.

[22] Dutta, R.; Qin, L.; Inouye, M. *Molecular Microbiology* **1999**, *34*, 633–40.

[23] Mascher, T.; Helmann, J. D.; Unden, G. *Microbiology and Molecular Biology Reviews* **2006**, *70*, 910–938.

[24] Gao, R.; Stock, A. M. *Annu Rev Microbiol* **2009**, *63*, 133–54.

[25] Perego, M.; Hanstein, C.; Welsh, K. M.; Djavakhishvili, T.; Glaser, P.; Hoch, J. A. *Cell* **1994**, *79*, 1047–55.

[26] Kim, J.-R.; Cho, K.-H. *Comput Biol Chem* **2006**, *30*, 438–44.

[27] Grebe, T. W.; Stock, J. B. *Adv Microb Physiol* **1999**, *41*, 139–227.

[28] Gotoh, Y.; Eguchi, Y.; Watanabe, T.; Okamoto, S.; Doi, A.; Utsumi, R. *Current Opinion in Microbiology* **2010**, *13*, 232–9.

[29] Salis, H.; Tamsir, A.; Voigt, C. *Contrib Microbiol* **2009**, *16*, 194–225.

[30] Ninfa, A. J. *Current Opinion in Microbiology* **2010**, *13*, 240–5.

[31] Cheung, J.; Hendrickson, W. A. *Current Opinion in Microbiology* **2010**, *13*, 116–123.

[32] Sperandio, V.; Torres, A. G.; Jarvis, B.; Nataro, J. P.; Kaper, J. B. *Proc Natl Acad Sci USA* **2003**, *100*, 8951–6.

[33] Reinelt, S.; Hofmann, E.; Gerharz, T.; Bott, M.; Madden, D. R. *J Biol Chem* **2003**, *278*, 39189–96.

[34] Sevvana, M.; Vijayan, V.; Zweckstetter, M.; Reinelt, S.; Madden, D. R.; Herbst-Irmer, R.; Sheldrick, G. M.; Bott, M.; Griesinger, C.; Becker, S. *Journal of Molecular Biology* **2008**, *377*, 512–23.

[35] Taylor, B. L.; Zhulin, I. B.; Johnson, M. S. *Annu Rev Microbiol* **1999**, *53*, 103–28.

[36] Vreede, J.; van der Horst, M. A.; Hellingwerf, K. J.; Crielaard, W.; van Aalten, D. M. F. *J Biol Chem* **2003**, *278*, 18434–9.

[37] Cock, P. J. A.; Whitworth, D. E. *Mol Biol Evol* **2007**, *24*, 2355–7.

[38] Stewart, R. C. *Current Opinion in Microbiology* **2010**, *13*, 133–41.

[39] Surette, M. G.; Levit, M.; Liu, Y.; Lukat, G.; Ninfa, E. G.; Ninfa, A.; Stock, J. B. *J Biol Chem* **1996**, *271*, 939–45.

[40] Tomomori, C.; Tanaka, T.; Dutta, R.; Park, H.; Saha, S. K.; Zhu, Y.; Ishima, R.; Liu, D.; Tong, K. I.; Kurokawa, H.; Qian, H.; Inouye, M.; Ikura, M. *Nat Struct Biol* **1999**, *6*, 729–34.

[41] Heermann, R.; Altendorf, K.; Jung, K. *Biochim Biophys Acta* **1998**, *1415*, 114–24.

[42] Park, H.; Saha, S. K.; Inouye, M. *Proc Natl Acad Sci USA* **1998**, *95*, 6728–32.

[43] Purcell, E. B.; McDonald, C. A.; Palfey, B. A.; Crosson, S. *Biochemistry* **2010**, *49*, 6761–70.

[44] Fabret, C.; Feher, V. A.; Hoch, J. A. *Journal of Bacteriology* **1999**, *181*, 1975–83.

[45] Filippou, P. S.; Kasemian, L. D.; Panagiotidis, C. A.; Kyriakidis, D. A. *Biochim Biophys Acta* **2008**, *1780*, 1023–31.

[46] Cai, S.-J.; Inouye, M. *Journal of Molecular Biology* **2003**, *329*, 495–503.

[47] Ninfa, E. G.; Atkinson, M. R.; Kamberov, E. S.; Ninfa, A. J. *Journal of Bacteriology* **1993**, *175*, 7024–32.

[48] Swanson, R. V.; Bourret, R. B.; Simon, M. I. *Molecular Microbiology* **1993**, *8*, 435–41.

[49] Wolfe, A. J.; Stewart, R. C. *Proc Natl Acad Sci USA* **1993**, *90*, 1518–22.

[50] Casino, P.; Rubio, V.; Marina, A. *Cell* **2009**, *139*, 325–36.

[51] McCleary, W. R.; Zusman, D. R. *Journal of Bacteriology* **1990**, *172*, 6661–8.

[52] Potter, C. A.; Ward, A.; Laguri, C.; Williamson, M. P.; Henderson, P. J. F.; Phillips-Jones, M. K. *Journal of Molecular Biology* **2002**, *320*, 201–13.

[53] Shapiro, L.; Losick, R. *Science* **1997**, *276*, 712–8.

[54] Simms, S. A.; Keane, M. G.; Stock, J. *J Biol Chem* **1985**, *260*, 10161–8.

[55] Shaulsky, G.; Fuller, D.; Loomis, W. F. *Development* **1998**, *125*, 691–9.

[56] Thomason, P. A.; Traynor, D.; Cavet, G.; Chang, W. T.; Harwood, A. J.; Kay, R. R. *The EMBO Journal* **1998**, *17*, 2838–45.

[57] Bourret, R. B. *Current Opinion in Microbiology* **2010**, *13*, 142–149.

[58] Burbulys, D.; Trach, K. A.; Hoch, J. A. *Cell* **1991**, *64*, 545–52.

[59] Appleby, J. L.; Parkinson, J. S.; Bourret, R. B. *Cell* **1996**, *86*, 845–8.

[60] Stock, J. B.; Ninfa, A. J.; Stock, A. M. *Microbiol Rev* **1989**, *53*, 450–90.

[61] Volz, K.; Matsumura, P. *J Biol Chem* **1991**, *266*, 15511–9.

[62] Lukat, G. S.; McCleary, W. R.; Stock, A. M.; Stock, J. B. *Proc Natl Acad Sci USA* **1992**, *89*, 718–22.

[63] Stewart, R. C.; VanBruggen, R. *Biochemistry* **2004**, *43*, 8766–77.

[64] Janiak-Spens, F.; Cook, P. F.; West, A. H. *Biochemistry* **2005**, *44*, 377–86.

[65] Porter, S. L.; Armitage, J. P. *Journal of Molecular Biology* **2002**, *324*, 35–45.

[66] Jagadeesan, S.; Mann, P.; Schink, C. W.; Higgs, P. I. *J Biol Chem* **2009**, *284*, 21435–45.

[67] Zhao, R.; Collins, E. J.; Bourret, R. B.; Silversmith, R. E. *Nat Struct Biol* **2002**, *9*, 570–5.

[68] Pioszak, A. A.; Ninfa, A. J. *Journal of Bacteriology* **2004**, *186*, 5730–40.

[69] Pazy, Y.; Motaleb, M. A.; Guarnieri, M. T.; Charon, N. W.; Zhao, R.; Silversmith, R. E. *Proc Natl Acad Sci USA* **2010**, *107*, 1924–9.

[70] Martínez-Hackert, E.; Stock, A. M. *Journal of Molecular Biology* **1997**, *269*, 301–12.

[71] Baikalov, I.; Schröder, I.; Kaczor-Grzeskowiak, M.; Grzeskowiak, K.; Gunsalus, R. P.; Dickerson, R. E. *Biochemistry* **1996**, *35*, 11053–61.

[72] Weiss, D. S.; Batut, J.; Klose, K. E.; Keener, J.; Kustu, S. *Cell* **1991**, *67*, 155–67.

[73] Morett, E.; Segovia, L. *Journal of Bacteriology* **1993**, *175*, 6067–74.

[74] Osuna, J.; Soberón, X.; Morett, E. *Protein Sci* **1997**, *6*, 543–55.

[75] Goulian, M. *Current Opinion in Microbiology* **2010**, *13*, 184–9.

[76] Li, J.; Swanson, R. V.; Simon, M. I.; Weis, R. M. *Biochemistry* **1995**, *34*, 14626–36.

[77] Armitage, J. P. *Adv Microb Physiol* **1999**, *41*, 229–89.

[78] Szurmant, H.; Ordal, G. W. *Microbiol Mol Biol Rev* **2004**, *68*, 301–19.

[79] Jiang, M.; Shao, W.; Perego, M.; Hoch, J. A. *Molecular Microbiology* **2000**, *38*, 535–42.

[80] Ninfa, A. J.; Ninfa, E. G.; Lupas, A. N.; Stock, A.; Magasanik, B.; Stock, J. *Proc Natl Acad Sci USA* **1988**, *85*, 5492–6.

[81] Igo, M. M.; Ninfa, A. J.; Stock, J. B.; Silhavy, T. J. *Genes & Development* **1989**, *3*, 1725–34.

[82] Skerker, J. M.; Prasol, M. S.; Perchuk, B. S.; Biondi, E. G.; Laub, M. T. *Plos Biol* **2005**, *3*, e334.

[83] Biondi, E. G.; Reisinger, S. J.; Skerker, J. M.; Arif, M.; Perchuk, B. S.; Ryan, K. R.; Laub, M. T. *Nature* **2006**, *444*, 899–904.

[84] Groban, E. S.; Clarke, E. J.; Salis, H. M.; Miller, S. M.; Voigt, C. A. *Journal of Molecular Biology* **2009**, *390*, 380–393.

[85] Grimshaw, C. E.; Huang, S.; Hanstein, C. G.; Strauch, M. A.; Burbulys, D.; Wang, L.; Hoch, J. A.; Whiteley, J. M. *Biochemistry* **1998**, *37*, 1365–75.

[86] Fisher, S. L.; Jiang, W.; Wanner, B. L.; Walsh, C. T. *J Biol Chem* **1995**, *270*, 23143–9.

[87] Silva, J. C.; Haldimann, A.; Prahalad, M. K.; Walsh, C. T.; Wanner, B. L. *Proc Natl Acad Sci USA* **1998**, *95*, 11951–6.

[88] Siryaporn, A.; Goulian, M. *Molecular Microbiology* **2008**, *70*, 494–506.

[89] Siryaporn, A.; Perchuk, B. S.; Laub, M. T.; Goulian, M. *Mol Syst Biol* **2010**, *6*, 1–7.

[90] Wolfe, A. J. *Microbiology and Molecular Biology Reviews* **2005**, *69*, 12–50.

[91] Cai, S. J.; Inouye, M. *J Biol Chem* **2002**, *277*, 24155–61.

[92] Batchelor, E.; Goulian, M. *Proc Natl Acad Sci USA* **2003**, *100*, 691–6.

[93] Kremling, A.; Heermann, R.; Centler, F.; Jung, K.; Gilles, E. D. *BioSystems* **2004**, *78*, 23–37.

[94] Laub, M. T.; Goulian, M. *Annu Rev Genet* **2007**, *41*, 121–45.

[95] Miyashiro, T.; Goulian, M. *Proceedings of the National Academy of Sciences* **2008**, *105*, 17457–62.

[96] Wanner, B. L.; Latterell, P. *Genetics* **1980**, *96*, 353–66.

[97] Wanner, B. L.; Wilmes, M. R.; Young, D. C. *Journal of Bacteriology* **1988**, *170*, 1092–102.

[98] Amemura, M.; Makino, K.; Shinagawa, H.; Nakata, A. *Journal of Bacteriology* **1990**, *172*, 6300–7.

[99] Verhamme, D. T.; Arents, J. C.; Postma, P. W.; Crielaard, W.; Hellingwerf, K. J. *Microbiology (Reading, Engl)* **2002**, *148*, 69–78.

[100] Alves, R.; Savageau, M. A. *Molecular Microbiology* **2003**, *48*, 25–51.

[101] Koretke, K. K.; Lupas, A. N.; Warren, P. V.; Rosenberg, M.; Brown, J. R. *Mol Biol Evol* **2000**, *17*, 1956–70.

[102] Ohta, N.; Newton, A. *Journal of Bacteriology* **2003**, *185*, 4424–31.

[103] Seok, J.-S.; Kaplan, S.; Oh, J.-I. *Microbiology (Reading, Engl)* **2006**, *152*, 2479–90.

[104] Skerker, J. M.; Perchuk, B. S.; Siryaporn, A.; Lubin, E. A.; Ashenberg, O.; Goulian, M.; Laub, M. T. *Cell* **2008**, *133*, 1043–54.

[105] Allen, M. P.; Zumbrennen, K. B.; McCleary, W. R. *Journal of Bacteriology* **2001**, *183*, 2204–11.

[106] Bock, A.; Bantscheff, M.; Perraud, A. L.; Rippe, K.; Weiss, V.; Glocker, M. O.; Gross, R. *Journal of Molecular Biology* **2001**, *310*, 283–90.

[107] Howell, A.; Dubrac, S.; Andersen, K. K.; Noone, D.; Fert, J.; Msadek, T.; Devine, K. *Molecular Microbiology* **2003**, *49*, 1639–55.

[108] Robinson, V. L.; Wu, T.; Stock, A. M. *Journal of Bacteriology* **2003**, *185*, 4186–94.

[109] Walthers, D.; Tran, V. K.; Kenney, L. J. *Journal of Bacteriology* **2003**, *185*, 317–24.

[110] Wadhams, G. H.; Warren, A. V.; Martin, A. C.; Armitage, J. P. *Molecular Microbiology* **2003**, *50*, 763–70.

[111] Thanbichler, M. *Current Opinion in Microbiology* **2009**, *12*, 715–21.

[112] Tsokos, C. G.; Perchuk, B. S.; Laub, M. T. *Developmental Cell* **2011**, *20*, 329–41; JC, 19.07.11.

[113] Mitrophanov, A. Y.; Groisman, E. A. *Genes & Development* **2008**, *22*, 2601–2611.

[114] Eguchi, Y.; Ishii, E.; Hata, K.; Utsumi, R. *Journal of Bacteriology* **2011**, *193*, 1222–1228.

[115] Kox, L. F.; Wösten, M. M.; Groisman, E. A. *The EMBO Journal* **2000**, *19*, 1861–72.

[116] Kato, A.; Groisman, E. A. *Genes & Development* **2004**, *18*, 2302–13.

[117] Perego, M.; Hoch, J. A. *Proc Natl Acad Sci USA* **1996**, *93*, 1549–53.

[118] Hellingwerf, K. J.; Postma, P. W.; Tommassen, J.; Westerhoff, H. V. *FEMS Microbiol Rev* **1995**, *16*, 309–21.

[119] Hellingwerf, K. J. *Trends Microbiol* **2005**, *13*, 152–8.

[120] Bijlsma, J. J. E.; Groisman, E. A. *Trends Microbiol* **2003**, *11*, 359–66.

[121] Hoffer, S. M.; Westerhoff, H. V.; Hellingwerf, K. J.; Postma, P. W.; Tommassen, J. *Journal of Bacteriology* **2001**, *183*, 4914–7.

[122] Blauwkamp, T. A.; Ninfa, A. J. *Molecular Microbiology* **2003**, *48*, 1017–28.

[123] Brown, D. A.; Berg, H. C. *Proc Natl Acad Sci USA* **1974**, *71*, 1388–92.

[124] Aiso, T.; Ohki, R. *Genes Cells* **2003**, *8*, 179–87.

[125] Gunn, J. S.; Miller, S. I. *Journal of Bacteriology* **1996**, *178*, 6857–64.

[126] Volkman, B. F.; Lipson, D.; Wemmer, D. E.; Kern, D. *Science* **2001**, *291*, 2429–33.

[127] Burger, L.; Nimwegen, E. V. *Mol Syst Biol* **2008**, *4*, 1–14.

[128] Nixon, B. T.; Ronson, C. W.; Ausubel, F. M. *Proc Natl Acad Sci USA* **1986**, *83*, 7850–4.

[129] Grob, P.; Michel, P.; Hennecke, H.; Göttfert, M. *Mol Gen Genet* **1993**, *241*, 531–41.

[130] Matsubara, M.; Kitaoka, S. I.; Takeda, S. I.; Mizuno, T. *Genes Cells* **2000**, *5*, 555–69.

[131] Li, Y.-H.; Lau, P. C. Y.; Tang, N.; Svensäter, G.; Ellen, R. P.; Cvitkovitch, D. G. *Journal of Bacteriology* **2002**, *184*, 6333–42.

[132] Oka, A.; Sakai, H.; Iwakoshi, S. *Genes Genet Syst* **2002**, *77*, 383–91.

[133] Stewart, V.; Chen, L.-L.; Wu, H.-C. *Molecular Microbiology* **2003**, *50*, 1391–1399.

[134] Darwin, A. J.; Tyson, K. L.; Busby, S. J.; Stewart, V. *Molecular Microbiology* **1997**, *25*, 583–95.

[135] Howell, A.; Dubrac, S.; Noone, D.; Varughese, K. I.; Devine, K. *Molecular Microbiology* **2006**, *59*, 1199–215.

[136] Yamamoto, K.; Hirao, K.; Oshima, T.; Aiba, H.; Utsumi, R.; Ishihama, A. *J Biol Chem* **2005**, *280*, 1448–56.

[137] Goodman, A. L.; Merighi, M.; Hyodo, M.; Ventre, I.; Filloux, A.; Lory, S. *Genes & Development* **2009**, *23*, 249–59.

[138] Mouslim, C.; Latifi, T.; Groisman, E. A. *J Biol Chem* **2003**, *278*, 50588–95.

[139] Delgado, M. A.; Mouslim, C.; Groisman, E. A. *Molecular Microbiology* **2006**, *60*, 39–50.

[140] Batchelor, E.; Walthers, D.; Kenney, L. J.; Goulian, M. *Journal of Bacteriology* **2005**, *187*, 5723–31.

[141] Jubelin, G.; Vianney, A.; Beloin, C.; Ghigo, J.-M.; Lazzaroni, J.-C.; Lejeune, P.; Dorel, C. *Journal of Bacteriology* **2005**, *187*, 2038–49.

[142] Procaccini, A.; Lunt, B.; Szurmant, H.; Hwa, T.; Weigt, M. *PLoS ONE* **2011**, *6*, e19729.

[143] Li, L.; Shakhnovich, E. I.; Mirny, L. A. *Proc Natl Acad Sci USA* **2003**, *100*, 4463–8.

[144] Alm, E.; Huang, K.; Arkin, A. *PLoS Comput Biol* **2006**, *2*, e143.

[145] Rietkötter, E.; Hoyer, D.; Mascher, T. *Molecular Microbiology* **2008**, *68*, 768–85.

[146] Vendeville, A.; Larivière, D.; Fourmentin, E. *FEMS Microbiol Rev* **2011**, *35*, 395–414.

[147] Graumann, P. L. *Annu Rev Microbiol* **2007**, *61*, 589–618.

[148] Kentner, D.; Sourjik, V. *Annu Rev Microbiol* **2010**, *64*, 373–90.

[149] Marles-Wright, J.; Grant, T.; Delumeau, O.; van Duinen, G.; Firbank, S. J.; Lewis, P. J.; Murray, J. W.; Newman, J. A.; Quin, M. B.; Race, P. R.; Rohou, A.; Tichelaar, W.; van Heel, M.; Lewis, R. J. *Science* **2008**, *322*, 92–6.

[150] Zusman, D. R.; Scott, A. E.; Yang, Z.; Kirby, J. R. *Nat Rev Micro* **2007**, *5*, 862–72.

[151] Mignot, T.; Shaevitz, J. W. *Current Opinion in Microbiology* **2008**, *11*, 580–5.

[152] Leonardy, S.; Bulyha, I.; Søgaard-Andersen, L. *Mol Biosyst* **2008**, *4*, 1009–14.

[153] Mignot, T.; Merlie, J. P.; Zusman, D. R. *Science* **2005**, *310*, 855–7.

[154] Kaiser, D. *Annu Rev Genet* **2008**, *42*, 109–30.

[155] Kentner, D.; Thiem, S.; Hildenbeutel, M.; Sourjik, V. *Mol Microbiol* **2006**, *61*, 407–417.

[156] Hazelbauer, G. L.; Falke, J. J.; Parkinson, J. S. *Trends Biochem Sci* **2008**, *33*, 9–19.

[157] Neumann, S.; Hansen, C. H.; Wingreen, N. S.; Sourjik, V. *The EMBO Journal* **2010**, *29*, 3484–95.

[158] Maddock, J. R.; Shapiro, L. *Science* **1993**, *259*, 1717–23.

[159] Sourjik, V.; Berg, H. C. *Molecular Microbiology* **2000**, *37*, 740–51.

[160] Thiem, S.; Kentner, D.; Sourjik, V. *The EMBO Journal* **2007**, *26*, 1615–23.

[161] Sourjik, V. *Trends Microbiol* **2004**, *12*, 569–76.

[162] Gestwicki, J. E.; Lamanna, A. C.; Harshey, R. M.; McCarter, L. L.; Kiessling, L. L.; Adler, J. *Journal of Bacteriology* **2000**, *182*, 6499–502.

[163] Porter, S. L.; Wadhams, G. H.; Armitage, J. P. *Trends Microbiol* **2008**, *16*, 251–60.

[164] Collier, J.; Shapiro, L. *Curr Opin Biotechnol* **2007**, *18*, 333–40.

[165] Wheeler, R. T.; Shapiro, L. *Mol Cell* **1999**, *4*, 683–94.

[166] Jenal, U. *Res Microbiol* **2009**, *160*, 687–95.

[167] Lam, H.; Schofield, W. B.; Jacobs-Wagner, C. *Cell* **2006**, *124*, 1011–23.

[168] Fukushima, T.; Szurmant, H.; Kim, E.-J.; Perego, M.; Hoch, J. A. *Molecular Microbiology* **2008**, *69*, 621–632.

[169] Scheu, P.; Sdorra, S.; Liao, Y.-F.; Wegner, M.; Basche, T.; Unden, G.; Erker, W. *Microbiology* **2008**, *154*, 2463–2472.

[170] Golby, P.; Davies, S.; Kelly, D. J.; Guest, J. R.; Andrews, S. C. *Journal of Bacteriology* **1999**, *181*, 1238–48.

[171] Kaspar, S.; Perozzo, R.; Reinelt, S.; Meyer, M.; Pfister, K.; Scapozza, L.; Bott, M. *Molecular Microbiology* **1999**, *33*, 858–72.

[172] Boyd, J. M. *Molecular Microbiology* **2000**, *36*, 153–62.

[173] Mileykovskaya, E.; Dowhan, W. *Journal of Bacteriology* **2000**, *182*, 1172–5.

[174] Shiomi, D.; Margolin, W. *Journal of Bacteriology* **2007**, *189*, 236–43.

[175] Ramamurthi, K. S.; Losick, R. *Proc Natl Acad Sci USA* **2009**, *106*, 13541–5.

[176] Batchelor, E.; Goulian, M. *Mol Microbiol* **2006**, *59*, 1767–1778.

[177] Sciara, M. I.; Spagnuolo, C.; Jares-Erijman, E.; Véscovi, E. G. *Molecular Microbiology* **2008**, *70*, 479–493.

[178] Véscovi, E. G.; Sciara, M. I.; Castelli, M. E. *Current Opinion in Microbiology* **2010**, *13*, 210–218.

[179] Miyawaki, A. *Developmental Cell* **2003**, *4*, 295–305.

[180] Chalfie, M.; Tu, Y.; Euskirchen, G.; Ward, W. W.; Prasher, D. C. *Science* **1994**, *263*, 802–5.

[181] Tsien, R. Y. *Annu Rev Biochem* **1998**, *67*, 509–44.

[182] Matz, M. V.; Fradkov, A. F.; Labas, Y. A.; Savitsky, A. P.; Zaraisky, A. G.; Markelov, M. L.; Lukyanov, S. A. *Nat Biotechnol* **1999**, *17*, 969–73.

[183] Shaner, N. C.; Steinbach, P. A.; Tsien, R. Y. *Nat Meth* **2005**, *2*, 905–909.

[184] Giepmans, B. N. G.; Adams, S. R.; Ellisman, M. H.; Tsien, R. Y. *Science* **2006**, *312*, 217–24.

[185] Zaslaver, A.; Bren, A.; Ronen, M.; Itzkovitz, S.; Kikoin, I.; Shavit, S.; Liebermeister, W.; Surette, M. G.; Alon, U. *Nat Meth* **2006**, *3*, 623–628.

[186] Nagai, T.; Ibata, K.; Park, E. S.; Kubota, M.; Mikoshiba, K.; Miyawaki, A. *Nat Biotechnol* **2002**, *20*, 87–90.

[187] Rizzo, M. A.; Springer, G. H.; Granada, B.; Piston, D. W. *Nat Biotechnol* **2004**, *22*, 445–449.

[188] Shaner, N. C.; Campbell, R. E.; Steinbach, P. A.; Giepmans, B. N. G.; Palmer, A. E.; Tsien, R. Y. *Nat Biotechnol* **2004**, *22*, 1567–1572.

[189] Nguyen, A. W.; Daugherty, P. S. *Nat Biotechnol* **2005**, *23*, 355–360.

[190] Zacharias, D. A.; Violin, J. D.; Newton, A. C.; Tsien, R. Y. *Science* **2002**, *296*, 913–6.

[191] Cormack, B. P.; Valdivia, R. H.; Falkow, S. *Gene* **1996**, *173*, 33–8.

[192] Förster, T. *Annalen der Physik* **1948**, *437*, 55–75.

[193] Wouters, F. S.; Verveer, P. J.; Bastiaens, P. I. *Trends Cell Biol* **2001**, *11*, 203–11.

[194] Sourjik, V.; Vaknin, A.; Shimizu, T. S.; Berg, H. C. *Meth Enzymol* **2007**, *423*, 365–91.

[195] Selvin, P. R. *Meth Enzymol* **1995**, *246*, 300–34.

[196] Sourjik, V.; Berg, H. C. *Proc Natl Acad Sci USA* **2002**, *99*, 12669–74.

[197] Datsenko, K. A.; Wanner, B. L. *Proc Natl Acad Sci USA* **2000**, *97*, 6640–5.

[198] Baba, T.; Ara, T.; Hasegawa, M.; Takai, Y.; Okumura, Y.; Baba, M.; Datsenko, K. A.; Tomita, M.; Wanner, B. L.; Mori, H. *Mol Syst Biol* **2006**, *2*, 1–11.

[199] Cherepanov, P. P.; Wackernagel, W. *Gene* **1995**, *158*, 9–14.

[200] Guzman, L. M.; Belin, D.; Carson, M. J.; Beckwith, J. *Journal of Bacteriology* **1995**, *177*, 4121–30.

[201] Chung, C. T.; Niemela, S. L.; Miller, R. H. *Proc Natl Acad Sci USA* **1989**, *86*, 2172–5.

[202] Herring, C. D.; Glasner, J. D.; Blattner, F. R. *Gene* **2003**, *311*, 153–63.

[203] Laemmli, U. K. *Nature* **1970**, *227*, 680–5.

[204] Lugtenberg, B.; Meijers, J.; Peters, R.; van der Hoek, P.; van Alphen, L. *FEBS Lett* **1975**, *58*, 254–8.

[205] Miller, J. H. *A Short Course In Bacterial Genetics: A Laboratory Manual and Handbook for Escherichia coli and Related Bacteria*, 1st ed.; Cold Spring Harbor Laboratory Press, 1992; Vol. 1.

[206] Kollmann, M.; Løvdok, L.; Bartholomé, K.; Timmer, J.; Sourjik, V. *Nature* **2005**, *438*, 504–7.

[207] Kentner, D.; Sourjik, V. *Molecular Systems Biology* **2009**, *5*, 238.

[208] Dong, X.; Stothard, P.; Forsythe, I. J.; Wishart, D. S. *Nucleic Acids Research* **2004**, *32*, W660–4.

[209] Amann, E.; Ochs, B.; Abel, K. J. *Gene* **1988**, *69*, 301–15.

[210] Rodriguez, C.; Kwon, O.; Georgellis, D. *Journal of Bacteriology* **2004**, *186*, 2085–90.

[211] Theodorou, M. C.; Tiligada, E.; Kyriakidis, D. A. *Biochem. J.* **2009**, *417*, 667.

[212] Nishino, K.; Nikaido, E.; Yamaguchi, A. *Journal of Bacteriology* **2007**, *189*, 9066–9075.

[213] Hagiwara, D.; Yamashino, T.; Mizuno, T. *Biosci Biotechnol Biochem* **2004**, *68*, 1758–67.

[214] Munson, G. P.; Lam, D. L.; Outten, F. W.; O'Halloran, T. V. *Journal of Bacteriology* **2000**, *182*, 5864–71.

[215] Kleefeld, A.; Ackermann, B.; Bauer, J.; Kramer, J.; Unden, G. *Journal of Biological Chemistry* **2008**, *284*, 265–275.

[216] Leonhartsberger, S.; Huber, A.; Lottspeich, F.; Böck, A. *Journal of Molecular Biology* **2001**, *307*, 93–105.

[217] Atkinson, M. R.; Kamberov, E. S.; Weiss, R. L.; Ninfa, A. J. *J Biol Chem* **1994**, *269*, 28288–93.

[218] Minagawa, S.; Ogasawara, H.; Kato, A.; Yamamoto, K.; Eguchi, Y.; Oshima, T.; Mori, H.; Ishihama, A.; Utsumi, R. *Journal of Bacteriology* **2003**, *185*, 3696–702.

[219] Ansaldi, M.; Jourlin-Castelli, C.; Lepelletier, M.; Théraulaz, L.; Méjean, V. *Journal of Bacteriology* **2001**, *183*, 2691–5.

[220] Island, M. D.; Kadner, R. J. *Journal of Bacteriology* **1993**, *175*, 5028–34.

[221] Keseler, I. M.; Collado-Vides, J.; Gama-Castro, S.; Ingraham, J.; Paley, S.; Paulsen, I. T.; Peralta-Gil, M.; Karp, P. D. *Nucleic Acids Research* **2005**, *33*, D334–7.

[222] Vaknin, A.; Berg, H. C. *Proc Natl Acad Sci USA* **2006**, *103*, 592–6.

[223] Vaknin, A.; Berg, H. C. *Journal of Molecular Biology* **2007**, *366*, 1416–23.

[224] Méjean, V.; Iobbi-Nivol, C.; Lepelletier, M.; Giordano, G.; Chippaux, M.; Pascal, M. C. *Molecular Microbiology* **1994**, *11*, 1169–79.

[225] Jourlin, C.; Ansaldi, M.; Méjean, V. *Journal of Molecular Biology* **1997**, *267*, 770–7.

[226] Bock, A.; Gross, R. *Eur J Biochem* **2002**, *269*, 3479–84.

[227] Endres, R. G.; Oleksiuk, O.; Hansen, C. H.; Meir, Y.; Sourjik, V.; Wingreen, N. S. *Molecular Systems Biology* **2008**, *4*, 211.

[228] Yamamoto, K.; Ishihama, A. *Molecular Microbiology* **2005**, *56*, 215–227.

[229] Wolfe, A. J.; Parikh, N.; Lima, B. P.; Zemaitaitis, B. *Journal of Bacteriology* **2008**, *190*, 2314–2322.

[230] Stewart, V.; Bledsoe, P. J.; Williams, S. B. *Journal of Bacteriology* **2003**, *185*, 5862–70.

[231] Smoot, M. E.; Ono, K.; Ruscheinski, J.; Wang, P.-L.; Ideker, T. *Bioinformatics* **2011**, *27*, 431–2.

[232] Krämer, J.; Fischer, J. D.; Zientz, E.; Vijayan, V.; Griesinger, C.; Lupas, A.; Unden, G. *Journal of Bacteriology* **2007**, *189*, 4290–8.

[233] Fleischer, R.; Heermann, R.; Jung, K.; Hunke, S. *J Biol Chem* **2007**, *282*, 8583–93.

[234] Gunn, J. S.; Richards, S. M. *Cell Host Microbe* **2007**, *1*, 163–5.

[235] Prost, L. R.; Miller, S. I. *Cell Microbiol* **2008**, *10*, 576–82.

[236] Kaspar, S.; Bott, M. *Arch Microbiol* **2002**, *177*, 313–21.

[237] Kenney, L. J. *Current Opinion in Microbiology* **2010**, *13*, 168–176.

[238] Fujita, M.; Losick, R. *Genes & Development* **2005**, *19*, 2236–44.

[239] Waters, C. M.; Bassler, B. L. *Genes & Development* **2006**, *20*, 2754–67.

[240] Hanahan, D. *Journal of Molecular Biology* **1983**, *166*, 557–80.

Appendix

Table 6.1: **Plasmids used in this study.**

Plasmid	Vector	Gene(s)	Cloning sites	Marker	Induction	ORI	Source/reference
-	pUA66	*asr-gfp*	*Xho*I, *BamH*I	kan	-	pSC101	[185]
-	pUA66	*creA-gfp*	*Xho*I, *BamH*I	kan	-	pSC101	[185]
-	pUA66	*ygjJ-gfp*	*Xho*I, *BamH*I	kan	-	pSC101	[185]
-	pUA66	*tdcB-gfp*	*Xho*I, *BamH*I	kan	-	pSC101	[185]
pACBSR	-	I-*Sce*I, λ Red	-	cam	ara	p15A	[202]
pAE-1	pTrc99A	*cusS-yfp*	*Nco*I, *BamH*I	amp	IPTG	pBR	this work
pAM90	pUA66	*citC-gfp*	*Xho*I, *BamH*I	kan	-	pSC101	this work
pAM91	pUA66	*fdnG-gfp*	*Xho*I, *BamH*I	kan	-	pSC101	this work
pAM92	pUA66	*frdA-gfp*	*Xho*I, *BamH*I	kan	-	pSC101	this work
pAM93	pUA66	*sdhC-gfp*	*Xho*I, *BamH*I	kan	-	pSC101	this work
pAM95	pUA66	*glnA-gfp*	*Xho*I, *BamH*I	kan	-	pSC101	this work
pAM96	pUA66	*cusC-gfp*	*Xho*I, *BamH*I	kan	-	pSC101	this work
pAM97	pUA66	*uhpT-gfp*	*Xho*I, *BamH*I	kan	-	pSC101	this work
pAM100	pUA66	*citT-gfp*	*Xho*I, *BamH*I	kan	-	pSC101	this work
pAM101	pUA66	*zraP-gfp*	*Xho*I, *BamH*I	kan	-	pSC101	this work
pAM103	pUA66	*mdtA-gfp*	*Xho*I, *BamH*I	kan	-	pSC101	this work
pAM104	pUA66	*flhD-gfp*	*Xho*I, *BamH*I	kan	-	pSC101	this work
pAM106	pUA66	*pstS-gfp*	*Xho*I, *BamH*I	kan	-	pSC101	this work
pAM107	pUA66	*ompC-gfp*	*Xho*I, *BamH*I	kan	-	pSC101	this work
pAM108	pUA66	*phoA-gfp*	*Xho*I, *BamH*I	kan	-	pSC101	this work
pAM110	pUA66	*htrA-gfp*	*Xho*I, *BamH*I	kan	-	pSC101	this work
pAM111	pUA66	*nrfA-gfp*	*Xho*I, *BamH*I	kan	-	pSC101	this work

Plasmid	Vector	Gene(s)	Cloning sites	Marker	Induction	ORI	Source/reference
pAM102	pUA66	*dcuB-gfp*	*Xho*I, *BamH*I	kan	-	pSC101	this work
pES165	pBAD33	*ntrC-cfp*	*Spe*I, *Hin*dIII	cam	ara	pACYC	this work
pAM113	pUA66	*ytfE-gfp*	*Xho*I, *BamH*I	kan	-	pSC101	this work
pBAD33	-	expression plasmid	MCS	cam	ara	pACYC	[200]
pCP20	pMMC6	FLP^{+}	-	amp, cam	-	Rep^{ts}	[199]
pDK-112	pTrc99A	*frontlinker-yfp*	*Nco*I, *BamH*I	amp	IPTG	pBR	D. Kentner
pDK-113	pTrc99A	*frontlinker-cfp*	*Nco*I, *BamH*I	amp	IPTG	pBR	D. Kentner
pES15	pTrc99A	*cheY-venus*	*Sac*I, *Xba*I	amp	IPTG	pBR	this work
pES16	pTrc99A	*cheY-mCherry*	*Sac*I, *Xba*I	amp	IPTG	pBR	this work
pES17	pBAD33	*cheZ-cerulean*	*Sac*I, *Xba*I	cam	ara	pACYC	this work
pES18	pTrc99A	*cheY-YPet*	*Sac*I, *Xba*I	amp	IPTG	pBR	this work
pES19	pBAD33	*cheZ-CyPet*	*Sac*I, *Xba*I	cam	ara	pACYC	this work
pES20	pTrc99A	*baeS-yfp*	*Nco*I, *BamH*I	amp	IPTG	pBR	this work
pES21	pTrc99A	*uhpB-yfp*	*Nco*I, *BamH*I	amp	IPTG	pBR	this work
pES22	pTrc99A	*phoR-yfp*	*Nco*I, *BamH*I	amp	IPTG	pBR	this work
pES24	pTrc99A	*qseC-yfp*	*Nco*I, *BamH*I	amp	IPTG	pBR	this work
pES25	pTrc99A	*dcuS-yfp*	*Nco*I, *BamH*I	amp	IPTG	pBR	this work
pES26	pTrc99A	*rstB-yfp*	*Nco*I, *BamH*I	amp	IPTG	pBR	this work
pES27	pTrc99A	*envZ-yfp*	*Nco*I, *BamH*I	amp	IPTG	pBR	this work
pES28	pTrc99A	*cpxA-yfp*	*Nco*I, *BamH*I	amp	IPTG	pBR	this work
pES30	pTrc99A	*yedV-yfp*	*Nco*I, *BamH*I	amp	IPTG	pBR	this work
pES31	pTrc99A	*ypdA-yfp*	*Nco*I, *BamH*I	amp	IPTG	pBR	this work
pES32	pTrc99A	*narQ-yfp*	*Nco*I, *BamH*I	amp	IPTG	pBR	this work
pES33	pTrc99A	*narX-yfp*	*Nco*I, *BamH*I	amp	IPTG	pBR	this work
pES34	pTrc99A	*creC-yfp*	*Nco*I, *BamH*I	amp	IPTG	pBR	this work
pES35	pTrc99A	*ntrB-yfp*	*Nco*I, *BamH*I	amp	IPTG	pBR	this work

Plasmid	Vector	Gene(s)	Cloning sites	Marker	Induction	ORI	Source/reference
pAM102	pUA66	*dcuB-gfp*	*Xho*I, *BamH*I	kan	-	pSC101	this work
pES165	pBAD33	*ntrC-cfp*	*Spe*I, *Hin*dIII	cam	ara	pACYC	this work
pES37	pTrc99A	*citA-yfp*	*Nco*I, *Bgl*II	amp	IPTG	pBR	this work
pES38	pTrc99A	*basS-yfp*	*Nco*I, *BamH*I	amp	IPTG	pBR	this work
pES39	pTrc99A	*yfhk-yfp*	*Nco*I, *BamH*I	amp	IPTG	pBR	this work
pES40	pTrc99A	*atoS-yfp*	*Nco*I, *BamH*I	amp	IPTG	pBR	this work
pES41	pTrc99A	*kdpD-yfp*	*Nco*I, *BamH*I	amp	IPTG	pBR	this work
pES42	pTrc99A	*torS-yfp*	*Nco*I, *BamH*I	amp	IPTG	pBR	this work
pES43	pTrc99A	*phoQ-yfp*	*Nco*I, *BamH*I	amp	IPTG	pBR	this work
pES44	pTrc99A	*arcB-yfp*	*BspH*I, *BamH*I	amp	IPTG	pBR	this work
pES45	pTrc99A	*lytS-yfp*	*Nco*I, *BamH*I	amp	IPTG	pBR	this work
pES46	pTrc99A	*barA-yfp*	*Nco*I, *BamH*I	amp	IPTG	pBR	this work
pES47	pTrc99A	*baeS-cfp*	*Nco*I, *BamH*I	amp	IPTG	pBR	this work
pES48	pTrc99A	*uhpB-cfp*	*Nco*I, *BamH*I	amp	IPTG	pBR	this work
pES49	pTrc99A	*phoR-cfp*	*Nco*I, *BamH*I	amp	IPTG	pBR	this work
pES50	pTrc99A	*evgS-yfp*	*Nco*I, *BamH*I	amp	IPTG	pBR	this work
pES51	pTrc99A	*qseC-cfp*	*Nco*I, *BamH*I	amp	IPTG	pBR	this work
pES52	pTrc99A	*dcuS-cfp*	*Nco*I, *BamH*I	amp	IPTG	pBR	this work
pES53	pTrc99A	*cusS-cfp*	*Nco*I, *BamH*I	amp	IPTG	pBR	this work
pES55	pTrc99A	*rstB-cfp*	*Nco*I, *BamH*I	amp	IPTG	pBR	this work
pES56	pTrc99A	*envZ-cfp*	*Nco*I, *BamH*I	amp	IPTG	pBR	this work
pES57	pTrc99A	*cpxA-cfp*	*Nco*I, *BamH*I	amp	IPTG	pBR	this work
pES58	pTrc99A	*yedV-cfp*	*Nco*I, *BamH*I	amp	IPTG	pBR	this work
pES59	pTrc99A	*hydH-cfp*	*Nco*I, *BamH*I	amp	IPTG	pBR	this work
pES60	pTrc99A	*ypdA-cfp*	*Nco*I, *BamH*I	amp	IPTG	pBR	this work
pES61	pTrc99A	*narQ-cfp*	*Nco*I, *BamH*I	amp	IPTG	pBR	this work
pES62	pTrc99A	*narX-cfp*	*Nco*I, *BamH*I	amp	IPTG	pBR	this work
pES63	pTrc99A	*creC-cfp*	*Nco*I, *BamH*I	amp	IPTG	pBR	this work
pES64	pTrc99A	*ntrB-cfp*	*Nco*I, *BamH*I	amp	IPTG	pBR	this work
pES65	pTrc99A	*citA-cfp*	*Nco*I, *BamH*I	amp	IPTG	pBR	this work
pES66	pTrc99A	*basS-cfp*	*Nco*I, *BamH*I	amp	IPTG	pBR	this work
pES67	pTrc99A	*yfhK-cfp*	*Nco*I, *BamH*I	amp	IPTG	pBR	this work
pES68	pTrc99A	*atoS-cfp*	*Nco*I, *BamH*I	amp	IPTG	pBR	this work
pES70	pTrc99A	*torS-cfp*	*Nco*I, *BamH*I	amp	IPTG	pBR	this work

Plasmid	Vector	Gene(s)	Cloning sites	Marker	Induction	ORI	Source/reference
pAM102	pUA66	*dcuB-gfp*	*Xho*I, *BamH*I	kan	-	pSC101	this work
pES165	pBAD33	*ntrC-cfp*	*Spe*I, *Hin*dIII	cam	ara	pACYC	this work
pES71	pTrc99A	*phoQ-cfp*	*Nco*I, *BamH*I	amp	IPTG	pBR	this work
pES72	pTrc99A	*arcB-cfp*	*Spe*I, *BamH*I	amp	IPTG	pBR	this work
pES73	pTrc99A	*lytS-cfp*	*Nco*I, *BamH*I	amp	IPTG	pBR	this work
pES74	pTrc99A	*barA-cfp*	*Nco*I, *BamH*I	amp	IPTG	pBR	this work
pES75	pBAD33	*baeS-cfp*	*Spe*I, *Hin*dIII	cam	ara	pACYC	this work
pES76	pBAD33	*uhpB-cfp*	*Spe*I, *Hin*dIII	cam	ara	pACYC	this work
pES77	pBAD33	*phoR-cfp*	*Spe*I, *Hin*dIII	cam	ara	pACYC	this work
pES78	pTrc99A	*evgS-cfp*	*Nco*I, *BamH*I	amp	IPTG	pBR	this work
pES79	pBAD33	*qseC-cfp*	*Spe*I, *Hin*dIII	cam	ara	pACYC	this work
pES80	pBAD33	*dcuS-cfp*	*Spe*I, *Hin*dIII	cam	ara	pACYC	this work
pES81	pBAD33	*cusS-cfp*	*Spe*I, *Hin*dIII	cam	ara	pACYC	this work
pES83	pBAD33	*envZ-cfp*	*Spe*I, *Hin*dIII	cam	ara	pACYC	this work
pES84	pBAD33	*hydH-cfp*	*Spe*I, *Hin*dIII	cam	ara	pACYC	this work
pES85	pBAD33	*ypdA-cfp*	*Spe*I, *Hin*dIII	cam	ara	pACYC	this work
pES86	pBAD33	*narQ-cfp*	*Spe*I, *Hin*dIII	cam	ara	pACYC	this work
pES87	pBAD33	*yedV-cfp*	*Spe*I, *Hin*dIII	cam	ara	pACYC	this work
pES88	pBAD33	*creC-cfp*	*Spe*I, *Hin*dIII	cam	ara	pACYC	this work
pES89	pBAD33	*narX-cfp*	*Spe*I, *Hin*dIII	cam	ara	pACYC	this work
pES90	pBAD33	*ntrB-cfp*	*Spe*I, *Hin*dIII	cam	ara	pACYC	this work
pES91	pBAD33	*basS-cfp*	*Spe*I, *Hin*dIII	cam	ara	pACYC	this work
pES92	pBAD33	*yfhK-cfp*	*Spe*I, *Hin*dIII	cam	ara	pACYC	this work
pES93	pBAD33	*phoQ-cfp*	*Spe*I, *Hin*dIII	cam	ara	pACYC	this work
pES94	pBAD33	*cpxA-cfp*	*Spe*I, *Hin*dIII	cam	ara	pACYC	this work
pES95	pBAD33	*rstB-cfp*	*Spe*I, *Hin*dIII	cam	ara	pACYC	this work
pES96	pBAD33	*atoS-cfp*	*Spe*I, *Hin*dIII	cam	ara	pACYC	this work
pES97	pBAD33	*barA-cfp*	*Spe*I, *Hin*dIII	cam	ara	pACYC	this work
pES101	pBAD33	*arcB-cfp*	*Spe*I, *Hin*dIII	cam	ara	pACYC	this work
pES102	pBAD33	*torS-cfp*	*Spe*I, *Hin*dIII	cam	ara	pACYC	this work
pES103	pTrc99A	*ompR-yfp*	*Nco*I, *BamH*I	amp	IPTG	pBR	this work
pES104	pTrc99A	*arcA-yfp*	*Nco*I, *BamH*I	amp	IPTG	pBR	this work
pES105	pTrc99A	*kdpE-yfp*	*Nco*I, *Bgl*II	amp	IPTG	pBR	this work
pES107	pTrc99A	*torR-yfp*	*Nco*I, *BamH*I	amp	IPTG	pBR	this work

Plasmid	Vector	Gene(s)	Cloning sites	Marker	Induction	ORI	Source/reference
pAM102	pUA66	*dcuB-gfp*	*Xho*I, *BamH*I	kan	-	pSC101	this work
pES165	pBAD33	*ntrC-cfp*	*Spe*I, *Hin*dIII	cam	ara	pACYC	this work
pES108	pTrc99A	*phoP-yfp*	*Nco*I, *BamH*I	amp	IPTG	pBR	this work
pES109	pTrc99A	*phoB-yfp*	*Nco*I, *BamH*I	amp	IPTG	pBR	this work
pES110	pTrc99A	*cusR-yfp*	*Nco*I, *BamH*I	amp	IPTG	pBR	this work
pES111	pTrc99A	*basR-yfp*	*Nco*I, *BamH*I	amp	IPTG	pBR	this work
pES112	pTrc99A	*citB-yfp*	*Nco*I, *BamH*I	amp	IPTG	pBR	this work
pES113	pTrc99A	*evgA-yfp*	*Nco*I, *BamH*I	amp	IPTG	pBR	this work
pES114	pTrc99A	*qseB-yfp*	*Nco*I, *BamH*I	amp	IPTG	pBR	this work
pES115	pTrc99A	*cpxR-yfp*	*Nco*I, *BamH*I	amp	IPTG	pBR	this work
pES116	pTrc99A	*ypdB-yfp*	*Nco*I, *Bgl*II	amp	IPTG	pBR	this work
pES117	pTrc99A	*creB-yfp*	*Nco*I, *BamH*I	amp	IPTG	pBR	this work
pES119	pTrc99A	*uhpA-yfp*	*Nco*I, *BamH*I	amp	IPTG	pBR	this work
pES120	pTrc99A	*rstA-yfp*	*Nco*I, *BamH*I	amp	IPTG	pBR	this work
pES121	pTrc99A	*fimZ-yfp*	*Nco*I, *Bgl*II	amp	IPTG	pBR	this work
pES122	pTrc99A	*uvrY-yfp*	*BspH*I, *Bgl*II	amp	IPTG	pBR	this work
pES123	pTrc99A	*rcsB-yfp*	*Nco*I, *Bgl*II	amp	IPTG	pBR	this work
pES125	pTrc99A	*evgA-cfp*	*Nco*I, *BamH*I	amp	IPTG	pBR	this work
pES127	pTrc99A	*arcA-cfp*	*Nco*I, *BamH*I	amp	IPTG	pBR	this work
pES128	pTrc99A	*torR-cfp*	*Nco*I, *BamH*I	amp	IPTG	pBR	this work
pES129	pTrc99A	*phoP-cfp*	*Nco*I, *BamH*I	amp	IPTG	pBR	this work
pES130	pTrc99A	*phoB-cfp*	*Nco*I, *BamH*I	amp	IPTG	pBR	this work
pES131	pTrc99A	*basR-cfp*	*Nco*I, *BamH*I	amp	IPTG	pBR	this work
pES132	pTrc99A	*cpxR-cfp*	*Nco*I, *BamH*I	amp	IPTG	pBR	this work
pES133	pBAD33	*evgA-cfp*	*Spe*I, *Hin*dIII	cam	ara	pACYC	this work
pES134	pTrc99A	*rstA-cfp*	*Nco*I, *BamH*I	amp	IPTG	pBR	this work
pES135	pTrc99A	*yedW-yfp*	*Nco*I, *BamH*I	amp	IPTG	pBR	this work
pES136	pTrc99A	*citB-cfp*	*Nco*I, *BamH*I	amp	IPTG	pBR	this work
pES137	pTrc99A	*creB-cfp*	*Nco*I, *BamH*I	amp	IPTG	pBR	this work
pES138	pTrc99A	*cusR-cfp*	*Nco*I, *BamH*I	amp	IPTG	pBR	this work
pES139	pTrc99A	*ompR-cfp*	*Nco*I, *BamH*I	amp	IPTG	pBR	this work
pES140	pTrc99A	*qseB-cfp*	*Nco*I, *BamH*I	amp	IPTG	pBR	this work
pES141	pTrc99A	*yedW-cfp*	*Nco*I, *BamH*I	amp	IPTG	pBR	this work
pES142	pTrc99A	*dcuR-yfp*	*Nco*I, *Bgl*II	amp	IPTG	pBR	this work

Plasmid	Vector	Gene(s)	Cloning sites	Marker	Induction	ORI	Source/reference
pAM102	pUA66	*dcuB-gfp*	*Xho*I, *BamH*I	kan	-	pSC101	this work
pES165	pBAD33	*ntrC-cfp*	*Spe*I, *Hin*dIII	cam	ara	pACYC	this work
pES143	pTrc99A	*dcuR-cfp*	*Nco*I, *Bgl*II	amp	IPTG	pBR	this work
pES144	pBAD33	*arcA-cfp*	*Spe*I, *Hin*dIII	cam	ara	pACYC	this work
pES145	pBAD33	*torR-cfp*	*Spe*I, *Hin*dIII	cam	ara	pACYC	this work
pES146	pBAD33	*phoP-cfp*	*Spe*I, *Hin*dIII	cam	ara	pACYC	this work
pES147	pBAD33	*basR-cfp*	*Spe*I, *Hin*dIII	cam	ara	pACYC	this work
pES148	pBAD33	*qseB-cfp*	*Spe*I, *Hin*dIII	cam	ara	pACYC	this work
pES149	pBAD33	*yedW-cfp*	*Spe*I, *Hin*dIII	cam	ara	pACYC	this work
pES150	pTrc99A	*narP-yfp*	*Nco*I, *Bgl*II	amp	IPTG	pBR	this work
pES153	pBAD33	*citB-cfp*	*Spe*I, *Hin*dIII	cam	ara	pACYC	this work
pES154	pBAD33	*ompR-cfp*	*Spe*I, *Hin*dIII	cam	ara	pACYC	this work
pES155	pTrc99A	*uvrX-cfp*	*Bsp*HI, *BamH*I	amp	IPTG	pBR	this work
pES156	pBAD33	*citA-cfp*	*Spe*I, *Hin*dIII	cam	ara	pACYC	this work
pES159	pBAD33	*cpxR-cfp*	*Spe*I, *Hin*dIII	cam	ara	pACYC	this work
pES160	pBAD33	*uvrY-cfp*	*Spe*I, *Hin*dIII	cam	ara	pACYC	this work
pES163	pTrc99A	*ntrC-yfp*	*Nco*I, *Bgl*II	amp	IPTG	pBR	this work
pES164	pTrc99A	*ntrC-cfp*	*Nco*I, *Bgl*II	amp	IPTG	pBR	this work
pES166	pTrc99A	*narL-yfp*	*Nco*I, *BamH*I	amp	IPTG	pBR	this work
pES170	pTrc99A	*rssB-yfp*	*Nco*I, *BamH*I	amp	IPTG	pBR	this work
pES171	pTrc99A	*baeR-cfp*	*Nco*I, *BamH*I	amp	IPTG	pBR	this work
pKD13	-	rpsB, YFP, kan^R, tsf	multiple	amp, kan	-	R6Kgamma	A. Mogk
pKD46	-	λ Red	-	amp	ara	R101	[197]
pTrc99A	-	expression plasmid	MCS	amp	IPTG	pBR	[209]

Table 6.3: **Primers used in this study.** Restriction sites in nucleotide sequences are underlined.

Primer	Nucleotide sequence (5´-3´)	Restriction site	Target	Source
ERI14	GTAACTTCTAGACTTG	*Xba*I	reverse fusion PCR primer XFP	this work
	TACAGCTCGTCC		+ variants C-terminal fusions	
ERI15	CCGGACAGGAGCTCC	*Sac*I	sense fusion PCR primer CheY	this work
	GTATTTAAATC		C-terminal fusion	
ERI16a	GGCGGAGGAGTGTC	-	sense fusion PCR primer YPet	this work
	TAAAGGTGAAG		C-terminal fusion to CheY	
ERI17	GGAGGCGGAGGCGGA	-	sense fusion PCR primer CyPet	this work
	GTGTCTAAAGGTGAAG		C-terminal fusion to CheZ	
ERI19a	ATATACCATGGTGCT	*Nco*I	sense primer *phoR* His-kinase	this work
	GGAAC GGCTGTC		C-terminal XFP fusions	
ERI19b	TATATGGATCCATCG	*BamH*I	reverse primer *phoR* His-kinase	this work
	CTGTTTTTGGC		C-terminal XFP fusions	
ERI20a	ATATACCATGGTGAA	*Nco*I	sense primer *rstB* His-kinase	this work
	AAAACTGTTTATCC		C-terminal XFP fusions	
ERI20b	TATATGGATCCGCAG	*BamH*I	reverse primer *rstB* His-kinase	this work
	AGGTAAATTGC		C-terminal XFP fusions	
ERI21a	ATATACCATGGTGAG	*Nco*I	sense primer *envZ* His-kinase	this work
	GCGATTGCGCTTC		C-terminal XFP fusions	
ERI21b	TATATGGATCCCCCT	*BamH*I	reverse primer *envZ* His-kinase	this work
	TCTTTTGTCGTGCC		C-terminal XFP fusions	
ERI22a	ATATACCATGGTGAT	*Nco*I	sense primer *cpxA* His-kinase	this work
	AGGCAGCTTAACC		C-terminal XFP fusions	
ERI22b	TATATGGATCCACTC	*BamH*I	reverse primer *cpxA* His-kinase	this work
	CGCTTATACAGCGG		C-terminal XFP fusions	
ERI23a	ATATACCATGGTGAAA	*Nco*I	sense primer *yedV* His-kinase	this work
	AGACTATCTATAACC		C-terminal XFP fusions	
ERI23b	TATATGGATCCATTT	*BamH*I	reverse primer *yedV* His-kinase	this work
	CTTTGCGGTAACG		C-terminal XFP fusions	
ERI24a	ATATACCATGGTGC	*Nco*I	sense primer *hydH* His-kinase	this work
	GTTTTATGCAACG		C-terminal XFP fusions	

Primer	Nucleotide sequence (5´-3´)	Restriction site	Target	Source
ERI24b	TATATGGATCCTCCT	*BamH*I	reverse primer *hydH* His-kinase	this work
	TGTGGGTCCTTACG		C-terminal XFP fusions	
ERI25a	ATATACCATGGTGT	*Nco*I	sense primer *citA* His-kinase	this work
	TGCAGCTTAACGAG		C-terminal XFP fusions	
ERI26a	ATATACCATGGTGA	*Nco*I	sense primer *dcuS* His-kinase	this work
	GACATTCATTGCCC		C-terminal XFP fusions	
ERI26b	TATATGGATCCTCT	*BamH*I	reverse primer *dcuS* His-kinase	this work
	GTTCGACCTCTCCC		C-terminal XFP fusions	
ERI27b	ATATACCATGGTGT	*Nco*I	sense primer *lytS* His-kinase	this work
	CGATTTTAATCTGG		C-terminal XFP fusions	
ERI28a	ATATACCATGGTGGTG	*Nco*I	sense primer *ypdA* His-kinase	this work
	CACGAAATATTCAAC		C-terminal XFP fusions	
ERI28b	TATATGGATCCAAGCA	*BamH*I	reverse primer *ypdA* His-kinase	this work
	ATAACGTAGCCTGTG		C-terminal XFP fusions	
ERI29a	ATATACCATGGTGCT	*Nco*I	sense primer *narX* His-kinase	this work
	TAAACGTTGTCTC		C-terminal XFP fusions	
ERI29b	TATATGGATCCCTCA	*BamH*I	reverse primer *narX* His-kinase	this work
	TGGGTATCTCCTTG		C-terminal XFP fusions	
ERI30a	ATATACCATGGTGAT	*Nco*I	sense primer *narQ* His-kinase	this work
	TGTTAAACGACCC		C-terminal XFP fusions	
ERI30b	TATATGGATCCCATT	*BamH*I	reverse primer *narQ* His-kinase	this work
	AACTGACTTTCCTC		C-terminal XFP fusions	
ERI31	TCGGTGCCGGTTGA	-	sequencing primer *rcsC* (sense)	this work
	TAAGGT			
ERI32	TATATAGATCTACGA	*Bgl*II	reverse primer *citA* His-kinase	this work
	TCAATAGGGTTAATG		C-terminal XFP fusions	
ERI33	GCAAAGCCGGTGTGG	-	sequencing primer binding to CheZ (sense)	this work
ERI34a	ATATACCATGGGTCA	*Nco*I	sense primer *basS* His-kinase	this work
	TTTTCTGCGCCG		C-terminal XFP fusions	
ERI34b	TATATGGATCCTATC	*BamH*I	reverse primer *basS* His-kinase	this work
	TGGTTTGCCACGTAC		C-terminal XFP fusions	
ERI35a	ATATACCATGGTGCG	*Nco*I	sense primer *creC* His-kinase	this work
	TATCGGCATGCGG		C-terminal XFP fusions	

Primer	Nucleotide sequence (5´-3´)	Restriction site	Target	Source
ERI35b	TATATGGATCCTGTG	*BamH*I	reverse primer *creC* His-kinase	this work
	AAGTGACGGTGAAG		C-terminal XFP fusions	
ERI36a	ATATACCATGGTGGC	*Nco*I	sense primer *ntrB* His-kinase	this work
	AACAGGCACGCAG		C-terminal XFP fusions	
ERI36b	TATATGGATCCTTTC	*BamH*I	reverse primer *ntrB* His-kinase	this work
	CTGATAGGCAGG		C-terminal XFP fusions	
ERI37a	ATATACCATGGTGAAA	*Nco*I	sense primer *yfhK* His-kinase	this work
	CGCTGGCCCGTTTTTC		C-terminal XFP fusions	
ERI37b	TATATGGATCCTTTC	*BamH*I	reverse primer *yfhK* His-kinase	this work
	GTGTTTTTCGACGAC		C-terminal XFP fusions	
ERI40a	ATATACCATGGTGAA	*Nco*I	sense primer *kdpD* His-kinase	this work
	TAACGAACCCTTAC		C-terminal XFP fusions	
ERI40b	TATATGGATCCCATA	*BamH*I	reverse primer *kdpD* His-kinase	this work
	TCCTCATGAAATTC		C-terminal XFP fusions	
ERI41a	ATATACCATGGTGAA	*Nco*I	sense primer *torS* His-kinase	this work
	TTTAACCCTGACC		C-terminal XFP fusions	
ERI41b	TATATGGATCCAATC	*BamH*I	reverse primer *torS* His-kinase	this work
	GCGTTCAGGTCTTTC		C-terminal XFP fusions	
ERI42b	TATATGGATCCTTCA	*BamH*I	reverse primer *phoQ* His-kinase	this work
	TCTTTCGGCGCAG		C-terminal XFP fusions	
ERI43a	ATATATCATGATCAA	*BspH*I	sense primer *arcB* His-kinase	this work
	GCAAATTCGTCTGC		C-terminal XFP fusions	
ERI43b	TATATGGATCCTTTT	*BamH*I	reverse primer *arcB* His-kinase	this work
	TTAGTGGCTTTTGCC		C-terminal XFP fusions	
ERI44a	ATATACCATGGTGAC	*Nco*I	sense primer *barA* His-kinase	this work
	CAACTACAGCCTG		C-terminal XFP fusions	
ERI44b	TATATGGATCCCCC	*BamH*I	reverse primer *barA* His-kinase	this work
	GAGAATTTTGCTGG		C-terminal XFP fusions	
ERI45a	ATATACCATGGTGAA	*Nco*I	sense primer *evgS* His-kinase	this work
	GTTTTTACCCTATAT		C-terminal XFP fusions	
ERI45b	TATATGGATCCGTCA	*BamH*I	reverse primer *evgS* His-kinase	this work
	TTTTTCTGACAG		C-terminal XFP fusions	
ERI46a	ATATACCATGGTGC	*Nco*I	sense primer *atoS* His-kinase	this work
	ATTATATGAAGTGG		C-terminal XFP fusions	

Primer	Nucleotide sequence (5´-3´)	Restriction site	Target	Source
ERI46b	TATATGGATCCTACA GTCTGATTTCCCTG	*BamH*I	reverse primer *atoS* His-kinase C-terminal XFP fusions	this work
ERI47	GTAACTACTAGTTTT GTACAATTCATCC	*Spe*I	reverse primer CyPet, C-terminal CheZ fusion (fusion PCR)	this work
ERI48	GAAGAGATGCAG CACAATAT	-	sequencing primer *barA* (sense)	this work
ERI49	GACCGCGTGGGT AAACGTC	-	sequencing primer *arcB* (sense)	this work
ERI50	TGCGCGCCTGGC GGGGGCATC	-	sequencing primer *kdpD* (sense)	this work
ERI51	CAGCTCAATAATG CGGTG	-	sequencing primer o *torS* (sense)	this work
ERI52	CCGCGTCAATATA ATTTTTTC	-	sequencing primer *evgS* (sense)	this work
ERI53a	ATATACCATGGCAG CGAGACGTATTCTG	*Nco*I	sense primer *phoB* response regulator, C-terminal XFP fusions	this work
ERI53b	TATATGGATCCAAAG CGGGTTGAAAAACG	*BamH*I	reverse primer *phoB* response regulator, C-terminal XFP fusions	this work
ERI54a	ATATACCATGGCAAC AAACGTTCTGATTG	*Nco*I	sense primer *kdpE* response regulator, C-terminal XFP fusions	this work
ERI54b	TATATAGATCTAAGC ATAAACCGATAGCC	*Bgl*II	reverse primer *kdpE* response regulator, C-terminal XFP fusions	this work
ERI55a	ATATACCATGGCACCA CATCACATTGTTATTG	*Nco*I	sense primer *torR* response regulator, C-terminal XFP fusions	this work
ERI55b	TATATGGATCCGCAC ACATCAGCGGCTAAG	*BamH*I	reverse primer *torR* response regulator, C-terminal XFP fusions	this work
ERI56a	ATATACCATGGCACGC GTACTGGTTGTTGAAG	*Nco*I	sense primer *phoP* response regulator, C-terminal XFP fusions	this work
ERI56b	TATATGGATCCGCGC AATTCGAACAGATAG	*BamH*I	reverse primer *phoP* response regulator, C-terminal XFP fusions	this work
ERI57a	ATATACCATGGCAAAT GTTATGAACACTATC	*Nco*I	sense primer *rstA* response regulator, C-terminal XFP fusions	this work
ERI57b	TATATGGATCCTTCC CATGCATGAGGCGC	*BamH*I	reverse primer *rstA* response regulator, C-terminal XFP fusions	this work

Primer	Nucleotide sequence (5´-3´)	Restriction site	Target	Source
ERI58b	TATATGGATCCAACG ATGCGGCAGGCGTC	*BamH*I	reverse primer *baeR* response regulator, C-terminal XFP fusions	this work
ERI59a	ATATACCATGGCACAGA CCCCGCACATTCTTATC	*Nco*I	sense primer *arcA* response regulator, C-terminal XFP fusions	this work
ERI59b	TATATGGATCCATCT TCCAGATCACCGC	*BamH*I	reverse primer *arcA* response regulator, C-terminal XFP fusions	this work
ERI60a	ATATACCATGGCACAA GAGAACTACAAGATTC	*Nco*I	sense primer *ompR* response regulator, C-terminal XFP fusions	this work
ERI60b	TATATGGATCCTGCT TTAGAGCCGTCCGG	*BamH*I	reverse primer *ompR* response regulator, C-terminal XFP fusions	this work
ERI61	TACGACCATGGCGAA AAAATTACTGCGTCTT	*Nco*I	sense primer *phoQ* His-kinase, C-terminal XFP fusions	this work
ERI62	ACTGACTCTGGTGA ATCG	-	sequencing primer *torS* II (sense)	this work
ERI63	CGTAGTCGCACTGA TGGC	-	sequencing primer *torS* III (sense)	this work
ERI64a	TACGACCATGGCAAA TAAAATCCTGTTAG	*Nco*I	sense primer *cpxR* response regulator C-terminal XFP fusions	this work
ERI64b	TATATGGATCCTGA AGCAGAAACCATC	*BamH*I	reverse primer *cpxR* response regulator C-terminal XFP fusions	this work
ERI65a	TACGACCATGGCAAA AATTCTGATTGTTG	*Nco*I	sense primer *basR* response regulator C-terminal XFP fusions	this work
ERI65b	TATATGGATCCGTTT TCCTCATTCGCG	*BamH*I	reverse primer *basR* response regulator C-terminal XFP fusions	this work
ERI66a	TACGACCATGGCAC AACGGGAAACGGTC	*Nco*I	sense primer *creB* response regulator C-terminal XFP fusions	this work
ERI66b	TATATGGATCCCAGGC CCCTCAGGCTATATC	*BamH*I	reverse primer *creB* response regulator C-terminal XFP fusions	this work
ERI67a	TACGACCATGGCAA AACTGTTGATTGTC	*Nco*I	sense primer *cusR* response regulator C-terminal XFP fusions	this work
ERI67b	TATATGGATCCCTG ACCATCCGGCACC	*BamH*I	reverse primer *cusR* response regulator C-terminal XFP fusions	this work
ERI68a	TACGACCATGGCAC GAATTTTACTGATAG	*Nco*I	sense primer *qseB* response regulator C-terminal XFP fusions	this work

Primer	Nucleotide sequence (5´-3´)	Restriction site	Target	Source
ERI68b	TATATGGATCCTTTC	*BamH*I	reverse primer *qseB* response	this work
	TCACCTAATGTG		regulator C-terminal XFP fusions	
ERI69a	TACGACCATGGCAA	*Nco*I	sense primer *yedW* response	this work
	AGATTCTACTTATTG		regulator C-terminal XFP fusions	
ERI69b	TATATGGATCCTTTT	*BamH*I	reverse primer *yedW* response	this work
	TTTACCGCTACG		regulator C-terminal XFP fusions	
ERI70a	TACGACCATGGCAAC	*Nco*I	sense primer *citB* response	this work
	AGCTCCATTAACCC		regulator C-terminal XFP fusions	
ERI70b	TATATGGATCCCCCA	*BamH*I	reverse primer *citB* response	this work
	CTGTGGTATATGCG		regulator C-terminal XFP fusions	
ERI71a	TACGACCATGGCAATC	*Nco*I	sense primer *dcuR* response	this work
	AATGTATTAATTATCG		regulator C-terminal XFP fusions	
ERI71b	TATATAGATCTTTGG	*Bgl*II	reverse primer *dcuR* response	this work
	CAATATTGTTTCAG		regulator C-terminal XFP fusions	
ERI74	GTCGTAAAGTCAT	-	sequencing primer binding to *evgS*	this work
	TCAGGGTG		II (sense)	
ERI75a	TACGACCATGGCAAT	*Nco*I	sense primer *lytR* response	this work
	TAAAGTCTTAATTGTC		regulator C-terminal XFP fusions	
ERI75b	TATATAGATCTCAGGCC	*Bgl*II	reverse primer *lytR* response	this work
	AATCGCCTCTTTTAAGC		regulator C-terminal XFP fusions	
ERI76a	TACGACCATGGCAAAA	*Nco*I	sense primer *ypdB* response	this work
	GTCATCATTGTTGAAG		regulator C-terminal XFP fusions	
ERI76b	TATATAGATCTAAGA	*Bgl*II	reverse primer *ypdB* response	this work
	TGCATTAACTGGCG		regulator C-terminal XFP fusions	
ERI77a	TACGACCATGGCAAAA	*Nco*I	sense primer *fimZ* response	this work
	CCAACGTCGGTGATC		regulator C-terminal XFP fusions	
ERI77b	TATATAGATCTTATTA	*Bgl*II	reverse primer *fimZ* response	this work
	ATTCGTATAATTTGG		regulator C-terminal XFP fusions	
ERI78a	TACGACCATGGCAAG	*Nco*I	sense primer *narL* response	this work
	TAATCAGGAACCGGC		regulator C-terminal XFP fusions	
ERI79a	TACGATCATGATAAT	*BspH*I	sense primer *uvrY* response	this work
	CAACGTTCTACTTG		regulator C-terminal XFP fusions	
ERI81a	TACGACCATGGCAAAC	*Nco*I	sense primer *evgA* response	this work
	GCAATAATTATTGATG		regulator C-terminal XFP fusions	

Primer	Nucleotide sequence (5´-3´)	Restriction site	Target	Source
ERI81b	TATATAGATCTGCCGA TTTTGTTACGTTG	*Bgl*II	reverse primer *evgA* response regulator C-terminal XFP fusions	this work
ERI82a	TACGACCATGGCACCT GAAGCAACACCTTTTC	*Nco*I	sense primer *narP* response regulator C-terminal XFP fusions	this work
ERI82b	TATATAGATCTTTGTG CCCCGCGTTGTTG	*Bgl*II	reverse primer *narP* response regulator C-terminal XFP fusions	this work
ERI83a	TACGACCATGGCAATC ACCGTTGCCCTTATAG	*Nco*I	sense primer *uhpA* response regulator C-terminal XFP fusions	this work
ERI83b	TATATAGATCTCCAGC CATCAAACATGCG	*Bgl*II	reverse primer *uhpA* response regulator C-terminal XFP fusions	this work
ERI84a	TACGACCATGGCAACT GCTATTAATCGCATC	*Nco*I	sense primer *atoC* response regulator C-terminal XFP fusions	this work
ERI85a	TACGACCATGGCAAC GCACGATAATATCG	*Nco*I	sense primer *hydG* response regulator C-terminal XFP fusions	this work
ERI85b	TATATAGATCTACGCGA CAGTTTTGCCAATAG	*Bgl*II	reverse primer *hydG* response regulator C-terminal XFP fusions	this work
ERI86a	TACGACCATGGCACAA CGAGGGATAGTCTG	*Nco*I	sense primer *ntrC* response regulator C-terminal XFP fusions	this work
ERI86b	TATATAGATCTCTCCAT CCCCAGCTCTTTTAAC	*Bgl*II	reverse primer *ntrC* response regulator C-terminal XFP fusions	this work
ERI87a	TACGACCATGGCAAG CCATAAACCTGCGC	*Nco*I	sense primer *yfhA* response regulator C-terminal XFP fusions	this work
ERI87b	TATATAGATCTTTCCTT GAAATCGTTTGC	*Bgl*II	reverse primer *yfhA* response regulator C-terminal XFP fusions	this work
ERI88a	TACGACCATGGCAACG CAGCCATTGGTCGG	*Nco*I	sense primer *rssB* response regulator C-terminal XFP fusions	this work
ERI90a	TACGACCATGGCAAAC AATATGAACG	*Nco*I	sense primer *rcsB* response regulator C-terminal XFP fusions	this work
ERI90b	TATATAGATCTGTCTT TATCTGCCGGAC	*Bgl*II	reverse primer *rcsB* response regulator C-terminal XFP fusions	this work
ERI95a	ATATACCATGGGTAAA TACCTTGCTTCTTTTCG	*Nco*I	sense primer *rcsC* His-kinase C-terminal YFP fusions (extended N-term)	this work

Primer	Nucleotide sequence (5´-3´)	Restriction site	Target	Source
ERI95b	TACGAAAGCTTCGATATT TATTGATGCGTTCATGCA	*Hind*III	reverse primer *rcsC* His-kinase (extended N-term)	this work
ERI97	GGCGTGCGTTATCAG	-	sequencing primer *kdpD* II (sense)	this work
ERI101	TACGACCATGGCATGA AGCACATAATGG	*Nco*I	sense primer *baeR* response regulator with additional 100bp upstream	this work
ERI105	TATATGGATCCCTGAC TTGATAATGTCTC	*BamH*I	reverse primer *uvrY* response regulator C-terminal XFP fusions	this work
ERI109	ATCGTCTCGAGGTTG GAGTCATTACCC	XhoI	new sense primer *flhD* promotor region	this work
ERI110	AGCTAGGATCTGAAA ATGCGCTCCTGATG	*BamH*I	reverse primer *narL* response regulator C-terminal XFP fusions	this work
ERI111	AGCTAGGATCTTTCTG CAGACAACATCAAG	*BamH*I	reverse primer *rssB* response regulator C-terminal XFP fusions	this work
ERI112a	ATCTGCCATGGGTATGA TTAAAGTCTTAATTG	*Nco*I	sense primer *yehT* response regulator C-terminal XFP fusions	this work
ERI112b	AGCTAGGATCCCAGGC CAATCGCCTCTTTTAAG	*BamH*I	reverse primer *yehT* response regulator C-terminal XFP fusions	this work
ERI113a	ATCTGTCATGAGTATGT ACGATTTTAATCTGG	*BspH*I	sense primer *yehU* histidine kinase C-terminal XFP fusions	this work
ERI113b	AGCTAGGATCCTGCCT CGTCCCTCCATGG	*BamH*I	reverse primer *yehU* histidine kinase C-terminal XFP fusions	this work
ERI119	TACGAGGATCCTACAT CCGCCGGATCGATAC	*BamH*I	new reverse primer *atoC* response regulator C-terminal XFP fusions	this work
ERI120	ATATATCATGATGTAC GATTTTAATCTGG	*BspH*I	sense primer *lytS* His-kinase C-terminal XFP fusions	this work
ERI121	CAGTCATAGCCGAATAGCCT	-	verification primer k1 kanamycin cassette knockouts (Datsenko and Wanner)	this work
ERI122	CGGTGCCCTGAATGA ACTGC	-	verification primer k2 kanamycin cassette knockouts (Datsenko and Wanner)	this work
ERI123a	ATCTGAAGCTTGGTAA GTTCAAACTTAACC	*Hind*III	300 bp upstream *envZ* deletion, sense primer	this work

Primer	Nucleotide sequence (5´-3´)	Restriction site	Target	Source
ERI124a	ATCTGCATATGATAAAC GGGAGGCGAAGGTG	*Nde*I	300 bp downstream *envZ* deletion, sense primer	this work
ERI124b	TAGCTGTTAACCGCCA TCCTCAACGGTTCG	*Hpa*I	300 bp downstream *envZ* deletion, reverse primer	this work
ERI125a	ATCTGAAGCTTCTGTA CTACAGCGTCTAAGTG	*Hind*III	300 bp upstream *ntrB* deletion, sense primer	this work
ERI126a	TAGCTCATATGAGGTG ACGTTTATGCAACGAG	*Nde*I	300 bp downstream *ntrB* deletion, sense primer	this work
ERI126b	TAGCTGTTAACCTTGTT GATAGGCGCTGACG	*Hpa*I	300 bp downstream *ntrB* deletion, reverse primer	this work
ERI127a	ATCTGAAGCTTCTCTGA TGCGCCGAACCAAC	*Hind*III	300 bp upstream *qseC* deletion, sense primer	this work
ERI128a	ATCTGCATATGCTTCTC TGTCTATGAGAGCCG	*Nde*I	300 bp downstream *qseC* deletion, sense primer	this work
ERI128b	TAGCTGTTAACGCTTT CAATAAGTATGACTGG	*Hpa*I	300 bp downstream *qseC* deletion, sense primer	this work
ERI129a	ATCTGAAGCTTCTACGA TATAACCAATAGTAAG	*Hind*III	300 bp upstream *rcsC* deletion, sense primer	this work
ERI130a	ATCTGCATATGGACGGA TAAGGCGTTTACGC	*Nde*I	300 bp downstream *rcsC* deletion, sense primer	this work
ERI130b	TAGCTGTTAACGCCAGA AGAAATCTGCGATG	*Hpa*I	300 bp downstream *rcsC* deletion, reverse primer	this work
ERI131	TAGCTGCGGCCGCTCAT GCTTTAGAGCCGTCC	*Not*I	300 bp upstream *envZ* deletion, reverse primer	this work
ERI132	TAGCTGCGGCCGCAAAG CAGTCTCCTGAACAGG	*Not*I	300 bp upstream *ntrB* deletion, reverse primer	this work
ERI133	TAGCTGCGGCCGCTCATT TCTCACCTAATGTGTAAC	*Not*I	300 bp upstream *qseC* deletion, reverse primer	this work
ERI134	TAGCTGCGGCCGCGTAG CGCGAGGCTTTCAGGG	*Not*I	300 bp upstream *rcsC* deletion, reverse primer	this work
ERI135	CCTTCTTGACGAGTTC	-	sequencing primer binding to end of kan-cassette (sense)	this work

Primer	Nucleotide sequence (5´-3´)	Restriction site	Target	Source
ERI140a	TACGAGCTAGCCTTAC CCATCTGGGGGC	*Nhe*I	500 bp upstream *evgS* chromosomal C-terminal YFP fusion, sense primer	this work
ERI140b	TAGCTGGTACCGTCA TTTTTCTGACAG	*Kpn*I	500 bp upstream *evgS* chromosomal C-terminal YFP fusion, reverse primer	this work
ERI140c	TACGAGAATTCATAGC GGCTCCCACAATG	*Hind*III	500 bp downstream *evgS* chromosomal C-terminal YFP fusion, sense primer	this work
ERI140d	TAGCTGTTAACCTACA TGGCACCTTTTG	*Hpa*I	500 bp downstream *evgS* chromosomal C-terminal YFP fusion, reverse primer	this work
ERI141a	TACGAAAGCTTGGCA CAGCAATATCCGTC	*Hind*III	500 bp upstream *torS* chromosomal C-terminal YFP fusion, sense primer	this work
ERI141b	TAGCTGGTACCAATCG CGTTCAGGTCTTTC	*Kpn*I	500 bp upstream *torS* chromosomal C-terminal YFP fusion, reverse primer	this work
ERI141c	TACGAGAATTCATCAA TATCAGCCAGTTAAG	*Eco*RI	500 bp downstream *torS* chromosomal C-terminal YFP fusion, sense primer	this work
ERI141d	TAGCTCTTAAGGCCGA CCAAACAGTTTG	*Afl*II	500 bp downstream *torS* chromosomal C-terminal YFP fusion, reverse primer	this work
ERI142a	TACGAAAGCTTCTGCT GGAAGTGGCGG	*Hind*III	500 bp upstream *baeS* chromosomal C-terminal YFP fusion, sense primer	this work
ERI142b	TAGCTGGTACCTACTT CTCTCTGTAAATC	*Kpn*I	500 bp upstream *baeS* chromosomal C-terminal YFP fusion, reverse primer	this work
ERI142c	TACGACATATGGGGA TTTACAGAGAGAAG	*Nde*I	500 bp downstream *baeS* chromosomal C-terminal YFP fusion, sense primer	this work

Primer	Nucleotide sequence (5´-3´)	Restriction site	Target	Source
ERI142d	TAGCTCTTAAGCAGCA GACGAAATTCCGC	*Afl*II	500 bp downstream *baeS* chromosomal C-terminal YFP fusion, reverse primer	this work
ERI143a	TACGAAGCTTCGCGG TTAACAGAGAAC	*Hind*III	500 bp upstream *yedV* chromosomal C-terminal YFP fusion, sense primer	this work
ERI143b	TAGCTGGTACCATTTC TTTGCGGTAACG	*Kpn*I	500 bp upstream *yedV* chromosomal C-terminal YFP fusion, reverse primer	this work
ERI143c	TACGACATATGCATAG GGCTTCAGTACGC	*Nde*I	500 bp downstream *yedV* chromosomal C-terminal YFP fusion, sense primer	this work
ERI143d	TAGCTACGCGTGTGGTC ATGGCGCACTTATTGG	*Afl*III	500 bp downstream *yedV* chromosomal C-terminal YFP fusion, reverse primer	this work
ERI144a	TACGAAAGCTTGGTCA GCGATATGCTGTTTC	*Hind*III	500 bp upstream *cusS* chromosomal C-terminal YFP fusion, sense primer	this work
ERI144b	TAGCTGGTACCAGCG GGTAATGTGATAAC	*Kpn*I	500 bp upstream *cusS* chromosomal C-terminal YFP fusion, reverse primer	this work
ERI144c	TACGAGAATTCTCCTT CAGCAAACGGCAAC	*Eco*RI	500 bp downstream *cusS* chromosomal C-terminal YFP fusion, sense primer	this work
ERI144d	TAGCTCTTAAGAACAT CACGCTGAGTATCG	*Afl*II	500 bp downstream *cusS* chromosomal C-terminal YFP fusion, reverse primer	this work
ERI145a	TACGAAGCTTGCCTG CGCGAGGCGTTTG	*Hind*III	500 bp upstream *citA* chromosomal C-terminal YFP fusion, sense primer	this work
ERI145b	TAGCTGATATCACGA TCAATAGGGTTAATG	*Eco*RV	500 bp upstream *citA* chromosomal C-terminal YFP fusion, reverse primer	this work

Primer	Nucleotide sequence (5´-3´)	Restriction site	Target	Source
ERI145c	TACGAGAATTCGCTC CATTAACCCTATTG	*Eco*RI	500 bp downstream *citA* chromosomal C-terminal YFP fusion, sense primer	this work

Table 6.5: **Bacterial strains used in this study.**

Strain	Relevant genotype	Source or Reference
***E. coli* K-12**		
BW25113	($lacI^q$ $rrnB_{T14}$ $\Delta lacZ_{WJ16}$ *hsdR514* $\Delta araBAD_{AH33}$ $\Delta rhaBAD_{LD78}$)	[197]
DH5α	F Φ80*lacZ*Δ(*lacZYA*-argF)U169 deoR recA1 endA1	Invitrogen, Karlsruhe
	hsdR17($r^-_k m^-_k$)phoA supE44 thi-1 gyrA96 relA1 λ^-)	[240]
ES1	Δ*uhpB* (removed kan^r from JW3643)	this work
ES2	Δ*phoQ* (removed kan^r from JW1115)	this work
ES3	Δ*yedV* (removed kan^r from JW1951)	this work
ES4	Δ*barA* (removed kan^r from JW2757)	this work
ES5	Δ*dcuS* (removed kan^r from JW4086)	this work
JW0390	Δ*phoR::kanR*	Keio collection
JW0611	Δ*citA::kanR*	Keio collection
JW1115	Δ*phoQ::kanR*	Keio collection
JW1213	Δ*narX::kanR*	Keio collection
JW1951	Δ*yedV::kanR*	Keio collection
JW2063	Δ*baeS::kanR*	Keio collection
JW2213	Δ*atoS::kanR*	Keio collection
JW2453	Δ*narQ::kanR*	Keio collection
JW2994	Δ*qseC::kanR*	Keio collection
JW3367	Δ*envZ::kanR*	Keio collection
JW3643	Δ*uhpB::kanR*	Keio collection
JW3882	Δ*cpxA::kanR*	Keio collection
JW3967	Δ*hydH(zraS)::kanR*	Keio collection
JW4073	Δ*basS::kanR*	Keio collection
JW4086	Δ*dcuS::kanR*	Keio collection
JW4362	Δ*creC::kanR*	Keio collection
JW5082	Δ*cusS::kanR*	Keio collection
JW5388	Δ*ypdA::kanR*	Keio collection
JW5407	Δ*yfhK::kanR*	Keio collection
JW5917	Δ*rcsC::kanR*	Keio collection
LL5	Δ*(cheR-cheZ)*, Δ*flgM*	L. Løvdok, personal gift
MG1655	wild type strain	[11]

Table 6.6: **Chemicals and consumables.**

1 kB plus ladder (1 µg/µL)	Invitrogen, Karlsruhe
α-Ketoglutaric acid	Applichem, Darmstadt
Acetoacetate	Applichem, Darmstadt
Agar bacteriology	Applichem, Darmstadt
Agarose electrophoresis grade	Invitrogen, Karlsruhe
Amoniumsulfate	Merck, Darmstadt
Ampicillin	Applichem, Darmstadt
Bacto tryptone	Difco, Hamburg
Bacto yeast extract	Difco, Hamburg
Bromphenol blue	Applichem, Darmstadt
Casein hydrolysate	Oxoid, Wesel
Chloramphenicol	Applichem, Darmstadt
Copper sulfate	Applichem, Darmstadt
D-glucose	Applichem, Darmstadt
di-Potassium hydrophosphate	Grüssing, Filsum
DL-lactic acid	Sigma-Aldrich, Deisenhofen
dNTPs	Invitrogen, Karlsruhe
EDTA	Merck, Darmstadt
Ethanol	Applichem, Darmstadt
Ethidiumbromide	Applichem, Darmstadt
Ferric sulfate	Applichem, Darmstadt
Fumaric acid	Sigma-Aldrich, Deisenhofen
Glucose-6-phosphate	Applichem, Darmstadt
Glycerol	Roth, Karlsruhe
Indole	Sigma-Aldrich, Deisenhofen
IPTG	Roth, Karlsruhe
Kanamycin sulphate	Applichem, Darmstadt
L-arabinose	Sigma-Aldrich, Deisenhofen
L-methionine	Sigma-Aldrich, Deisenhofen
L-serine	Sigma-Aldrich, Deisenhofen
Magnesium chloride	Invitrogen, Karlsruhe
Magnesium sulfate	Merck, Darmstadt
Pageruler Prestained Protein Ladder	Fermentas, St. Leon-Rot
Polythyleneglycol	Sigma-Aldrich, Deisenhofen
Potassium chloride	Applichem, Darmstadt
Potassium hydrophosphate	Grüssing, Filsum
Potassium phosphate	Riedel de Haën, Seelze
Sodium Citrate	Applichem, Darmstadt
Sodium chloride	Applichem, Darmstadt
Sodium hydroxide	Applichem, Darmstadt
Sodium nitrate	Applichem, Darmstadt
Sodium nitrite	Applichem, Darmstadt
Sucrose	Roth, Karlsruhe
TEMED	Applichem, Darmstadt
TMANO	Sigma-Aldrich, Deisenhofen
Tris	Roth, Karlsruhe
Xylencyanol	Applichem, Darmstadt
Zinc chloride	Sigma-Aldrich, Deisenhofen